


1-1-2016

Torque Accuracy Improvement Via Explicit Torque Feedback Control For Internal Combustion Spark Ignition Engines

Anwar Alkeilani
Wayne State University,

Follow this and additional works at: https://digitalcommons.wayne.edu/oa_dissertations

 Part of the [Electrical and Computer Engineering Commons](#), and the [Mechanical Engineering Commons](#)

Recommended Citation

Alkeilani, Anwar, "Torque Accuracy Improvement Via Explicit Torque Feedback Control For Internal Combustion Spark Ignition Engines" (2016). *Wayne State University Dissertations*. 1418.
https://digitalcommons.wayne.edu/oa_dissertations/1418

This Open Access Dissertation is brought to you for free and open access by DigitalCommons@WayneState. It has been accepted for inclusion in Wayne State University Dissertations by an authorized administrator of DigitalCommons@WayneState.

**TORQUE ACCURACY IMPROVEMENT VIA EXPLICIT TORQUE
FEEDBACK CONTROL FOR INTERNAL COMBUSTION SPARK
IGNITION ENGINES**

by

ANWAR ALKEILANI

DISSERTATION

Submitted to the Graduate School,

of Wayne State University,

Detroit, Michigan

in partial fulfillment of the requirements

for the degree of

DOCTOR OF PHILOSOPHY

2016

MAJOR: ELECTRICAL ENGINEERING

Approved By:

Advisor Date

Advisor Date

DEDICATION

To my beloved parents, who raised me tenderly, Dr. Aref Alkeilani and Karama Albarazi,

to all of my dear sisters and brothers who supported me,

to my treasured wife and life partner

Ruqaia Muradagha who stood by and comforted me,

and our children Karama, Aref and Mustafa for their patience,

to my precious sisters-in-law and brothers-in-law for their encouragement,

and to Songping Yu, my previous manager, for all his assistance and cooperation.

ACKNOWLEDGEMENTS

I am much obliged perpetually to Professors Le Yi Wang and Hao Ying, who contributed time to my research. Without their support, encouragement and guidance, I would not be able to write this dissertation. Special thanks to Dr. Songping Yu and Dr. Tamer Badawy who taught me various concepts related to engine management systems and computer-aided simulations. Thanks are due to Professor Feng Lin for his constructive comments. On the other side, I am in debt for the remaining part of my life to my family who stood with me and supported me throughout my long educational voyage in every possible and impossible way.

TABLE OF CONTENTS

ACKNOWLEDGEMENTS	iii
LIST OF FIGURES	viii
LIST OF USED ACRONYMS.....	xi
LIST OF TABLES	xiii
CHAPTER 1: INTRODUCTION.....	1
1.1 Problem Statement.....	1
1.2 Objective and Motivation	2
1.3 Literature Review.....	5
1.4 Originality and Contribution	8
1.5 Dissertation Overview.....	9
CHAPTER 2: SYSTEM OVERVIEW.....	10
2.1 Selected Engine.....	10
2.2 Measuring Methods of Torque and Pressure Sensors	12
2.3 Torque Sensors Specifications	17
2.4 In-Cylinder Pressure Sensors Specifications.....	22
2.5 Hardware Setup	23
CHAPTER 3: INTEGRATED POWERTRAIN MODELS	25
3.1 Engine Plant Model.....	28

3.1.1	Throttle Body Model.....	28
3.1.2	VVT Actuator models.....	30
3.1.3	Engine Breathing Model.....	31
3.1.4	Torque Generation Model.....	33
3.1.5	Crankshaft Speed Dynamics.....	39
3.2	Automatic Transmission Plant Model.....	39
3.2.1	Torque Converter Model.....	39
3.2.2	Transmission Gear Box Model.....	40
3.3	Vehicle Dynamic Model.....	41
CHAPTER 4: PLANT MODEL CALIBRATION AND VALIDATION.....		42
4.1	GT Power Model.....	42
4.2	Engine Mapping Setup.....	46
4.3	Data Fitting Method.....	50
CHAPTER 5: EMS TYPICAL TORQUE REALIZATION SCHEMES.....		54
5.1	Overview of Typical Torque Control Subsystems.....	54
5.2	Driver Torque Demand.....	56
5.3	Torque Arbitration.....	56
5.4	Torque Realization.....	57
5.5	Estimations of Engine Losses.....	61

5.6	Estimations of Engine Torque	62
CHAPTER 6: ALGORITHMS & CASCADE CONTROL STRUCTURE		68
6.1	Brake Torque Sensor Signal Processing	68
6.2	In-Cylinder Pressure Sensors Signal Processing	71
6.3	Design of Feedback Control Systems	74
6.3.1	Control System Design Overview.....	74
6.3.2	Closed loop indicated torque control	78
6.3.3	Closed loop brake torque control.....	79
6.3.4	Combined closed-loop indicated and brake torque control.....	80
CHAPTER 7: SIMULATIONS AND RESULTS		83
7.1	Steady State Data Fitting Results	83
7.2	Transient Data Fitting Results	88
7.3	Controllers Simulation Results.....	92
CHAPTER 8: SYSTEM ANALYSIS AND CONCLUSION		101
8.1	Control System Analysis.....	101
8.2	Conclusion and Suggested Future Work	105
APPENDIX: LIST OF USED SYMBOLS		107
REFERENCES		111
ABSTRACT		121

AUTOBIOGRAPHICAL STATEMENT123

LIST OF FIGURES

Figure 1.1 Facsimile of dog-clutches (by Hofer powertrain Inc.).....	3
Figure 2.1 Flexplate attached to V6 3.6L engine selected for modeling and controls.....	10
Figure 2.2 Torque and power characteristic curves for V6 3.6L engine.....	11
Figure 2.3 (a) Reflective delay-line SAW, (b) one-port SAW resonator, (c) two-port SAW resonator, (d) Interrogation unit	16
Figure 2.4 Torque sensor's response to zero-applied-torque for non-rotating flexplate	18
Figure 2.5 Torque sensor's response to zero-applied-torque for rotating flexplate	19
Figure 2.6 Brake torque sensor raw reading (black) and ECU estimated brake torque (red) for random in city drive cycle	20
Figure 2.7 Brake torque sensor raw (black) and ECU's estimated brake torque (red) readings for random in-city drive cycle zoomed-in.....	21
Figure 2.8 Kistler in-cylinder pressure sensor	22
Figure 2.9 Experimental Hardware setup.....	24
Figure 3.1 Various levels of modeling complexity and their associated execution speed.....	25
Figure 3.2 Illustration of integrated models used in this work.....	27
Figure 3.3 Engine brake torque behavior during enabling and disabling of fuel injectors	36
Figure 3.4 Illustration of basic modeled torque quantities.....	38
Figure 4.1 Six-cylinder gasoline engine model captured by GT-SUITE.....	45
Figure 4.2 Hierarchy of operating point determination and related actuator positions.....	47
Figure 4.3 Operating points exercised on engine dyno.....	48
Figure 4.4 GT-SUITE Space of DoE selected operating points for engine mapping.	49
Figure 5.1 High level overview of typical torque control subsystem within ECU engine management system	55
Figure 5.2 Typical torque signals for open loop torque control	58
Figure 5.3 Averaged torque efficiency as a function of spark advance.....	60
Figure 5.4 Summary of fast path torque realization between spark advance and FSO	61

Figure 5.5 Torque efficiency curve as a function of LBT Delta.....	63
Figure 5.6 Illustration of existing control loops related to torque management.....	66
Figure 6.1 Raw SAW torque sensor reading and processed one.....	68
Figure 6.2 Three engine cycles zoomed-in view of SAW torque sensor reading and processed one during neutral engine idling.....	69
Figure 6.3 Requested engine brake torque, ECU's estimated one as well as the signal as measured by SAW torque sensor.....	70
Figure 6.4 Processed brake torque sensor reading (green) compared to ECU estimated brake torque and commanded fast and slow torques.....	71
Figure 6.5 Instantaneous pressure and derived net IMEP for each cylinder at 2500RPM and max torque	72
Figure 6.6 Superimposed instantaneous pressures for each cylinder and derived engine net IMEP at 2500RPM & max torque.....	73
Figure 6.7 Illustration of SISO slow and fast paths feedback controllers.....	75
Figure 6.8 Fast and slow paths coordination algorithm overview	76
Figure 6.9 Illustration of indicated torque feedback structure with adaption area.....	79
Figure 6.10 Illustration of brake torque feedback structure with adaption area	80
Figure 6.11 Illustration of brake and indicated torque feedback structure with adaptations area...	81
Figure 6.12 Pictorial diagram of torque sensors feedback with existing feedback loops	82
Figure 7.1 Steady state fitting of indicated torque and the error of fitting	83
Figure 7.2 Steady state fitting of cylinder MAF and the error of fitting	84
Figure 7.3 Steady state fitting of cylinder Torque Losses and fitting error.....	84
Figure 7.4 CdA data fitting.....	85
Figure 7.5 Fitting of AFR and spark efficiency data.....	85
Figure 7.6 Validation of modeled VVT positions against ECU measured ones	86
Figure 7.7 Validation of modeled against dyno measured torque data.....	87
Figure 7.8 Validation of modeled against sensor measured MAF data	87
Figure 7.9 GT-Power transient throttle opening data at engine speed = 2500RPM	89

Figure 7.10 Pedal and brake inputs and modeled vs measured values of MAP, transmission turbine speed and vehicle speed.....	90
Figure 7.11 Modeled vs measured values of transmission gear, engine speed, throttle and engine brake torque.....	91
Figure 7.12 Plots of initial vehicle launch simulation.....	94
Figure 7.13 Plots of activation of cruise control simulation using the same cruise control gains for the two strategies	95
Figure 7.14 Vehicle speed and engine brake torque with hill disturbance injection during cruise control whilst cruise control gains are kept the same between the two strategies	96
Figure 7.15 Activation of cruise control simulation results with aggressive cruise control gains for the closed loop strategy	97
Figure 7.16 Vehicle speed and engine brake torque with up-hill disturbance injection during cruise control with aggressive cruise control gains for the closed loop strategy	98
Figure 7.17 Open vs closed loop control response to fast torque request at engine speed 4500 RPM in dyno mode	99
Figure 7.18 Vehicle speed and engine brake torque with down-hill disturbance injection during cruise control with aggressive cruise control gains for the closed loop strategy	100
Figure 8.1 Illustration of plant and slow controller using linearized transfer functions	101
Figure 8.2 Overall open loop equivalent system with closed loop feedback closing the loop on vehicle speed.	104
Figure 8.3 Bode Plot of the OL torque control system.....	104
Figure 8.4 Bode plot of the system including inner torque control feedback loop	105

LIST OF USED ACRONYMS

Acronym	Description	Acronym	Description
ACC	Adaptive Cruise Control	IC	Internal Combustion
ATDC	After Top Dead Center	ICL	Intake Center Line
BTDC	Before Top Dead Center	IDTs	Inter-Digitated/Digital Transducers
CA	Crank Angle	I-term	Integral term
CAC	Cylinder Air Charge	KAM	Keep Alive Memory
CAD	Crank Angle Degrees	KF	K-Factor
CAS	Combustion Analysis System	LBT	Lean Best Torque
CMCV	Charge Motion Control Valve	LTI	Linear Time Invariant
COM	Control Oriented Model	MAF	Mass Airflow
CPS	Cylinder Pressure Sensors	MAP	Manifold Absolute Pressure
CPS	Crank Position Sensor	MBT	Maximum Brake Torque
DoE	Design of Experiment	MiL	Model in the Loop
DOHC	Dual-Overhead Camshaft	MTV	Manifold Tuning Valve
ECL	Exhaust Center Line	NVH	Noise, Vibration, and Harshness
ECU	Engine Control Unit	OBD	On-Board Diagnostics
EGO	Exhaust Gas Oxygen Content	ODE	Ordinary Differential Equation
EGR	Exhaust Gas Recirculation	OOP	Out-of-Plane

Acronym	Description	Acronym	Description
EMS	Engine Management Systems	PFI	Port Fuel Injection
ESS	Engine Stop-Start	RPM	Vehicle Wheel Speed
ETB	Throttle Body	SAD	Spark Advance Delta
ETC	Electronic Throttle Control	SAW	Surface Acoustic Wave
FRM	Fast Running Model	TIP	Throttle Inlet Pressure
FSO	Fuel Shut-Off	TOP	Throttle Outlet Pressure
HCCI	Homogeneous Charge Compression Ignition	TPMS	Tire-Pressure Monitoring Systems
HVAC	Heating, Ventilation and Air Conditioning	VVT	Variable Valve Timing
IAT	Inlet Air Temperature		

LIST OF TABLES

Table 2.1 Specifications of Selected V6 3.6L engine	12
---	----

CHAPTER 1: INTRODUCTION

1.1 Problem Statement

Design and control of internal combustion (IC) engines for automotive powertrain aim to achieve improved vehicle performance, including enhanced drivability, suppressed noise, vibration, and harshness (NVH), improved safety, increased fuel economy, and reduced emissions. Stringent governmental regulations on fuel economy standards and emission levels demand more sophisticated control systems that can balance these, often conflicting [1], performance criteria under diversified driving conditions and engine operating points. One common and key interface signal for control systems for engine, transmission, emission, traction, and vehicle stability is the engine brake or brake torque signal [2]. These systems require the engine to calculate the desired torque and deliver the actual torque with accuracy. The accuracy has two related aspects, one being the accuracy of torque estimation, namely the estimated engine brake torque with respect to the true one. The second is the accuracy of tracking control in delivering the requested torque.

Throughout the recent history of automotive powertrain, specifically since the introduction of microcontrollers into engine management systems (EMS), indicated and brake engine torques have been estimated indirectly using models that incorporate readings from various engine sensors. Sensors for the Intake manifold absolute pressure (MAP) or mass airflow (MAF), exhaust gas oxygen content (EGO), crank shaft speed, throttle position, inlet airflow temperature, engine oil temperature, etc., are examples of sensors that are employed within torques estimation models. For example, gross indicated torque is calculated as a function of the estimated air charge trapped in

the cylinders via a calibration lookup table assuming unity torque (combustion) efficiency [3]. The air charge itself is estimated on the basis of either the MAP or MAF [4] [5]. After the gross indicated torque is calculated, it is adjusted to take into account the effect of torque efficiency changes based on spark angle, air/fuel ratio, percentage of ethanol, fuel shut off, exhaust gas recirculation (EGR), and any other parameters that may affect torque efficiency. The combined effect of such parameters estimations poses a challenge for attaining high accuracy. To calculate engine brake torque, the effects of all torque losses that are also estimated from various calibration lookup tables need to be subtracted from the adjusted indicated torque. This includes estimation of friction, pumping losses, and all other losses incurred from driving the various accessory loads.

Accumulations of the sensors' measurement errors, structures and calibrations modeling inaccuracies, aging and drift factors of engines as well as cylinder-to-cylinder combustion variations have prevented developers from achieving optimum solution [6].

1.2 Objective and Motivation

The demand for better torque estimation and tracking control increased [7] [8] with the advent of Electronic Throttle Control (ETC) and "drive by wire" torque-based control systems (as opposed to pedal-follower-based control). Transmission clutch control requires accurate engine torque [9] especially during shift operations that utilize dog-clutches which are not capable of slipping, refer to Figure 1.1, such that shifting can be completed without the use of friction clutches, thus reducing wear and increasing reliability [10].

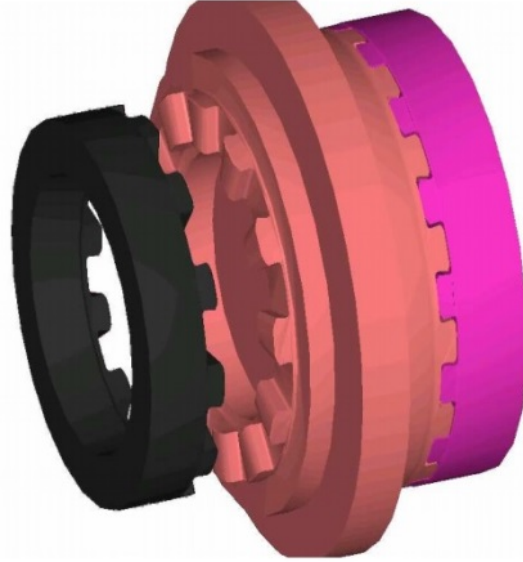


Figure 1.1 Facsimile of dog-clutches (by Hofer powertrain Inc.)

New generations of engines that employ direct injection or those that utilize advanced combustion techniques will have to switch between several operating modes (lean, rich and stoichiometric combustions modes; stratified and homogeneous charge modes) to achieve their best performance in terms of emissions and efficiency. In order to be able to switch operating modes without compromising drivability, the switching must be performed using a very precise controlled torque trajectory [11].

Engine Stop-Start (ESS) systems also demand very high torque accuracy levels in the first stages of engine start (typically within the first 350 ms). The required accuracy is difficult to achieve with the current adopted estimation methods mainly due to inaccuracies related to air charge and combustion efficiency estimations during the short time period following engine start.

Conventional as well as the more recently developed Adaptive Cruise Control (ACC) systems employ highly sophisticated control algorithms and require high levels of torque control accuracy since they are torque-based systems [12] [13].

The main motivations of this work can be summarized in the following points:

1. Achieves better torque estimation and control during engine starts which is crucial for applications equipped with engine stop-start feature for fast and smooth vehicle launches. This also means better engine speed flares trajectory control during normal key and ESS starts.
2. Enables enhanced management of garage shift maneuvers related to transmission shifts smoothness and quality in general as the transmission system, in such conditions, selects to perform up or down shifts near the zero torque line which is hard to measure and control accurately.
3. Achieves better idle torque control around the area where torque is hovering near the zero crossing torque level (positive and negative torque levels crossing).
4. Attains enhanced driveline control related to the prediction, prevention and control of driveline oscillations due to gears' backlash hysteresis.
5. Enables running torque adaptations, outside of idling regime, for friction, pumping and accessory loads'/torques' losses models all the time.
6. Allows investigation of potential opportunities to come up with a novel approach to provide and deliver fast control for transients step pedals.
7. Enables torque and/or air-fuel ratio balancing amongst individual cylinders.
8. Reduces the number of calibration parameters that requires tuning thus cutting the development time.

1.3 Literature Review

Since open-loop torque control approach is the adopted control approach by OEMs in current production vehicles, there has been significant amount of research activity to enhance torque estimation [6] [14–17]. The inverse models of the torque estimation algorithms are used to schedule the actuators such that the resultant engine torque is the requested one. The more accurate torque estimation model, the higher is the precision of open-loop feed-forward control. In order to control torque more accurately and robustly by using feedback control, a reliable direct torque measurement is needed.

Without reliable direct torque measurement, robust torque feedback control is challenging especially during transients. Research for using torque sensors in engine controls is gaining momentum due to the emergence of robust and cost-effective Surface Acoustic Wave (SAW) technology that is used in fabricating torque sensor [18] which permits researchers to implement direct engine torque feedback control as well as other functions. The work by Chalmers University of Technology documented in [19] [20], an inline torque sensor was used to perform optimal combustion phasing control. The 2003 paper [21] by Stefan Schagerberg and Tomas McKelvey describes how they developed a crankshaft torque model using information generated from the cylinder based pressure sensors. The modeled torque was validated against measured torque coming from a torque sensor that they installed within the crankshaft itself (closer to flywheel side). Perhaps this is the first documented work related to installing a torque sensor in such location. The inspiration and original intention of this work was to control combustion timing (phasing), not torque, using instantaneous information obtained from crankshaft

torque sensor using a reversal separation model. This is a different problem and is usually related to diesel engines and Homogeneous Charge Compression Ignition (HCCI) engines in general. Stefan Larsson and Stefan Schagerberg in the 2004 paper [22] demonstrated a reversal method concept that allows the estimation of in-cylinder pressures using the torque sensor.

In [23], H^∞ controller was designed to close the loop on torque but using the throttle only as an actuator. In [24] [25], PI controllers were designed to close the loop on torque by also using the throttle only as an actuator while feeding back the estimated engine torque as opposed to measured torque.

In [26], under the assumption that the rotary torque sensor is available, a model-based approach is employed to control engine torque by also adjusting only the throttle. Disturbance rejection controller is built by regarding the discrepancy between the actual plant and the nominal plant (with desired plant characteristics) as an equivalent disturbance input, which is estimated and for elimination.

Cylinder Pressure Sensors (CPS) have been used to close the loop on spark control, EGR control, Air/Fuel ratio control in [27] but not torque, because indicated torque is unpropitiously not the final engine output (brake torque is the main control objective). In [28], IMEP alone was used in feedback torque control but only after the friction losses were modeled and added in order to have an equivalent brake torque control. Cylinder pressure sensors in [29] were used in the evaluation of the distribution of cycle work, the estimation of net heat release during combustion, the assessment of cycle-to-cycle variability, and the diagnosis of abnormal combustion. Most of research that involves the study of in-cylinder pressure sensing and the usage of this information

rotates around topics related to combustion diagnosis, combustion phasing control, but never tried to use it effectively to control indicated torque or break torque such as in work that can be found in [30-32] and many other similar works for reasons that will be discussed in next chapters.

Based on the developed torque observer in [33], a closed-loop torque control method is designed to track a given torque demand (derived by means of solving an optimal speed tracking problem) using throttle as an actuator.

Neural networks technique is used for both torque estimation and torque tracking control in [34] but the results were showing steady state overshoot in torque possibly due to using the throttle as the only controlling actuator.

In these papers, fast torque control path (by means of using spark and fuel) is not considered in the sense that it is controlled only using open-loop. Also, the control of fast torque request is not coordinated with slow torque request feedback control suggested in some of the work done by others that I outlined.

Adaptive critic learning technique using neural networks in [35] showed promising results for torque and air/fuel ratio control but responding only to one type of input, namely driver torque request which is usually mapped to slow torque request. Hence, using spark and fuel pulse width as a control output along with the throttle in the absence of explicit fast torque request is not clear. In addition, neural networks are considered black box technique which in some cases could be problematic as far addressing issues or calibrating them.

1.4 Originality and Contribution

Seeking remedies to the estimation and tracking accuracy issues mentioned previously, this research takes an alternative approach by utilizing newly considered sensors, introduced primarily for other purposes and areas such as On-Board Diagnostics (OBD), and uses them for torque control. This approach will maximize the benefits from these sensors and justify the potential added cost. This dissertation shows an innovative advance in the utilization of an additional SAW brake engine torque and in-cylinder pressure sensors to accurately control the engine brake and indicated torques. The main innovative part in this research is the application of both the brake torque and in-cylinder pressure sensors to control engine brake torque and engine indicated torque, respectively, by tracking not only slow torque requests but also the fast torque requests. The developed control strategy is innovative in the sense that it utilizes both fast and slow torque paths at the same time to complement the effect of each other via inner-outer loop control structure [36] to control both indicated and brake torques. The usage of the fast torque control path in the feedback permits enhanced performance for rejecting disturbances. The control strategy includes adaptation of various components (that are part of torque estimation), namely, the adaption of potential torque and torque losses due to friction, pumping and accessory loads. The adaption of these quantities increases overall system accuracy. Using the newly developed innovative approach, I was able to get significant improvements in gain and phase margins compared to existing methods which enable using more aggressive gains for faster response without causing overshoot. I was able to achieve faster transient response and improved torque tracking accuracy during fast torque

interventions when compared to existing suggested methods outlined in the literature review section.

1.5 Dissertation Overview

Chapter 2 of this dissertation introduces the plant that is under research. It provides system overview by covering the engine, newly suggested sensors and the hardware setup utilized. Chapter 3 discusses the development of the control oriented mean value engine model. It also includes a simplified transmission and vehicle dynamics plant models. Chapter 4 details the calibration and validation of the plant model showing various simulation traces compared with data obtained from a representative vehicle. Chapter 5 lists a typical torque realization scheme and lays down the necessary foundations for the proposed work. Chapter 6 shows the four basic adopted control structures, discusses the proposed control algorithms and their implementations. Chapter 7 shows major relevant simulation results for the introduced control structures. Finally, Chapter 8 includes system analysis discussion followed by summary and conclusion.

CHAPTER 2: SYSTEM OVERVIEW

2.1 Selected Engine

A 2012 model year 3.6 Liter V-6 engine, shown in Figure 2.1, is the main focus of this research. The reason for selecting this engine is that it is highly considered as one of the most well matured and well developed engines amongst all engines that are currently in production by the manufacturing OEM.



Figure 2.1 Flexplate attached to V6 3.6L engine selected for modeling and controls

Hence, its EMS calibrations are optimized and kept up-to-date. The 3.6L V-6 engine design features state of the art technologies such as a Dual-Overhead Camshaft (DOHC) chain-driven Variable Valve Timing (VVT) with dual independent cam phasing system incorporating 24 valves (2 intake valves and 2 exhaust valves per cylinder) for enhanced breathing and volumetric efficiency during high torque demands with hydraulic end-pivot rocker rollers.

The engine has Charge Motion Control Valve (CMCV) for improved fuel economy and combustion stability. It also has Manifold Tuning Valve (MTV) for increased torque throughout the speed range. The engine has aluminum (die-cast) cylinder block for better power density outputs. The engine supports any percentage of blends between regular gasoline and E85 fuels. The selected engine is a Port Fuel Injection (PFI) engine. Figure 2.2 shows that the engine break torque peaks at around 362 N.m at 4700RPM and its break power is rated at 290 HP at 6800RPM.

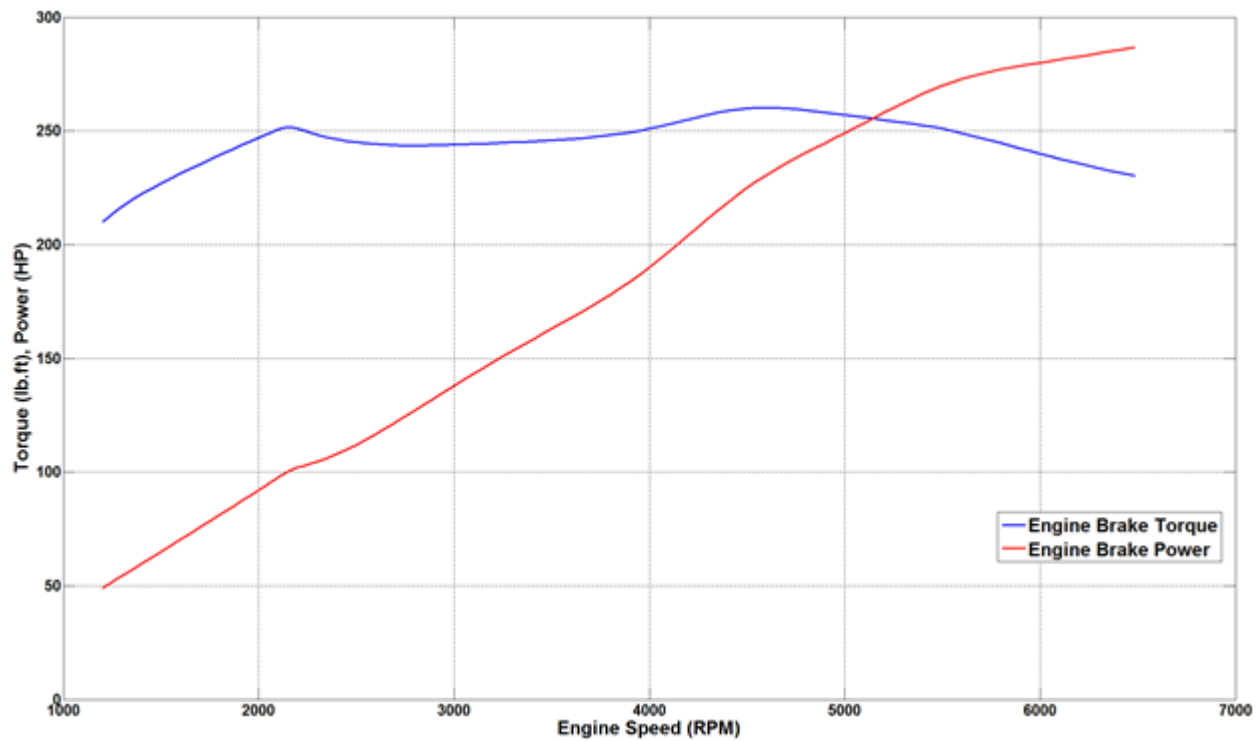


Figure 2.2 Torque and power characteristic curves for V6 3.6L engine

New generations and upgrades to this engine are currently being developed and hence this work is considered to feed into these efforts. Table 2.1 summarizes the main specifications of the selected engine.

Bore and Stroke	96mm x 83mm
Bore Spacing	106mm
Fuel Injection Pressure	400kPa
Engine Power (HP @ rpm)	280 @ 6400
Engine Torque (Nm @ rpm)	360 @ 4300
Engine capacity (cubic cm)	3604
Compression Ratio	10.2:1
Max. Controlled Engine Speed	6400 RPM
Firing Order	1-2-3-4-5-6
Intake Valve Diameter	39mm
Exhaust Valve Diameter	3mm
Throttle Body Bore Diameter	74mm
Minimum Throttle Air Flow	5.0Kg/hr @ 0.63°

Table 2.1 Specifications of Selected V6 3.6L engine

2.2 Measuring Methods of Torque and Pressure Sensors

Measuring torque or pressure quantities effectively is identical to measuring force. There are several measuring techniques used to sense a force that would translate into torque or pressure [14] [37]. Measurement of this quantity can be classified into direct and indirect sensing methods.

The most common direct method is based on the piezo-resistive principle or strain gauge technique that utilizes Hooke's Law [38]. The law states that resulting deformation due to an applied force is directly proportional to a change in mechanical

strain. Change in strain causes resistance of a measuring element to change and when this resistance is arranged in an H-bridge circuitry, the measured voltage across it translates into a force. This means that this sensor is an active sensor that must be supplied with electric current. This method is very accurate, precise and robust. However, due to the location of the torque to be measured (being in a rotating element), this method is not very practical for mass production applications as the measuring element has to be wired.

Another direct method for measuring force is based on magneto-elastic or magnetostrictive principle [39] [40]. The principle states that when a force is applied to a measuring element, its resultant relative magnetic permeability (that governs the relationship between magnetic induction and magnetic field strengths) changes. This change in the measuring element's permeability causes its inductance to change. By measuring the voltage across the sensing element, the force can be determined. This is a contactless type of sensor. Similarly, measuring voltage means that the sensing element has to be wired to pass electric current through it which makes it not a very attractive technique for flexplate torque sensing. This method is robust at high temperatures (up to 300°C) but suffers from non-linearity (mainly hysteresis) effects. These non-linearity effects, however, can be overcome by using special alloy compounds in the sensing element but at the expense of diminishing proportionality factor of the measuring effect. Because of these special compounds, this method is still costly for automotive applications. Due to sensor's sensitivity to magnetic fields, it is not capable of operating in harsh environment without proper magnetic shielding. This is another reason for its high cost. Eddy-current based torque sensors are another version

of this measuring technique that depends on Faraday's law. When torque is applied, magnetic permeability changes which in turn causes the magnetic field to change that results in attenuation or amplification of current.

Torsion or angle measuring is another direct method for measuring applied torque transmitted by a shaft. The torque can be sensed by measurement of relative twist angle, i.e., the torsional strain in the shaft. The relative torsion angle is defined as difference in angle measurements at two points on a shaft that are at certain distance from each other. The relative torsion angle that results in an automotive driveshaft when subjected to applied torque is, however, very small. At maximum applied torque, the twist angle is not larger than couple of degrees. Picking up these fractions of degrees is regarded as extremely too complicated for automotive applications. However, the advantage of this method is that it does not require modification to the shaft (to install a sensing element in-between the shaft) unlike the first two methods that require a certain level of shaft modification.

The torque and pressure signals can also be measured directly by using the emerging SAW technology [18]. The technology is wireless and passive which makes it very apt for automotive applications. In fact, at the time being, this technology is used in the harsh automotive environment in the field of Tire-Pressure Monitoring Systems (TPMS) in vehicles. The technology takes advantage of the piezoelectric effect phenomenon. The piezoelectric effect states that electric charge can accumulate in certain solid materials that have elasticity when mechanical stress or thermal strain across the material is applied. This effect is also reversible and works the other way around; that is applied electric charge can generate stress or strain in certain elastic

material. The SAW sensor works by responding back to a wireless interrogation RF signal (transmitted wirelessly via an interrogation unit shown in Figure 2.3 d). This response is also in the form of an RF signal but with electrical signal properties (mainly frequency and phase) that reflect the magnitude of applied torque or pressure. The transmitted interrogation RF signal is used to excite the sensing elements of the sensor that are made of piezoelectric substrate material, such as quartz or lithium tantalate [41]. Inter-Digitated/Digital Transducers (IDTs) are mounted on this substrate to guide the RF signal and convert it into a SAW signal. When mechanical strain or thermal stress is applied on the sensing element, the properties of the generated SAW signal change. When the interrogation signal is stopped, the already changed generated SAW signal gets transmitted back as an RF signal via the reverse process of the piezoelectric effect (using IDTs again) to the interrogation unit for processing. Signal processing is carried to measure the electrical properties on the final resultant RF signal to extract the torque, pressure or temperature values that are applied and are to be measured.

There are two main types of SAW sensors. Reflective delay-lines (shown in Figure 2.3 a) are one type of SAW devices that measure phase delay between the transmitted and received RF signal. The other most commonly spread and used type is the SAW resonators (being one-port or two-port resonators as shown in Figure 2.3 b and c) that measure change in the frequency of the transmitted RF signal after it is received back from the sensing element and comparing it to a reference resonator frequency. One-port resonator is a bi-directional port that is used to serve the purpose of being an input and output port of the RF signal at the same time using switching circuitry. One-port resonators are the most used type of SAW sensors and are typically

arranged in several pairs for increased accuracy by cancelling the influence of parasitic torque loads such as shaft bending.

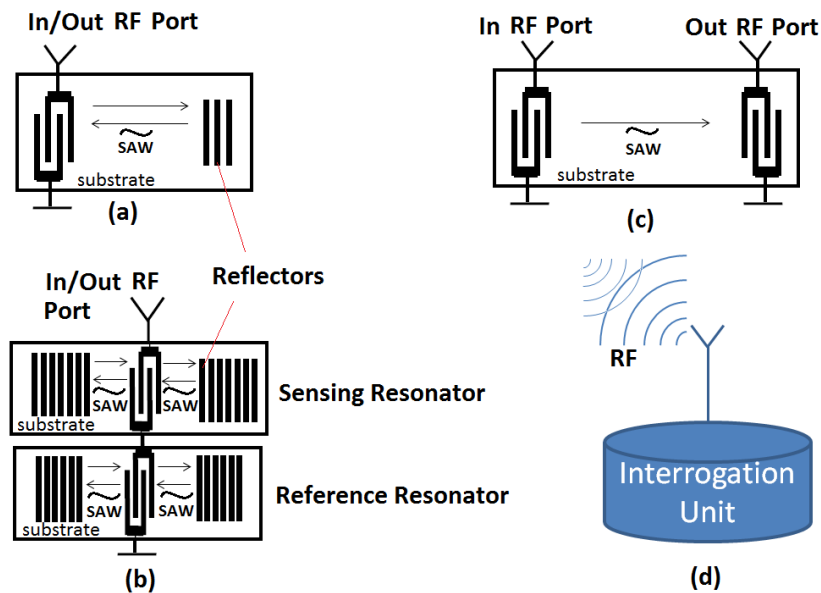


Figure 2.3 (a) Reflective delay-line SAW, (b) one-port SAW resonator, (c) two-port SAW resonator, (d) Interrogation unit

Indirectly, the engine torque can be estimated by measuring engine acceleration using crank position sensor [42] and then applying equation (3.31). This method is accurate as long as the load torque is negligible compared to inertia torque [43]. Also torque converter slip speed measurement for automatic transmissions can be used to indirectly estimate engine brake torque using equations (3.32) and (3.33) assuming engine brake torque is approximately equal to impeller torque [44] [45]. The most common indirect method employed in today's EMS is based on air flow measurement using MAF/MAP sensors but suffers from accuracy issues especially during transients [46] [47].

2.3 Torque Sensors Specifications

The torque sensor used in this project utilizes the SAW technology which exploits the piezoelectric effect phenomenon. The sensor is supplied by Transense Technologies plc. The sensor is installed on the engine's flexplate (automatic transmission counterpart to the flywheel which is related to manual transmissions).

The sensor's minimum torque update period (best possible sampling period) is 150 μ sec. The chosen sampling time is 300 μ sec as dictated by the CAN-bus available speed and bandwidth.

The sensor's resolution, defined as the tripled standard deviation of torque noise, is 1.29 Nm. The sensor's measured torque is affected by the surface temperature of its SAW IDTs which the sensor also measures to compensate for. This means that the temperature compensation has to be calibrated to be used during signal processing. The temperature dependency is due to the fact that piezoelectric effect, in general, is a temperature-dependent phenomenon [48].

The sensor measures the impacted strains due to torque on the flexplate. This means that the sensor does not distinguish between in-plane, Out-of-Plane (OOP), axial load and side applied torques (last three are parasitic loads) as measurement components. However, steady state data reveal that these measurement components are either negligible or can be filtered out to yield a rectified torque measurement.

As the flexplate revolves, the out-of-plane strain can be measured and corrected for during post-processing. In the current design, axial load would be difficult to compensate for, since it would be symmetric with respect to flexplate revolution. However, axial strain measurements show relatively low values (less than 0.2Nm) with

careful location of SAW sensor. The total maximum torque measurement error was up to 5.6Nm, non-linearity error was below 1.2Nm and the hysteresis was below 3.3Nm at applied maximum engine brake torque at all temperatures.

Sensitivity to side loads was 0.056Nm/Nm of side load applied. OOP refers to crank bending and sensitivity to OOP torques was up to 3 Nm/Nm per applied OOP torque. The instantaneous torque output signal at zero-applied-torque for non-rotating flexplate is shown in Figure 2.4.

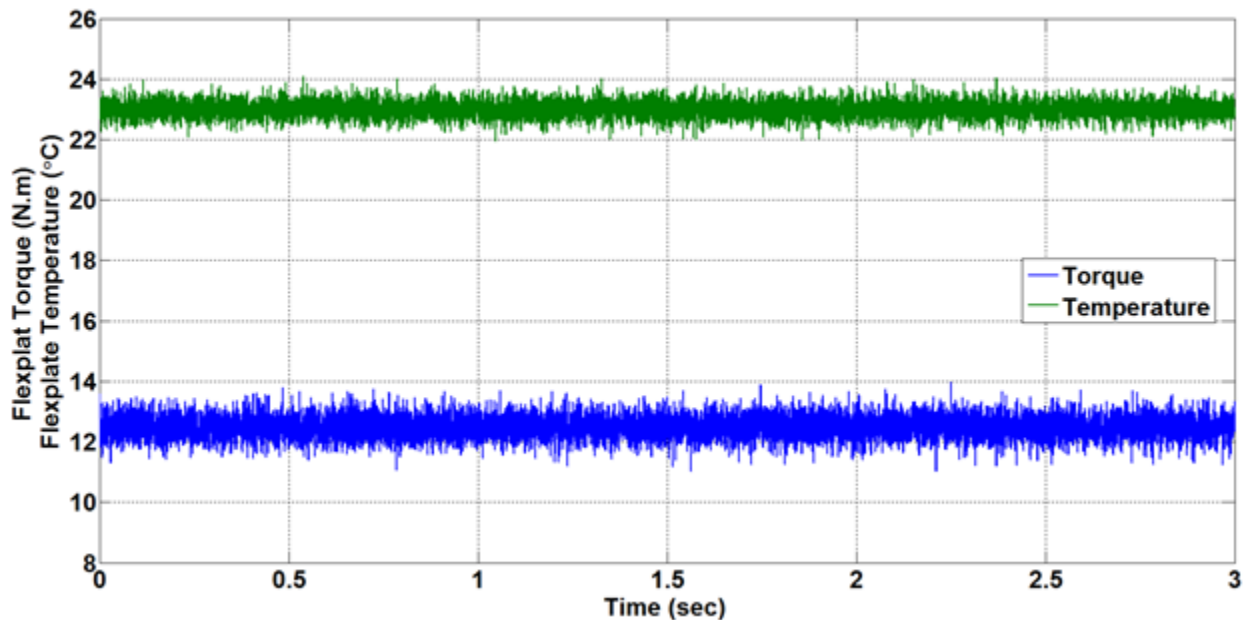


Figure 2.4 Torque sensor's response to zero-applied-torque for non-rotating flexplate

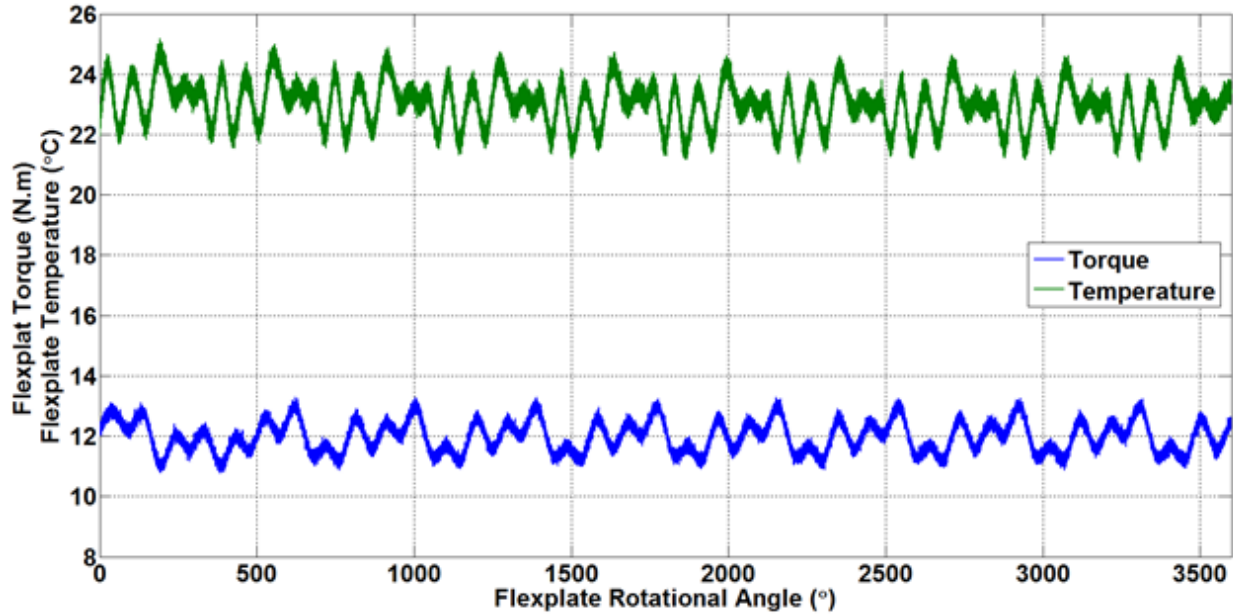


Figure 2.5 Torque sensor's response to zero-applied-torque for rotating flexplate

The instantaneous output torque signal at zero-applied-torque for rotating flex-plate is shown in Figure 2.5. As can be seen in Figure 2.5, the coupler rotational forces produce variations in peak amplitude torque reading of 0.9Nm roughly. This information suggests that careful attention and care must be paid when reading the torque sensor values in order not to react to parasitic loads and reject them via signal processing. Consequently, the sensor readings have to be developed and validated at an engine dynamometer capable of handling torque transients. This is a potential challenge for this project that has to be addressed.

Data was recently collected from a research vehicle equipped with the flexplate torque sensor that shows the nature of this sensor. During engine idle, it can be observed that the sensor outputs pulsations related to the torque spike produced by each firing event.

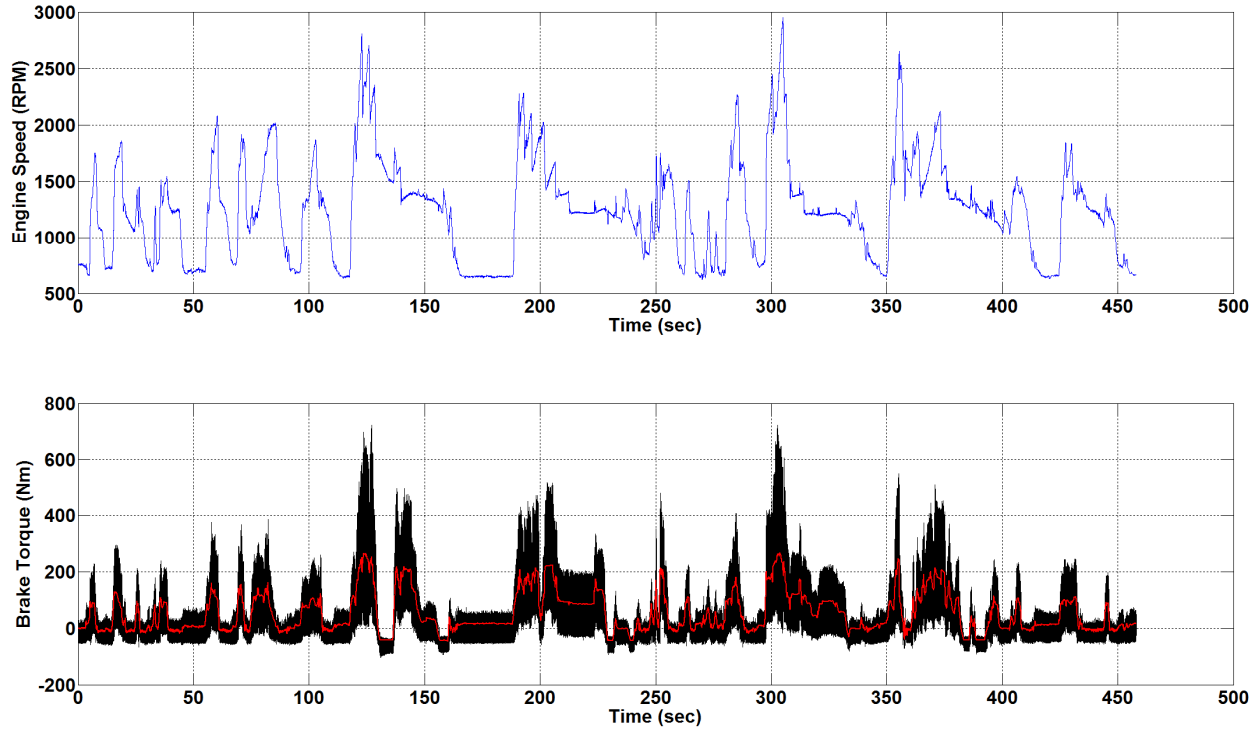


Figure 2.6 Brake torque sensor raw reading (black) and ECU estimated brake torque (red) for random in city drive cycle

From a first glance at the data presented in Figure 2.6, one may conceive the brake torque sensor reading to be noisy relative to the ECU's calculated estimate of engine brake torque. However, zooming in, for example, at an idle region as shown in Figure 2.7 reveals that the sensor is oversampled at a rate of 300 μ sec, since at an idle engine speed of 650RPM, the time between TDC of one cylinder to the next is only 30.77ms. It is oversampled relative to the sampling rate of the ECU's calculated estimate of engine brake torque as it is calculated and updated every TDC. The sampling rate of the sensor is capable of picking up the instantaneous torque signal. In order to compare the sensor reading with the ECU one, the sensor reading has to be processed such that we compare some sort of an average sensor reading using signal processing algorithm. This will be discussed in Chapter 6 in detail.

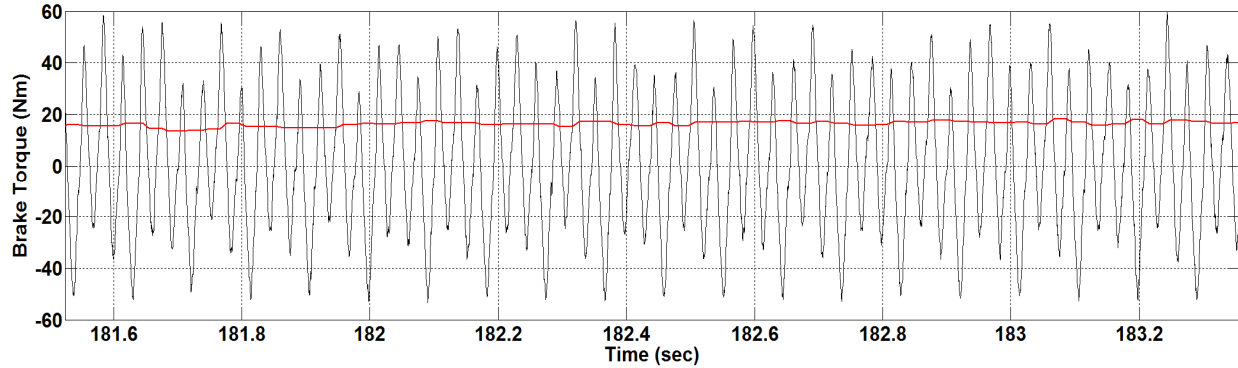


Figure 2.7 Brake torque sensor raw (black) and ECU's estimated brake torque (red) readings for random in-city drive cycle zoomed-in

At every TDC there is one out of the six cylinders producing torque. This is why we see oscillations or pulsations in the measured torque of about 90Nm in magnitude. The average measured sensor torque is close to zero, which is what one would expect at idle since the net torque will be zero (engine acceleration is 0). This info suggests that:

1. The sensor should be sampled at an event-based rate rather than time-based rate. The event rate should be every TDC.
2. The sensor's reading should be averaged every 6 TDCs to produce a reading that is comparable with the current estimate of the brake torque produced currently by the ECU.

The proper signal sampling, conditioning and usage present intriguing challenges. In addition, the proper sampled and conditioned sensor output will have to be tuned by including an offset term that guarantees a final brake torque reading close to zero at idle during park and neutral gears. This is referred to as "finding the zero point" of the sensor. This offset turned out to be the average torque shown in Figure 2.4.

2.4 In-Cylinder Pressure Sensors Specifications



The in-cylinder pressure sensors to be used in this project are piezoelectric pressure sensors that are supplied by Kistler Group. These sensors produce electrical charge when subjected to mechanical stress (in this case the stress being applied combustion pressure). The charge generated by the piezoelectric pressure sensor has to be converted into a voltage signal by a charge amplifier which is then passed to data recording and analysis equipment. Each sensor has minimum sensitivity to temperature variation. It is capable of measuring in-cylinder pressures up to

Figure 2.8 Kistler in-cylinder pressure sensor

300 bar (30MPa). The sensor is characterized by outstanding linearity performance. The sensor does not require additional cooling

which means less effort for integrating and packaging them. These sensors will be sampled at two rates. A fast time-based rate of 0.1ms will be used. An event-based rate of 0.5° Crank Angle (CA) will also be provided. The processing of the sensor's readings involves essentially amplification the charge, converting it to a voltage, looking up the voltage into pressure, and integrating the pressure over full engine cycle to obtain an averaged IMEP reading that will be used to calculate indicated torque cycle by cycle for individual cylinders. This task is performed via an external combustion analysis tool that is described in the next section. The tool fundamentally implements the integral given by

$$IMEP_{cyl} = \frac{W_{cyl}}{V_{dc}} = \frac{\oint P_{icyl} dV_{icyl}}{V_{dc}} \quad (2.1)$$

where V_{dc} is the maximum cylinder swept volume (m^3), P_{icyl} is the instantaneous in-cylinder pressure (Pascal), W_{cyl} is work done by cylinder (Joule) and V_{icyl} is

instantaneous displacement volume of cylinder (m^3).

For net $IMEP_{cyl}$, the integral in (2.1) is evaluated over the entire engine cycle. For gross $IMEP_{cyl}$, the integral is evaluated only from IVC to EVO (for compression and power strokes only). Clearly, this equation requires the change in cylinder volume as it travels within the cylinder which can be derived from the crank angle measurements using the Crank Position Sensor (CPS). The engine IMEP (either gross or net) is derived by averaging all corresponding cylinders' IMEP for each engine cycle:

$$IMEP = \frac{\sum_{cyl=1}^{engine\ total\ number\ of\ cylinders} IMEP_{cyl}}{engine\ total\ number\ of\ cylinders} \quad (2.2)$$

The engine indicated torque is then given by

$$T_{Ind} = \frac{IMEP \cdot V_d}{2\pi n_r} \quad (2.3)$$

where n_r is the number of revolutions per engine cycle which is 2 for a 4-stroke engine and V_d is engine displacement (Liter).

The resulting indicated torque type (gross or net) depends on the type of IMEP used (gross or net).

2.5 Hardware Setup

The OEM ECU will be connected to rapid-prototyping system, INTECRIO from ETAS Inc., via CAN bus. The INTECRIO system is where the new control and signal conditioning algorithms reside. The INTECRIO system in turn will be connected (also via CAN bus) to both a portable combustion analysis system (CAS), called Phoenix, which is a high-speed data acquisition system supplied by A&D Technology Inc. that performs the pressure signals processing (both hardware and software low-pass filtering and calculations of gross and net IMEPs) and the flexplate torque sensor'

readings as it is used as sensor's low-level driver. Figure 2.9 shows the main components used as part of the hardware setup that is utilized to collect vehicle-level data for analysis and verification.

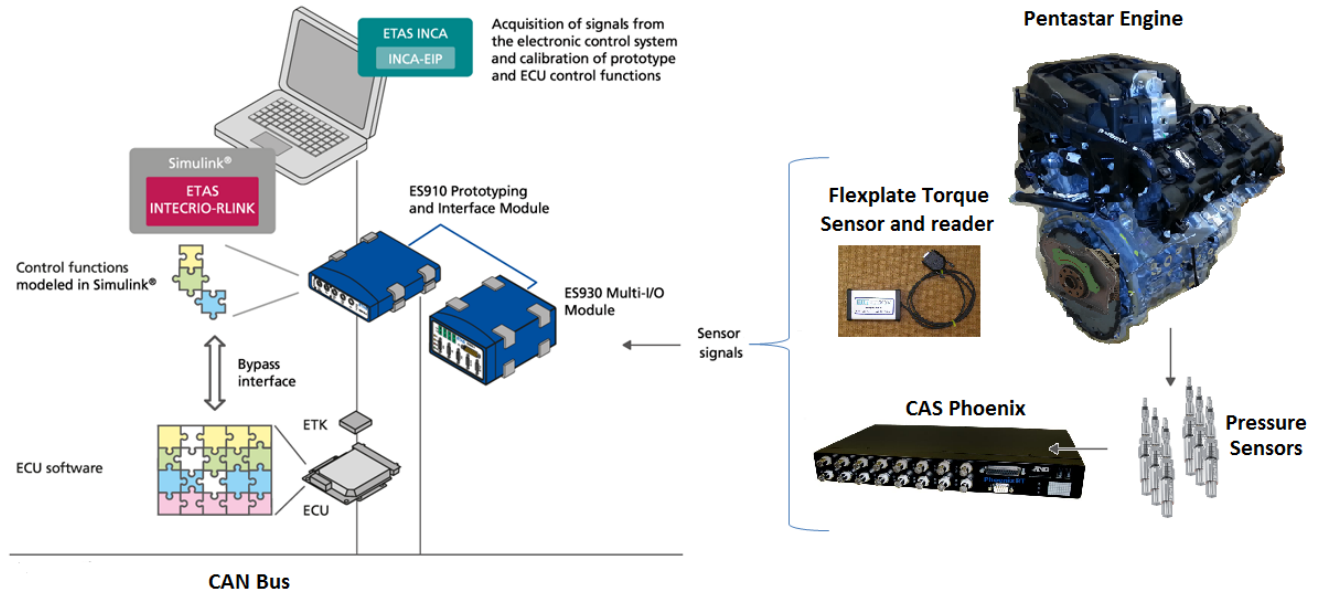


Figure 2.9 Experimental Hardware setup

CHAPTER 3: INTEGRATED POWERTRAIN MODELS

A mean-value model of the engine is developed and explained in this chapter. The advantage of this specific type of control oriented model (COM) which is shown in Figure 3.2 is to rapidly and iteratively develop new advanced control strategies using model in the loop (MiL) environment. The results of the advanced control strategies can be evaluated before building hardware or generating code and therefore minimizing cost and improving efficiency. The execution rate of the COM is typically faster than real-time at the expense of model's fidelity and accuracy. Figure 3.1 shows where the COM falls within the spectrum of available types of models. In this work, GT-SUITE 1-D detailed and fast running models are also used but to calibrate and validate the developed COM as explained in chapter 4 in detail.

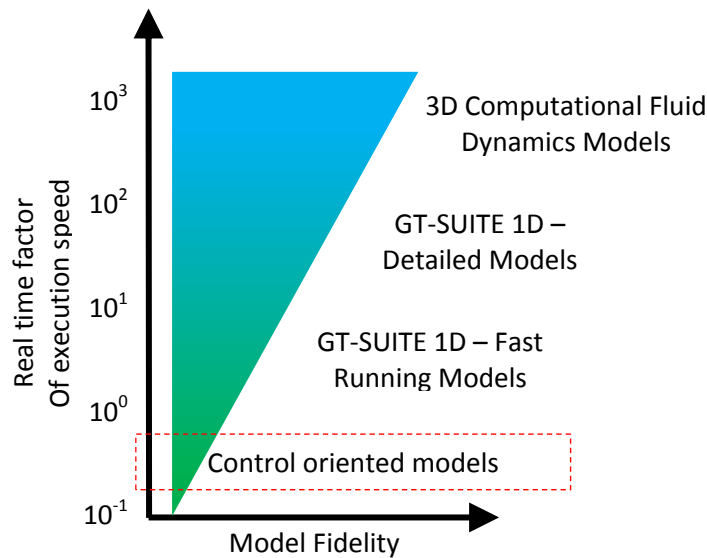


Figure 3.1 Various levels of modeling complexity and their associated execution speed

The proposed integrated powertrain plant model consists of three main subsystems: (1) engine, (2) automatic transmission and (3) vehicle dynamics. The engine subsystem is broken down into four subsystems: (1) throttle body, (2) engine breathing, (3) torque generation and (4) crankshaft dynamics. The automatic transmission subsystem consists of two main parts: (1) torque converter (2) gear box. In the next sections, these subsystems are discussed in detail.

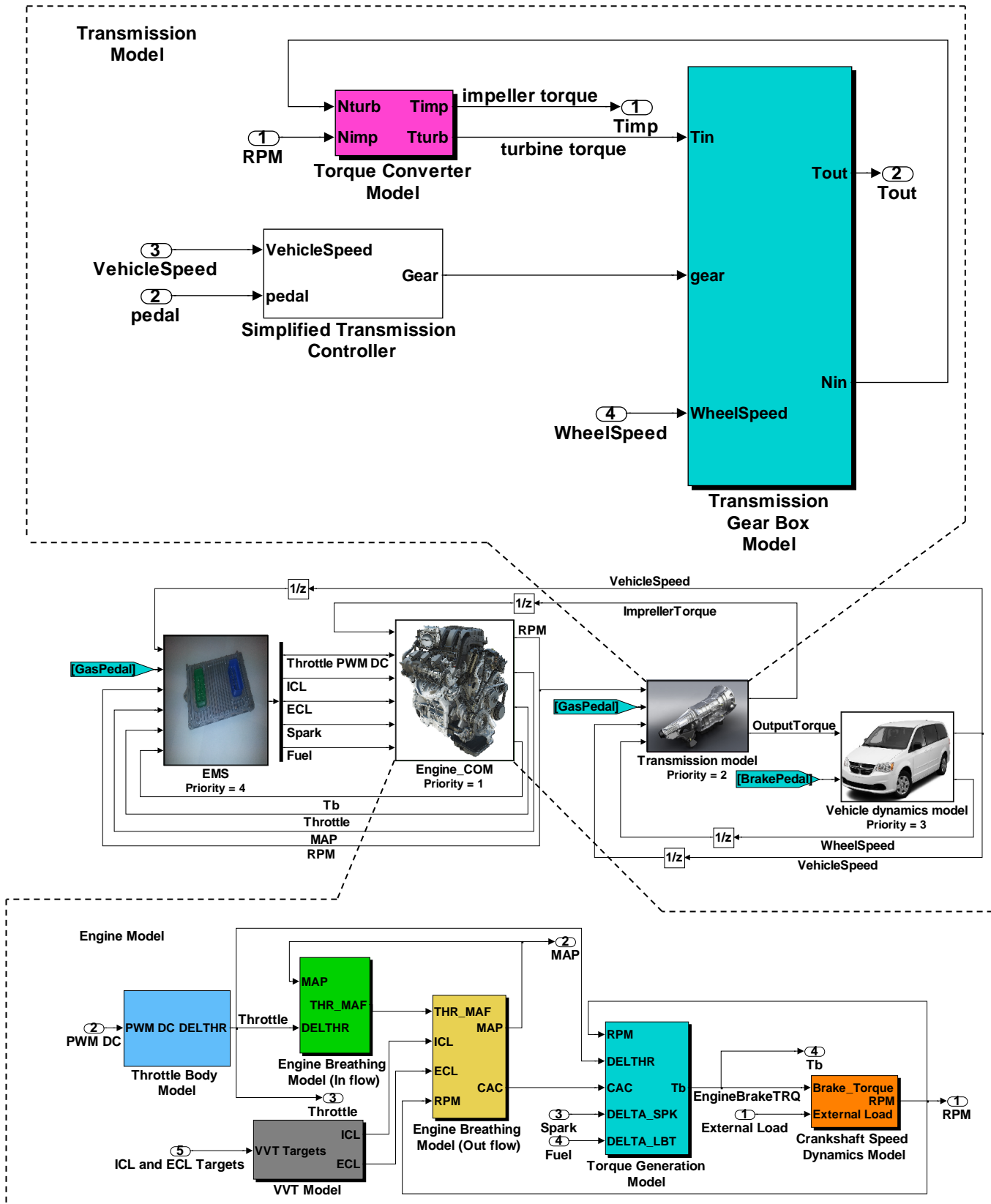


Figure 3.2 Illustration of integrated models used in this work

3.1 Engine Plant Model

In order to develop controllers and experiment with ideas related to their structures, plant engine model is developed. From this model a control law, \mathbf{U} , is then developed.

The modeled engine is a V6 3.6L engine with dual VVT. The engine plant model consists of the following four sub-models:

3.1.1 Throttle Body Model

The model of the throttle body that consists of a dc motor driving a throttle plate with a pre-loaded return spring and a set of gear trains is based on [49]. The input to the throttle body model is the PWM duty cycle DC_{PWM} that is applied on the voltage supply V_s , feeding the throttle body DC motor to control its output, namely the throttle angle, φ_{thr} . The DC motor is connected to the throttle plate shaft via two sets of reduction gear trains. Hence, knowing the total throttle gear ratio, GR_{thr} , one can always relate the angular speed of the motor ω_m (rad/s) to the angular speed of the throttle plate shaft ω_{thr} (rad/s) via

$$\omega_{thr} = \frac{\omega_m}{GR_{thr}} \quad (3.1)$$

The throttle body model can be divided into an electrical model and a mechanical model. The electrical model captures the first order dynamics of the equivalent armature RL circuit of the DC motor

$$DC_{PWM} \cdot V_s - R_a \cdot i_a - V_{emf} = L_a \frac{di_a}{dt} \quad (3.2)$$

where $V_{emf} = \omega_{thr} \times K_{me}$ is the back emf voltage, K_{me} the motor's back emf constant (V.s/rad), ω_{thr} the throttle plate angular velocity (rad/s), φ_{thr} the throttle plate angle (rad), DC_{PWM} the controller duty cycle of the PWM signal (%), V_s the throttle body DC

motor supply voltage (V), R_a the DC motor's armature equivalent resistance (Ω), i_a the current through the DC motor's armature (A), L_a the DC motor's armature equivalent inductance (H).

The mechanical part of the electronic throttle body (ETB) model consists of a safety spring with spring constant K_S . The spring has two advantages: (1) when the spring is at rest, the throttle angle has an opening (between 60° and 90°) to guarantee an elevated engine speed in case of ETB power loss or malfunction so that the vehicle remains drivable. (2) The spring can return the throttle plate to its rest position in case of malfunction or power loss during large throttle openings. The mechanical part of the model is derived from the torque balancing equation. The net torque is the applied torque by the DC motor excluding all torque losses such as damping and friction torques. This is captured by using the following second-order ODE:

$$J_{ETB} \frac{d^2 \varphi_{thr}}{dt} = T_m - K_b \omega_{thr} - T_f \text{sgn}(\omega_{thr}) - f n_1(\varphi_{thr}, K_S) - f n_2(\varphi_{thr}) \quad (3.3)$$

where J_{ETB} is the equivalent total inertia of the ETB, $T_m = K_{mt} \times i_a$ the DC motor applied torque (N.m), T_f the friction torque (N.m), K_{mt} the motor torque constant (N.m/A), ω_{thr} the directional angular speed of the throttle plate (rad/s), K_b the DC motor's viscous friction damping constant (N.m.s/rad), K_S the spring constant (N.m/rad), $\text{Sgn}(\omega_{thr})$ the signum function, $f n_1(\varphi_{thr}, K_S)$ the spring torque function (N.m), $f n_2(\varphi_{thr})$ the spring pre-loaded torque function (N.m).

$f n_1(\varphi_{thr}, K_S)$ is related to the throttle angle which is directly related to the spring position. Depending on whether or not the spring is compressed or stretched, $f n_1(\varphi_{thr}, K_S)$ is given by:

$$fn_1(\varphi_{thr}, K_s) = \begin{cases} K_s \varphi_{thr} & \text{if } \varphi_{thr} > \varphi|_{rest\ angle} \\ 0 & \text{if } \varphi_{thr} = \varphi|_{rest\ angle} \\ -K_s \varphi_{thr} & \text{if } \varphi_{thr} < \varphi|_{rest\ angle} \end{cases} \quad (3.4)$$

$fn_2(\varphi_{thr})$ is related to the constant spring pre-loaded torque T_{PL} (N.m) and it is given

by:

$$fn_2(\varphi_{thr}) = \begin{cases} T_{PL} & \text{if } \varphi_{thr} = \varphi_{min} \text{ or } \varphi_{thr} = \varphi_{max} \\ 0 & \text{else where} \end{cases} \quad (3.5)$$

$Sgn(\omega_{thr})$ is defined by:

$$sgn(\omega_{thr}) = \begin{cases} -1 & \text{if } \omega_{thr} < 0 \\ 0 & \text{if } \omega_{thr} = 0 \\ 1 & \text{if } \omega_{thr} > 0 \end{cases} \quad (3.6)$$

The throttle model can be changed to map the relationship between target throttle position (by ECU) to actual throttle position instead of mapping it from commanded throttle PWM DC to actual throttle position. This is done in order to simplify the analysis (will be explained in the analysis subsequent section) of the model and keep the analysis linear as suggested in [50]. However, for simulations, the PWM-DC model is still adopted and used to maintain model accuracy.

3.1.2 VVT Actuator models

These models are captured based on VVT plant models described in [51-53] with modification to the parameters of the suggested transfer functions in order to fit the collected data from the real engine. These models capture the dynamics associated with the VVT actuators. Given an ECU target Intake and Exhaust Center Line positions (ICL_T and ECL_T respectively), the outputs of these models are the actual Intake and Exhaust Center Line positions (ICL and ECL respectively). These models are summarized via the following two ODEs:

$$\frac{1}{vi_1} \frac{dICL_T}{dt} + \frac{vi_3}{vi_1} ICL_T = \frac{dICL}{dt} + \frac{vi_2}{vi_1} ICL \quad (3.7)$$

$$\frac{1}{ve_1} \frac{dECL_T}{dt} + \frac{ve_3}{ve_1} ECL_T = \frac{dECL}{dt} + \frac{ve_2}{ve_1} ECL \quad (3.8)$$

where vi_x and ve_x are the fitting coefficients

3.1.3 Engine Breathing Model

This model is based on the intake manifold filling and emptying dynamics [54][5] given by:

$$\frac{dm_{air_m}}{dt} = \dot{m}_{air_thr} - \sum_i^{total_cyls} \dot{m}_{air_cyl,i} \quad (3.9)$$

where i is the cylinder index, $\frac{dm_{air_m}}{dt}$ the air mass variation in the intake manifold (g/s), \dot{m}_{air_thr} the mass flow rate of air passing through the throttle (g/s), $\dot{m}_{air_cyl,i}$ the mass flow rate of air in a given individual cylinder i (g/s), $total_cyls$ the engine's total number of cylinders.

In-Flow model through the main throttle (\dot{m}_{air_thr}) is based on quasi-steady state model [55] [56] of flow through restriction orifice given by the following piece wise function:

$$\dot{m}_{air_thr} = \begin{cases} \frac{C_D A p_o}{\sqrt{RT_o}} (P_r)^{\frac{1}{\gamma}} \sqrt{\frac{2\gamma}{\gamma-1} \left(1 - (P_r)^{\frac{\gamma-1}{\gamma}}\right)} & \text{if } p_r > \left(\frac{2}{\gamma+1}\right)^{\frac{\gamma}{\gamma-1}} \\ \frac{C_D A p_o}{\sqrt{RT_o}} \gamma^{1/2} \left(\frac{2}{\gamma+1}\right)^{\frac{\gamma+1}{2(\gamma-1)}} & p_r \leq \left(\frac{2}{\gamma+1}\right)^{\frac{\gamma}{\gamma-1}} \end{cases} \quad (3.10)$$

where p_o is the pressure upstream of the throttle (kPa) or sometimes called Throttle Inlet Pressure (TIP), p_m the intake manifold pressure (kPa) downstream the throttle (throttle outlet pressure or sometimes called TOP), p_r the pressures ratio (p_m / p_o), of

downstream to upstream of the throttle pressures and when $p_r \leq \left(\frac{2}{\gamma+1}\right)^{\frac{\gamma}{\gamma-1}}$ this is called sonic or choked case. γ is the ratio of specific heat capacities (c_v/c_p) of inlet air, c_v the specific heat capacity at constant volume and c_p the specific heat capacity at constant pressure, γ function of temperature and molecular constituents of inlet air (gas composition). For example for fresh air $\gamma = 1.4$ at $T = 250K$ and $\gamma = 1.309$ at $T = 1500K$.

Once the throttle angle φ_{thr} is determined, the throttle cross sectional area can be calculated using geometry. C_D is the throttle discharge coefficient that is empirically determined by measuring the throttle mass air flow rate at the sonic or choked case [55]. C_d is meant to correct for the assumption that the flow through the throttle is isentropic flow. Typically the combined term $C_d A$ is determined as a whole [57] by fitting the throttle airflow data using equation (3.10) and the fitting coefficients a_x within $C_d A$ that is as a function of the throttle angle, φ_{thr} given by:

$$C_d A = a_1 \times \varphi_{thr}^5 + a_2 \times \varphi_{thr}^4 + a_3 \times \varphi_{thr}^3 + a_4 \times \varphi_{thr}^2 + a_5 \times \varphi_{thr} + a_6 \quad (3.11)$$

For the Out-Flow model, the outgoing flow from the intake manifold into the cylinder, $\dot{m}_{air_{cyl,i}}$ (g/s) can be written based on the speed density equation [58] derived from the ideal gas law as:

$$\sum_i^{total_cyls} \dot{m}_{air_{cyl,i}} = \frac{\eta_v \rho_{air} V_d N}{2} \quad (3.12)$$

where η_v is the engine volumetric efficiency, unitless, ρ_{air_m} the density of intake air inside the intake manifold (g/L), N engine speed (rev/s), V_d the engine displacement (L).

However, since η_v is a function of manifold pressure MAP, engine speed N , intake and exhaust CAM positions (ICL and ECL respectively) [59], equation (3.12) is rewritten

such that $\sum_i^{total_cyls} \dot{m}_{air_cyl,i} = f(N, MAP, ICL, ECL)$ and collected engine data are fitted to come up with an expression for $\sum_i^{total_cyls} \dot{m}_{air_cyl,i}$. The final fitted model is:

$$\begin{aligned} \sum_i^{total_cyls} \dot{m}_{air_cyl,i} &= b_1 + b_2 \times MAP + b_3 \times MAP^2 + b_4 \times MAP^3 + b_5 \times N \\ &+ b_6 \times N^2 + b_7 \times N^3 + b_8 \times N^4 + b_9 \times MAP \times N + b_{10} \\ &\times ICL + b_{11} \times ICL^2 + b_{12} \times ICL^3 + b_{13} \times ECL + b_{14} \times ECL^2 \\ &+ b_{15} \times ECL^3 + b_{16} \times ICL \times N + b_{17} \times ECL \times N \end{aligned} \quad (3.13)$$

where b_x is the fitting coefficients of the least square estimate that is used.

Finally, from the ideal gas law principle and from the equations (3.9), (3.10), (3.11) and (3.13) we have a first-order ODE with a single time constant $K = \frac{R_s IAT}{V_m}$ given by:

$$\dot{MAP} = K \frac{dm_{air_m}}{dt} \quad (3.14)$$

where $R_s = 287.058$ (J.kg⁻¹.K⁻¹) is the specific gas constant of air, IAT the inlet air temperature (K), and V_m the intake manifold volume (m³).

3.1.4 Torque Generation Model

The engine brake torque is calculated based on models of the gross indicated engine torque and engine torque losses [60]. The gross indicated torque is mainly a function of the total engine Cylinder Air Charge (CAC):

$$CAC = 2 \frac{\sum_i^{total_cyls} \dot{m}_{air_cyl,i}}{N} \quad (3.15)$$

The gross indicated torque at full efficiency, $T_{G_Ind}|_{full_eff}$, is determined without considering the effects of spark advance delta from the maximum brake torque (MBT)

spark, and deviation of air/fuel ratio away from the lean best torque (LBT) air/fuel ratio. Therefore, the CAC data that are collected at the MBT spark, and air/fuel ratio at LBT are fitted using the structure:

$$T_{G_Ind}|_{full_eff} = c_1 + c_2 \times CAC + c_3 \times N + c_4 \times CAC^2 + c_5 \times CAC \times N + c_6 \times N^2 \quad (3.16)$$

where c_x is the fitting coefficients from the least squares estimation. Using N in the fitting reduces modeling errors.

The effect of spark advance is captured by introducing spark efficiency function, η_{spk} . This efficiency is calculated by fitting torque ratio data at different engine load levels as indicated by CAC. The numerator of the ratio is torque that resulted when spark advance is modified from MBT spark. The denominator of the ratio is the torque that results when the spark is at the MBT (best efficiency). The spark efficiency is given by:

$$\eta_{spk} = s_1 + s_2 \times SAD + s_3 \times CAC + s_4 \times SAD^2 + s_5 \times SAD \times CAC + s_6 \times CAC^2 \quad (3.17)$$

where s_x is the fitting coefficients from the least squares estimation, SAD the Spark Advance Delta away from the MBT in (CAD).

Similarly, the effect from air/fuel ratios can be captured by introducing a lambda efficiency function, η_{af} . This efficiency is calculated by fitting torque ratio data. The numerator of the ratio is the torque that results when the air/fuel ratio is perturbed away from the LBT air/fuel ratio. The denominator of the ratio is the torque that results when air/fuel ratio is at LBT air/fuel ratio.

$$\eta_{af} = l_1 \times LBT D^3 + l_2 \times LBT D^2 + l_3 \times LBT D + l_4 \quad (3.18)$$

where l_x is the fitting coefficients from the least squares estimation that is used. LBTD is the air/fuel ratio delta away from LBT air/fuel ratio.

Combining the effect of all the aforementioned efficiencies [61], the instantaneous gross indicated torque is then given by

$$T_{G_Ind_Inst} = T_{G_Ind}|_{full_eff} \times \eta_{spk} \times \eta_{af} \times \eta_{FSO} \quad (3.19)$$

where η_{FSO} is the torque efficiency (%) associated with the cylinder fuel shut-off (FSO) defined by a factor that is the percentage of turned-off fuel injectors to the total number of cylinders of the engine. In reality, the engine torque does not get reduced instantly by this factor. The resultant torque when cylinder/s is/are turned OFF takes few engine cycles to be realized in a blended and filtered effect as can be seen from sensor data during FSO event in Figure 3.3. Hence, this effect is captured by introducing a first order low pass filter:

$$\tau_c(t) \frac{d\eta_{FSO}}{dt} + \eta_{FSO} = \eta_{RAW_FSO} \quad (3.20)$$

where η_{RAW_FSO} is the raw FSO efficiency (%) prior to filtering and is given by:

$$\eta_{RAW_FSO} = \frac{\text{number of shut off cylinders}}{\text{engine total number of cylinders}} \quad (3.21)$$

and $\tau_c(t)$ is the filter time constant given experimentally by:

$$\tau_c(t) = \frac{1}{2\pi N} \quad (3.22)$$

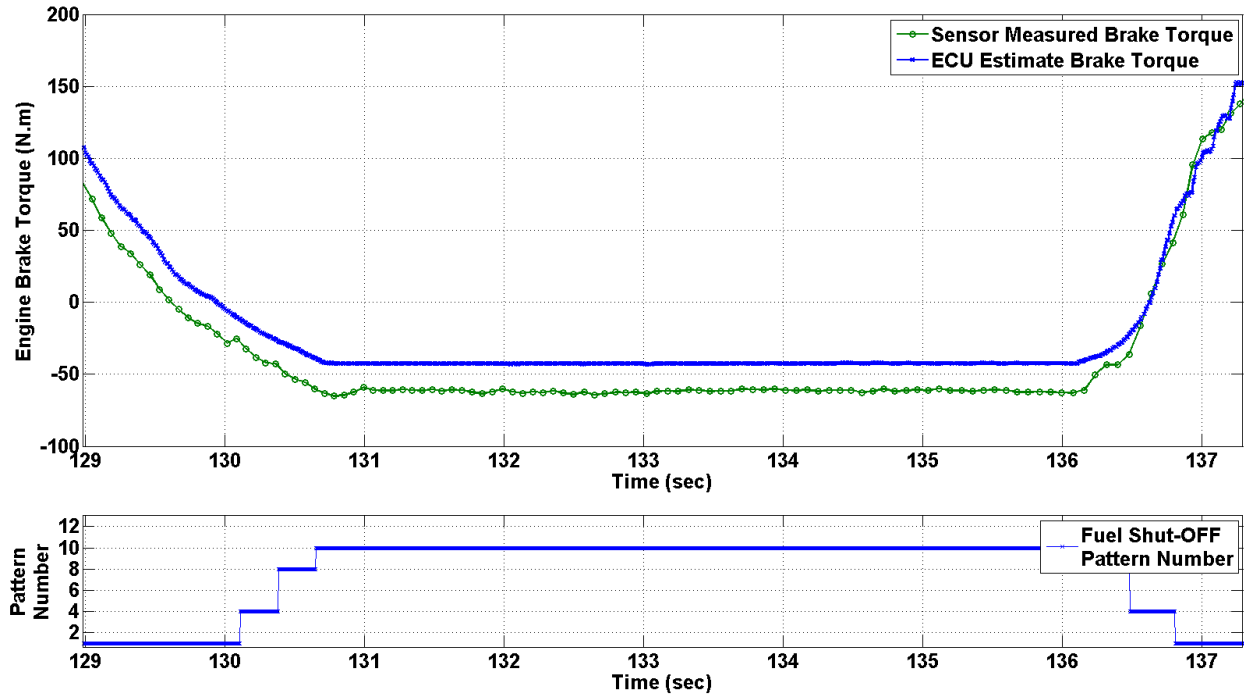


Figure 3.3 Engine brake torque behavior during enabling and disabling of fuel injectors

The torque given by (3.19) does not include any dynamics related to combustion delay and the time it takes for the torque to actually act on the engine crankshaft. To capture these effects a variable transport delay is introduced such that:

$$T_{G_Ind}(t) = T_{G_Ind_Inst}(t - t_d(t)) \quad (3.23)$$

where $T_{G_Ind}(t)$ is the final gross engine indicated torque and $t_d(t)$ is the variable torque production delay given by:

$$t_d(t) = \frac{1}{N} \quad (3.24)$$

In order to keep the linear form of ODE of the final indicated torque model, the transport delay between intake-TDC to power-TDC is approximated by Padé approximation method [62] as will be discussed in the analysis chapter. However, for modeling and simulations, the delay model is used as is for accuracy.

Engine pumping losses torque is modeled as a function of engine speed, and intake manifold pressure which is given by:

$$T_{P_Losses} = p_1 + p_2 \times N + p_3 \times MAP \quad (3.25)$$

The net indicated torque is given by:

$$T_{N_Ind} = T_{G_Ind} - T_{P_Losses} \quad (3.26)$$

The total engine torque losses (including effects of driving accessory loads) are derived by combining engine mechanical friction and pumping losses for a fully warmed-up engine. Based on [63], since friction torque losses depend on engine speed and volumetric efficiency (which mainly depends on MAP), the total combined losses are setup to take the form given by:

$$T_{T_Losses} = f_1 + f_2 \times N + f_3 \times MAP + f_4 \times N \times MAP + f_5 \times MAP^2 + f_6 \times N^2 \quad (3.27)$$

where f_x is the fitting coefficients from the least squares estimation.

Friction torque-losses is the difference between total combined losses and pumping losses:

$$T_{F_Losses} = T_{T_Losses} - T_{P_Losses} \quad (3.28)$$

The final engine brake torque is given by:

$$T_{Brake} = T_{G_Ind} - T_{T_Losses} \quad (3.29)$$

or using (3.26), (3.28) and (3.29)

$$T_{Brake} = T_{N_Ind} - T_{F_Losses} \quad (3.30)$$

Figure 3.4 captures pictorially these modeled torque values and summarizes visually.

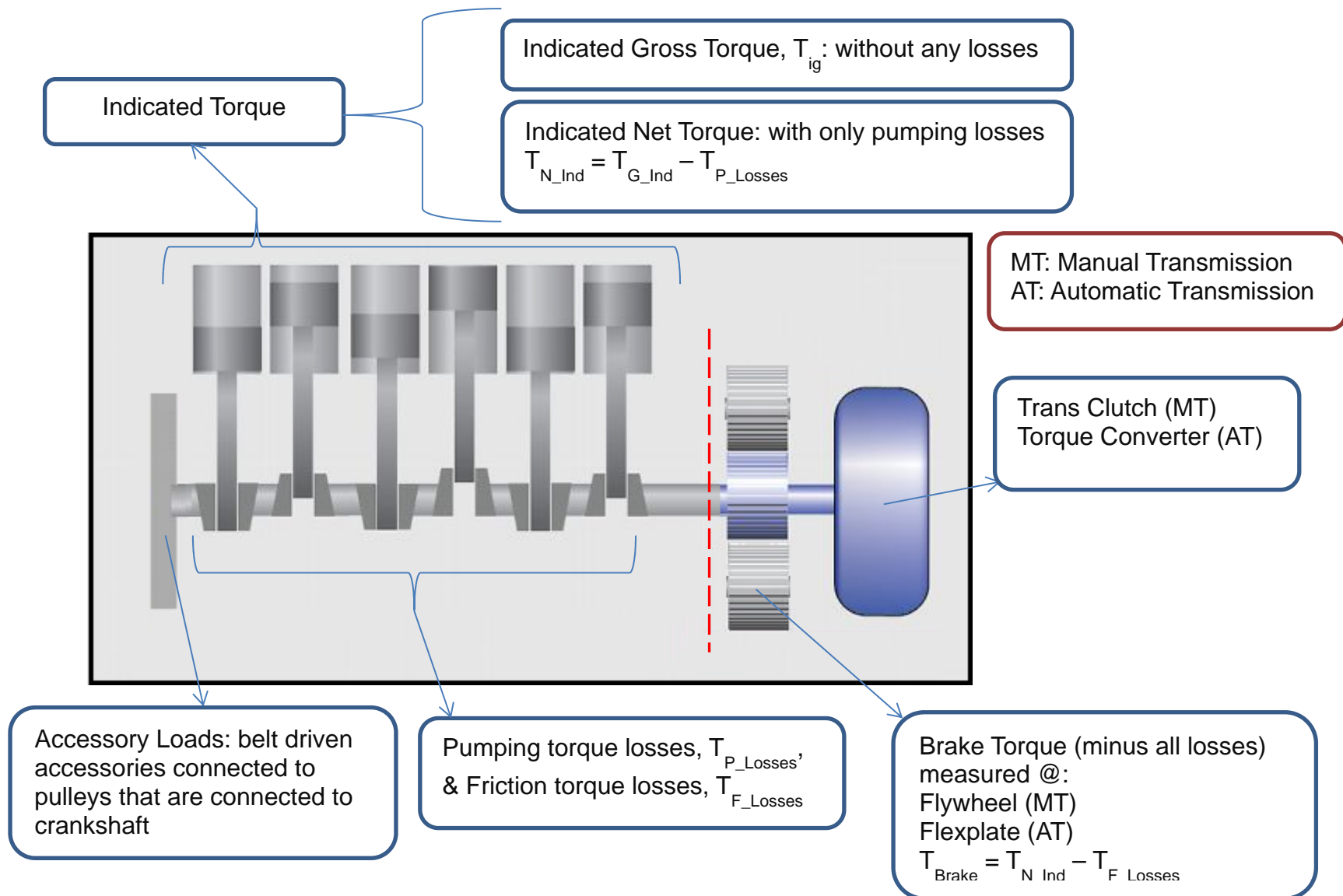


Figure 3.4 Illustration of basic modeled torque quantities

3.1.5 Crankshaft Speed Dynamics

The crankshaft is regarded as a rigid body [33]. Therefore, the second-order torque-balancing differential equation is used to calculate the engine speed:

$$J_{ei} \frac{d^2\theta}{dt^2} + C_{ei} \frac{d\theta}{dt} + K_{ei}\theta = T_{Brake} - T_{Load} \quad (3.31)$$

where θ is the crankshaft position (rad), $\frac{d\theta}{dt} = \omega_e$ the angular speed of the engine's crankshaft (rad/s), $\frac{d^2\theta}{dt^2} = \frac{d\omega_e}{dt} = \alpha_e$ the angular acceleration of engine's crankshaft (rad/s²), J_{ei} the equivalent moment of inertia of the engine and transmission impeller (N.m.s²/rad), C_{ei} the engine's and transmission impeller's damping coefficient or rotational friction (N.m.s/rad), K_{ei} the stiffness of engine and transmission impeller's or coefficient of torsion (N.m/rad). T_{Load} (N.m) is the engine external load torque that comes from transmission impeller torque. This is discussed in the next section.

3.2 Automatic Transmission Plant Model

The transmission model consists of the two submodels: (1) Torque Converter Model, and (2) Transmission Gear Box Model that are explained below.

3.2.1 Torque Converter Model

A torque converter consists mainly of an impeller connected to the engine and a turbine that is connected to the transmission input shaft. Both the impeller and turbine have speeds and torques associated with them. Paper [14] describes a basic model for a torque converter that is used as basis in this section. The external load torque on the engine, T_{Load} , is the impeller torque, T_{Imp}

$$T_{Load} = T_{Imp} = \left(\frac{N}{KF}\right)^2 \quad (3.32)$$

where KF (referred to as K-factor) is determined by fitting speeds data since it is defined as a function of the ratio of the turbine speed, N_T , to the engine speed, N

$$KF = fn_3\left(\frac{N_T}{N}\right) \quad (3.33)$$

N_T is given in the next section. The turbine torque, T_T is given by:

$$T_T = fn_4\left(\frac{N_T}{N}\right) * T_{Imp} \quad (3.34)$$

3.2.2 Transmission Gear Box Model

Papers [64] [65] have a basic automatic transmission model that is used as a foundation for the gear box model used in this research. The transmission gear box consists of an input shaft and output shaft connected by gear sets. Turbine speed, N_T , is the same as the transmission input speed, N_{in} , and is calculated from the equation:

$$N_T = N_{in} = R_{gear} \times N_{out} \quad (3.35)$$

where R_{gear} is the transmission gear ratio based on the current gear. N_{out} is the transmission output speed which given by:

$$N_{out} = spd_w \times FDR \quad (3.36)$$

where Spd_w is the vehicle wheel speed (RPM) derived from the vehicle model as shown in the next section, FDR is a constant for the vehicle's final drive ratio.

The transmission input shaft torque, T_{in} , is the same as the turbine torque T_T . The transmission output shaft torque T_{out} is given by:

$$T_{out} = R_{gear} \times T_{in} \quad (3.37)$$

A simplified transmission shift schedule as a function of driver requested torque percentage and vehicle speed with switching hysteresis is implemented as part of simplified transmission control unit.

3.3 Vehicle Dynamic Model

This model calculates vehicle speed. It is based on the torque balancing equation similar to the crankshaft speed dynamics model that was discussed previously. However, a first-order differential equation is used for simplification. The net torques involved here are the wheel torque, T_w , and the load torque, T_l . The wheel torque is derived from the transmission output shaft torque based on FDR, using the equation:

$$T_w = T_{out} \times FDR \quad (3.38)$$

The load torque consists of three main components [66]: (1) the drag and road-tire friction component, (2) the road grade load component, and (3) the braking load from the applied brake pedal:

$$T_l = fn_5(VS) + fn_6(VS, \theta_r) + T_{BP} \quad (3.39)$$

where the function fn_5 of vehicle speed, VS, represents the drag and road-tire friction load torque component of the load torque; fn_6 function of vehicle speed, VS, and the road grade angle, θ_r (°), and T_{BP} the braking torque applied by the driver's brake pedal (N.m),

The final torque balancing equation around the vehicle's wheels is given by:

$$J_v \alpha_v = T_w - T_l \quad (3.40)$$

where J_v is the vehicle's inertia (N.m.s²/rad), α_v the vehicle angular acceleration (rad/s²) from which the linear vehicle speed, VS (mph), can be calculated given the tire radius, R_t (ft), using the following ODE:

$$\dot{VS} = \frac{120\pi R_t (T_w - T_l)}{5280 J_v} \quad (3.41)$$

CHAPTER 4: PLANT MODEL CALIBRATION AND VALIDATION

Calibrating the plant model parameters, that are outlined in the previous chapter, requires data to be collected from the original plant under study. The data is then fitted by selecting the optimum values for the plant model parameters. The data needed for the fitting is generated from a surrogate but equivalent plant captured by GT-SUITE. The fitted model is then validated using real engine and vehicle data. The following sections summarize these steps.

4.1 GT Power Model

In order to shorten development cycle and save valuable physical testing resources (vehicles, engines and dynamometers), an existing desktop-simulated engine model developed using GT-SUITE is used to collect data required for plant modeling and simulations instead of testing on a real physical engine connected to a dynamometer. Using simulation data generated from GT-SUITE reduces number of required prototypes and enables design optimization with minimum laboratory testing.

GT-SUITE (or GT-Power as it is sometimes called) modelling software, produced by Gamma Technologies Inc., is a comprehensive vehicle simulation tool that consists of various simulation modeling libraries and blocks. It is primarily used for analyzing an entire powertrain system within a vehicle. This includes simulation of processes taking place within an engine, transmission, drive shaft, differential, and final drive components. In regards to engine modelling in particular, GT-SUITE is capable of performing detailed level of both static and dynamic simulations for many processes such as engine intake and exhaust valve-train processes, fuel injection and delivery systems, ignition timing systems, combustion processes, NVH, thermal management

systems, crankshaft dynamics, and lubrication systems and many others. These simulations are typically used to investigate components design, transient response, engine emissions, systems interactions, controls, and perform both system and component level verification and validation.

GT-SUITE engine model variables such as in-cylinder pressures, intake and exhaust manifolds pressures, various mass air and fuel flow rates, and engine speed, various torques measurements, etc. can all be estimated and virtually sensed by the GT-SUITE model and then logged.

Modelling the plant engine using GT-SUITE involves breaking down the engine into its main components and adding them from existing blocks within GT-SUITE library. These include various air restrictions (straight and bent pipes, splits, runners, ports ...etc.), air filters, intake throttle, intake manifold, intake valves, combustion chamber, fuel injectors, fuel system components, spark system, exhaust valves, exhaust manifold, catalyst, mufflers, resonators, crank train, etc. Each of these components has its own set of predefined properties and attributes that need to be entered. For example the throttle blade has inner and outer diameters, forward and reverse coefficients of discharge properties. The throttle body has diameters at inlet end and diameters at outlet end, length, wall temperature assumptions and models, forward and reverse pressure loss coefficients properties.

GT-SUITE model is based on one-dimensional gas dynamics, fluid flows and heat transfer. Each component in the model is discretized or partitioned in many smaller pieces. These pieces have very small differential volumes and hence the scalar properties in these volumes can be assumed to be constant. For example the scalar

properties of a fluid used within GT-SUITE include pressure, temperature, density, and internal energy. Each volume also has vector properties that can be transferred across its boundaries to the next surrounding pieces. These properties include mass flux, fluid velocity, momentum etc. GT-SUITE determines the change in the scalar properties by solving simultaneous one-dimensional thermodynamics differential equations. The main thermodynamic equations that GT-SUITE uses are the mass continuity, conservation of momentum, and conservation of energy equations.

Depending on the details provided in the engine combustion model as far as the number of components used, and the amount of details provided in the properties of these blocks, the model can become very complicated and capture many fluid and air flow dynamics and heat transfer aspects on the expense of simulation time. This is because the model will need to solve more and more one-dimensional differential equations. For this work, there are two available engine planet models that are used depending on the need. (1) A simplified GT-SUITE, called fast running model (FRM) that executes simulations fast (but still slower than real-time) with an impact on accuracy which is used for collecting steady state engine mapping data. (2) A high fidelity GT-SUITE model that is very slow but with higher accuracy which is used for generating transient data. Figure 4.1 shows the components used for the high fidelity model.

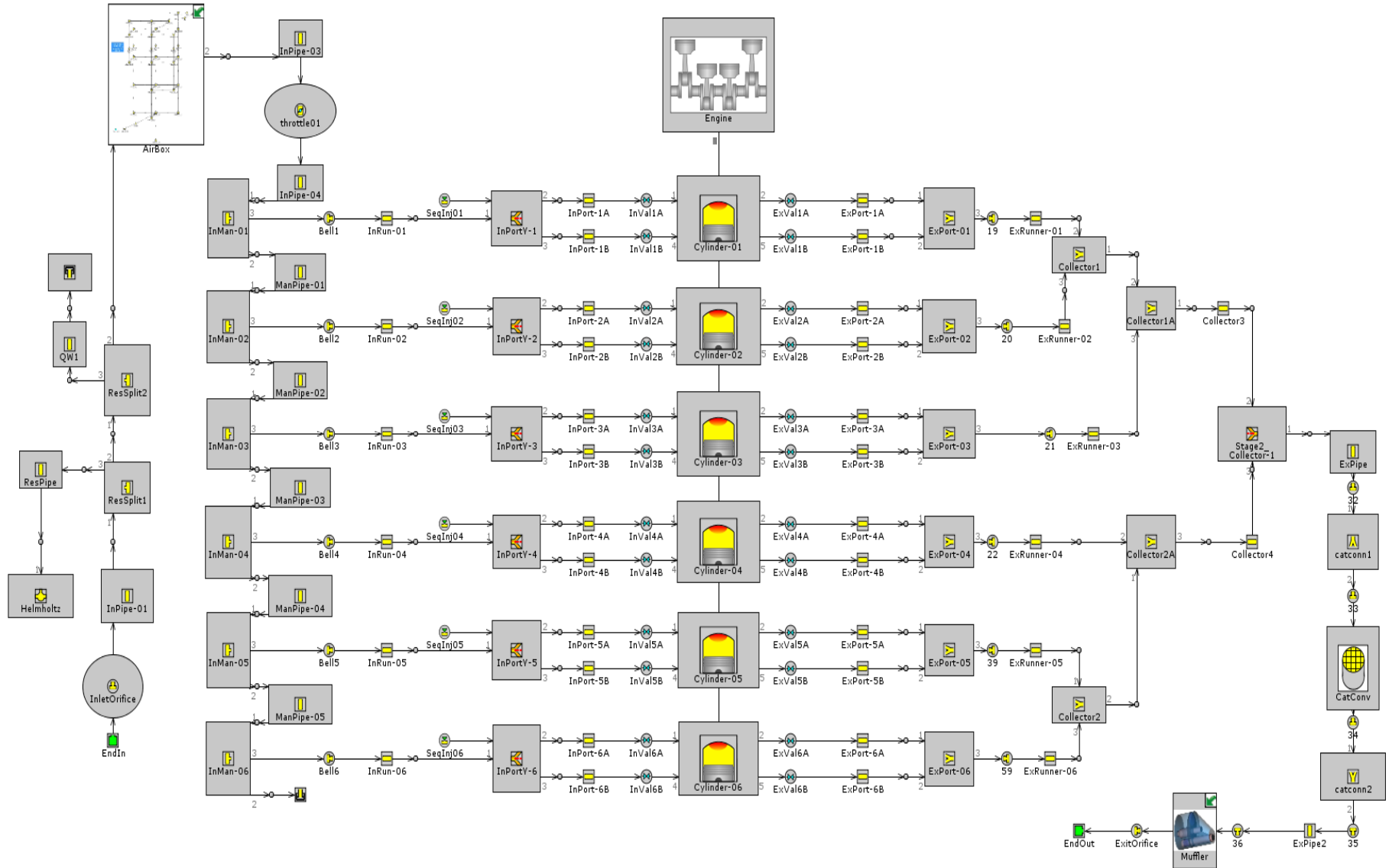


Figure 4.1 Six-cylinder gasoline engine model captured by GT-SUITE

4.2 Engine Mapping Setup

Various engine data have been collected at each engine operating point in order to map the entire engine and calibrate its model parameters as illustrated in [67]. The operating point is designated by engine speed in RPM and engine brake torque in N.m. For a given fixed engine speed the brake torque can be achieved by infinite number of actuator combinations. For example, at an operating point of 1000RPM and 70Nm, the following actuators positions sets may all achieve the same operating point:

Set1: ETC1, ECL1, ICL1, SA1, λ 1

Set2: ETC2, ECL2, ICL2, SA2, λ 2

Set3: ETC3, ECL3, ICL3, SA3, λ 3

where ETCx is the throttle position, ECLx and ICLx are the exhaust and intake cams center line positions of the VVT actuator, SAx is the spark advance angle and λ x is the normalized air fuel ratio.

Therefore, a design of experiment (DoE) has been formulated to produce the necessary data required for developing a calibrated engine plant model. The method that has been followed is to fix the engine speed (run in dyno mode), target a desired torque value to be achieved, sweep various VVT positions, SA, and lambda combinations. The different combinations of swept actuators positions form several test cases. For each test case, the necessary throttle position that is required to achieve the desired engine brake torque is then determined by scanning various throttle positions using a built-in throttle controller in GT-SUITE until the desired torque is achieved. Of course some operating points for some test cases cannot be achieved because of reaching the throttle position boundary (throttle control authority), which means these

operating points at these test cases are not reachable and cannot be realized. In these cases the operating point is not considered and is omitted. Figure 4.2 summarizes the procedure that is followed for one operating point:

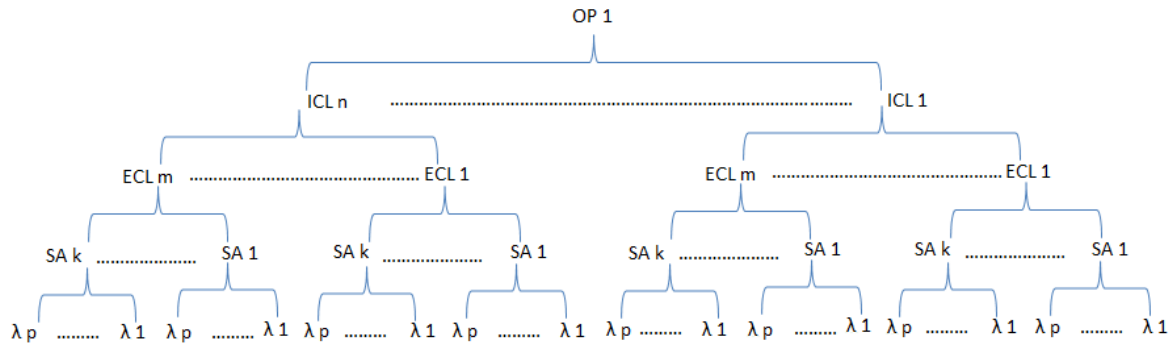


Figure 4.2 Hierarchy of operating point determination and related actuator positions

In Figure 4.2, the number of swept and exercised positions for ICL, ECL, SA, and λ is n , m , k and p respectively. For engine data mapping, typically, the number of operating points that are run is 30×30 . This means the total number of test cases is $30 \times 30 \times n \times m \times k \times p$. Each test case runs for at least 30 seconds in order to ensure that proper steady state conditions are reached and achieved. The data from the last 200 engine cycles within those 30 seconds is averaged and stored as the final data for each test case. This procedure was performed on an engine dynamometer as shown in Figure 4.3 but only with common actuator positions (i.e. n , m , k , p were limited to a max of 2 positions/settings each) and using engine operating points that are found on a common city drive cycle due to availability of resources. Total number of test cases collected on the dyno is around 1300 test for 700 operating points.

Therefore, this obtained engine dyno data is considered only a subset of the entire engine capability spectrum. This data is then used to only validate the models that are

obtained by using mapping data that is generated from GT-SUITE. The same engine data mapping procedure outlined previously is performed and repeated using the GT-SUITE engine model simulation in order to cover as much as possible of the entire space of possible actuator positions to establish the final control oriented nonlinear engine model that is used for developing controls and performing simulations.

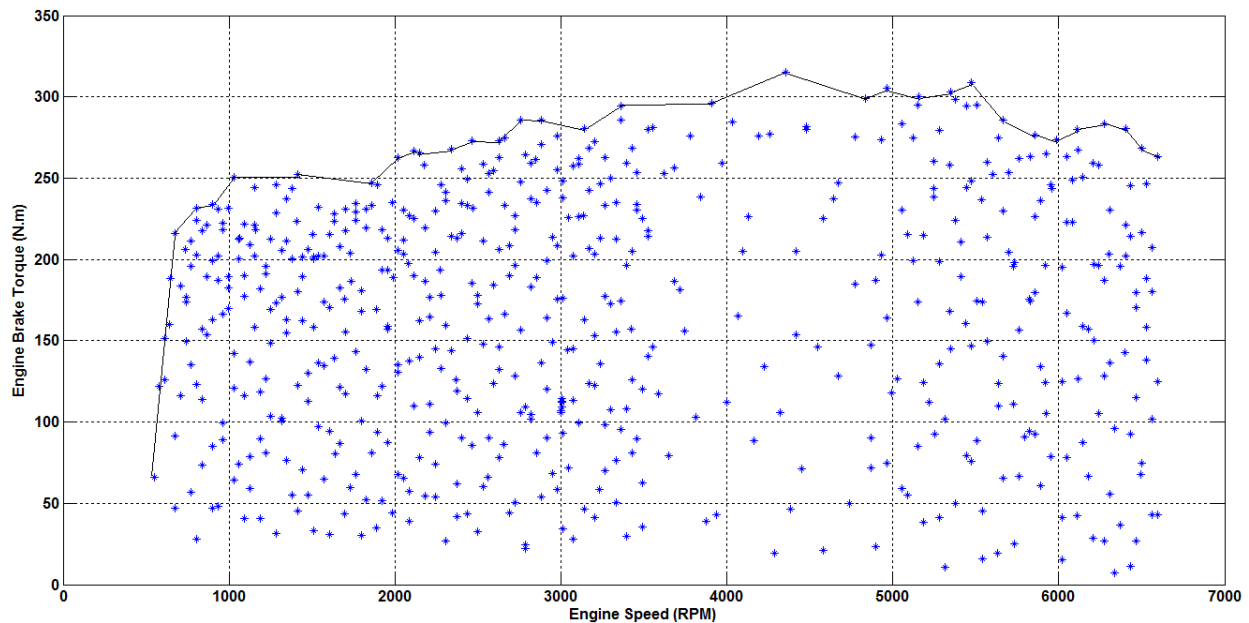


Figure 4.3 Operating points exercised on engine dyno

Starting from the high fidelity engine model established previously using GT-SUITE, a complete engine grid mapping DoE is executed for the entire space of possible engine operating points. The number of operating points exercised is around 1300 points. Several tests per each covered operating point are conducted based on number of swept actuators positions. The total number of tests conducted is around 65000 tests. Figure 4.4 shows the space of operating points that are exercised and covered by the DoE using steady state data from GT-SUITE.

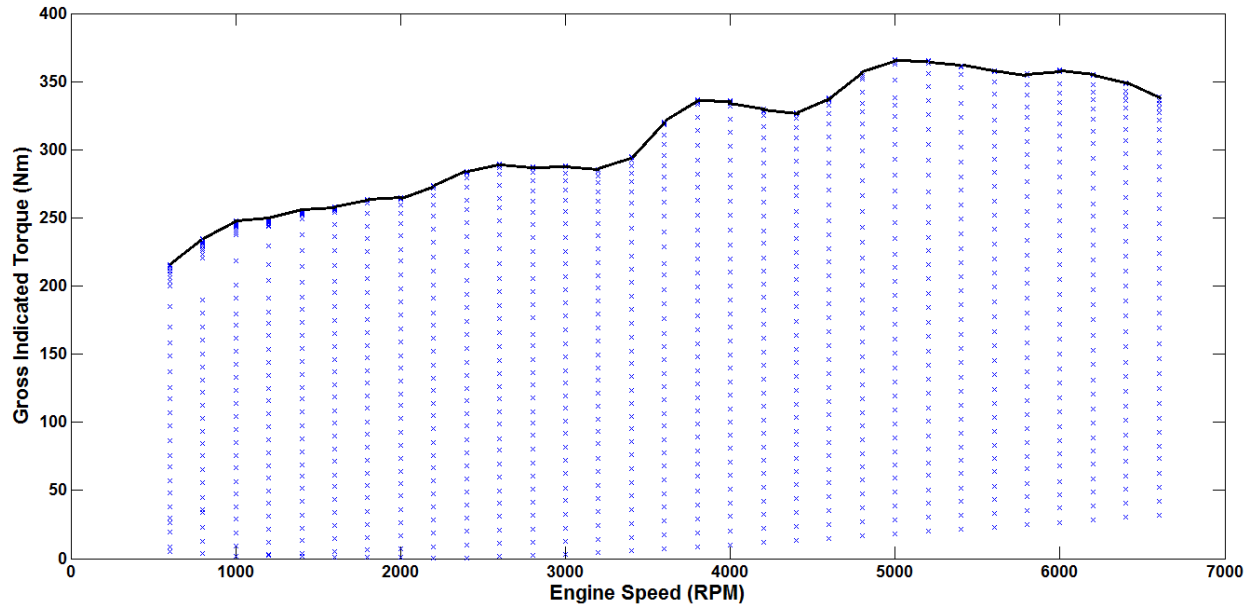


Figure 4.4 GT-SUITE Space of DoE selected operating points for engine mapping.

These steady state data are collected at each engine operating point for duration of time determined by GT-SUITE that ensures steady state conditions are met by comparing cycle to cycle variations in the results of the simulations. These data are used to fit equations (3.11), (3.13), (3.16), (3.17), (3.18), (3.27), (3.33), (3.34) and (3.39) describing the steady state behavior of the engine as lumped steady-state mean-value models.

4.3 Data Fitting Method

The method that is used for data fitting is the linear quadratic least square regression method [68]. The method consists of the following three outlined steps describing fitting of cylinder air charge as an example for illustrating the method:

1. A cylinder air charge fitting structure is initially assumed based on an educated guess that takes into account the expected forms of the various variables that the cylinder air charge depends on. From first principles that are outlined in the previous chapter, the cylinder air charge depends on intake MAP, and engine speed (N). It also depends on ICL and ECL positions of the VVT system. Hence, for example an initial structure for the estimated CAC may have the following form as starting point:

$$CAC \approx a_1 \times N + a_2 \times N^2 + a_3 \times ICL + a_4 \times ECL \times N + a_5 \times MAP + a_6 \times MAP^2$$

where, the coefficients a_1 through a_6 are referred to as the fitting linear coefficients that have to be estimated via regression. For the general case, the number of fitting coefficients that have to be estimated via regression is denoted by k . For this starting point, k is equal to 6.

2. Data for every obtained engine operating point from the engine mapping DoE is used to estimate these fitting parameters by writing 1.0 in a matrix format as the following [68]:

$$CAC_1 \approx [N_1 \quad N_1^2 \quad ICL_1 \quad ECL_1 \cdot N_1 \quad MAP_1 \quad MAP_1^2]_{1 \times k} \begin{bmatrix} a_1 \\ a_2 \\ a_3 \\ a_4 \\ a_5 \\ a_6 \end{bmatrix}_{k \times 1} \quad (4.1)$$

Or

$$CAC \approx \boldsymbol{\varphi}_1 \mathbf{A} \quad (4.2)$$

where $\boldsymbol{\varphi}$ is called vector of predictors and \mathbf{A} is vector of fitting parameters.

Similarly, the rest of the operating points data yield the following equations:

$$\begin{aligned} CAC_2 &\approx \boldsymbol{\varphi}_2 \mathbf{A} \\ &\vdots \\ CAC_n &\approx \boldsymbol{\varphi}_n \mathbf{A} \end{aligned} \quad (4.3)$$

where n is the number of measurement points.

Combining together the entire cylinder air charge equations for all operating points data yield:

$$CAC_{n \times k} \approx \boldsymbol{\Phi}_{n \times k} \mathbf{A}_{k \times 1} \quad (4.4)$$

This system of equations often has no exact solution. Therefore, the goal is instead to find the coefficients of the vector \mathbf{A} which best fit that system of equations in the sense of optimally governed by solving the quadratic minimization problem:

$$\hat{\mathbf{A}} = \arg \min_{\hat{\mathbf{A}}} S(\hat{\mathbf{A}}) \quad (4.5)$$

such that:

$$CAC_{n \times 1} = \boldsymbol{\Phi}_{n \times k} \hat{\mathbf{A}}_{k \times 1} + \mathbf{E}_{n \times 1} \quad (4.6)$$

Where, $\mathbf{E}_{n \times 1}$ is the fitting error vector associated with each data point.

and S is the objective function given by:

$$S(\hat{\mathbf{A}}) = \|\mathbf{CAC} - \boldsymbol{\Phi} \hat{\mathbf{A}}\|^2 \quad (4.7)$$

Expanding (4.7) yields

$$\begin{aligned} S(\hat{\mathbf{A}}) &= (\mathbf{CAC} - \boldsymbol{\Phi} \hat{\mathbf{A}})^T (\mathbf{CAC} - \boldsymbol{\Phi} \hat{\mathbf{A}}) \\ &= \mathbf{CAC}^T \mathbf{CAC} - \hat{\mathbf{A}}^T \boldsymbol{\Phi}^T \mathbf{CAC} - \mathbf{CAC}^T \boldsymbol{\Phi} \hat{\mathbf{A}} + \hat{\mathbf{A}}^T \boldsymbol{\Phi}^T \boldsymbol{\Phi} \hat{\mathbf{A}} \end{aligned} \quad (4.8)$$

Further reducing (4.8) gives

$$S(\hat{\mathbf{A}}) = \mathbf{CAC}^T\mathbf{CAC} - 2\hat{\mathbf{A}}^T\boldsymbol{\Phi}^T\mathbf{CAC} + \hat{\mathbf{A}}^T\boldsymbol{\Phi}^T\boldsymbol{\Phi}\hat{\mathbf{A}} \quad (4.9)$$

Differentiating both sides of (4.9) with respect to \mathbf{A} and equating the derivative of $S(\hat{\mathbf{A}})$ to zero gives:

$$\boldsymbol{\Phi}^T\mathbf{CAC} = (\boldsymbol{\Phi}^T\boldsymbol{\Phi})\hat{\mathbf{A}} \quad (4.10)$$

Solving for $\hat{\mathbf{A}}$ yields:

$$\hat{\mathbf{A}} = (\boldsymbol{\Phi}^T\boldsymbol{\Phi})^{-1}\boldsymbol{\Phi}^T\mathbf{CAC} \quad (4.11)$$

where,

$$\mathbf{CAC}_{n \times 1} = \begin{bmatrix} \text{CAC}_1 \\ \text{CAC}_2 \\ \vdots \\ \text{CAC}_{n-1} \\ \text{CAC}_n \end{bmatrix} \text{ is the measured mean cylinder air charge vector associated with}$$

each data point.

$$\boldsymbol{\Phi}_{n \times k} = \begin{bmatrix} \boldsymbol{\varphi}_1 \\ \boldsymbol{\varphi}_2 \\ \vdots \\ \boldsymbol{\varphi}_{n-1} \\ \boldsymbol{\varphi}_n \end{bmatrix} \text{ is the vector of linear or non-linear combinations of the assumed fitting}$$

data structure.

3. If the fitting is not acceptable according to a goodness of fitting criterion, then the fitting structure described in step#1 is modified and (4.11) is executed again. The modification could be by adding more dependent variables or changing the form of the dependent variable already selected to be based on another arithmetic function (such as introducing a cubic engine speed term)

The goodness of fitting criterion used is comparison of \bar{R}^2 (adjusted coefficient of determination) which is defined as:

$$\bar{R}^2 = 1 - \frac{(n-1) \sum_{i=1}^n (\widehat{CAC}_i - \overline{CAC})^2}{(n-k) \sum_{i=1}^n (CAC_i - \overline{CAC})^2} \quad (4.12)$$

where

\widehat{CAC}_i is the estimated cylinder air charge for the i^{th} operating point measurement

\overline{CAC} is the mean of all cylinder air charge measurements

CAC_i is the i^{th} operating point cylinder air charge measurement

The goal is to achieve \bar{R}^2 greater than 99%. This goal has been achieved for all fitted models except for spark and lambda efficiencies fitting (only ~80% has been achieved) for the reasons provided in the first chapter.

Based on the obtained GT-SUITE DoE data and after several iterations of fitting-structure changes, the cylinder air charge model described by equation (3.15) is obtained. The same procedure is followed to develop and fit the steady state equations described in the previous chapter.

CHAPTER 5: EMS TYPICAL TORQUE REALIZATION SCHEMES

5.1 Overview of Typical Torque Control Subsystems

Typical recent EMS control algorithms contain several subsystems that interact with one another to deliver certain outputs by the engine's actuators and process certain inputs from the engine's sensors [69]. One of the most important subsystems is Engine Torque Management Subsystem that gained extra importance with the introduction of drive by wire or ETC system. Typically, the torque subsystem administers over several underlying functions in order to ensure correct engine torque delivery. Figure 5.1 illustrates the basic functions that the engine torque management is comprised of. The fuel and spark subsystems are just shown for clarity as they are not part of the engine torque management subsystem. The goal in providing high level explanation of this subsystem is to give the reader a basic understanding of the foundations that is going to be modified to incorporate the new controls as will be explained in the next chapter.

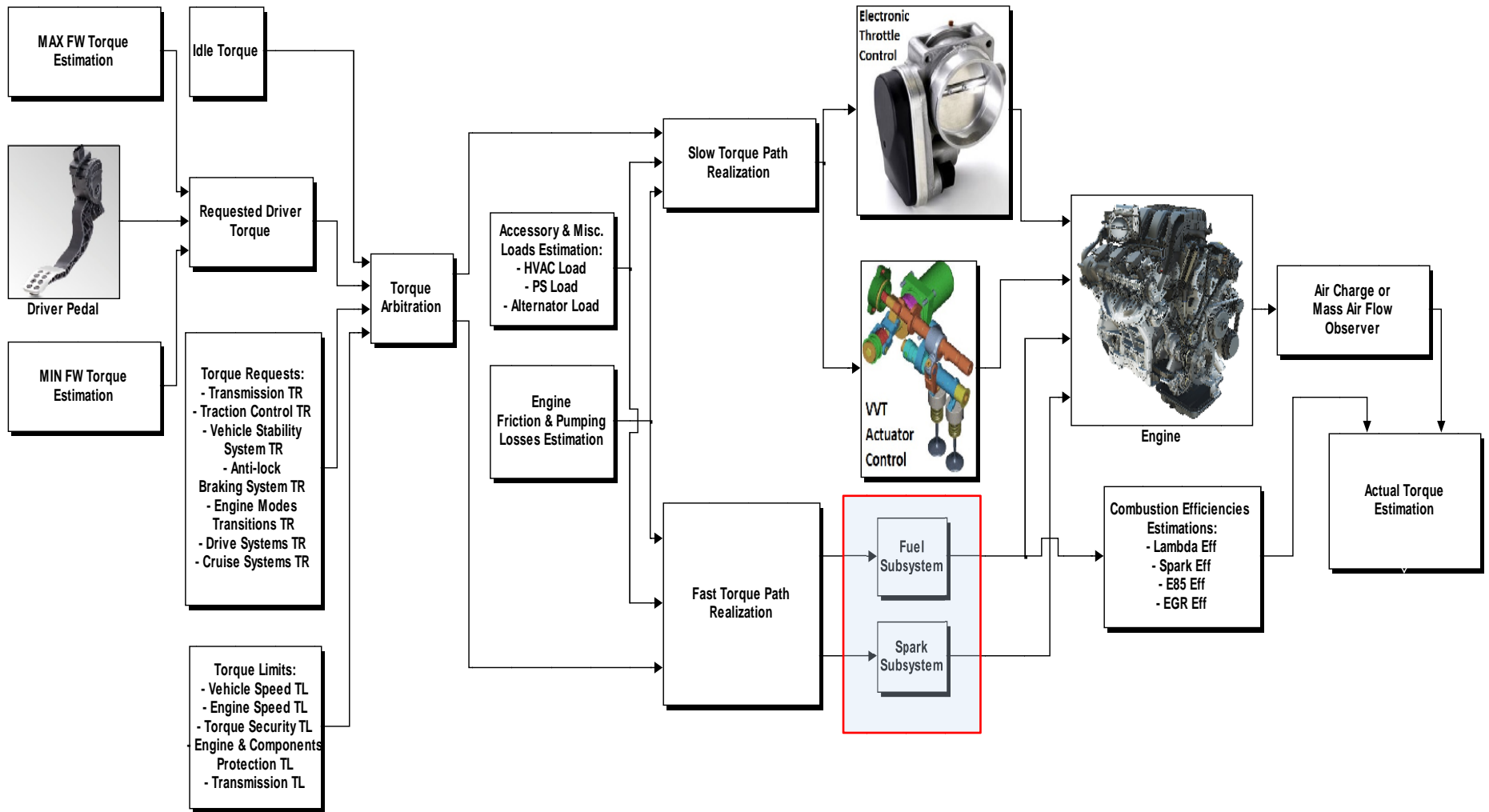


Figure 5.1 High level overview of typical torque control subsystem within ECU engine management system

5.2 Driver Torque Demand

Amongst them all, determining the final driver torque demand or request is one of the most critical functions that has to be performed by the engine torque management subsystem. It involves reading filtered inputs from the driver's accelerator pedal sensors and mapping the final reading to requested driver demand. This usually involves some requested torque filtering in order to prevent drive line oscillations related to pedal tip-ins and tip-outs during the vehicle's rolling [70]. This filtering potentially produces delay in torque realization relative to a step request generated by the driver and hence fast and accurate torque delivery is essential in order to avoid any additional unnecessary delays that would negatively impact transient response.

5.3 Torque Arbitration

The engine torque management subsystem has also to process other torque based requests from other subsystems within the engine control unit (ECU) or even from other external modules and arbitrate between all of them to determine the final torque to be delivered by the engine. Internal torque requestors to the ECU include for example cruise and active cruise control torque requests, engine over speed prevention torque request, vehicle over speed prevention torque request, torque-safety torque request, idle speed control torque request and others. External torque requestors include but not limited to: traction control torque request, vehicle stability torque request, transmission torque request, and driveline torque request. Some of these torque requestors set minimum or maximum limits, while others demand exact torque values that need to be controlled to. Often times, priority is assigned to these torque requestors to help aid in determining the winner of the torque arbitration should two or more torque requests

impose conflicting demands. All of these torque requests require high levels of torque accuracy as well as fast torque response.

5.4 Torque Realization

Another vital function that has to be performed by the engine torque management subsystem is the torque realization. This means that the various engine's actuators have to be utilized (typically in a coordinated fashion) in order to deliver the final requested torque. Typically, the final torque to be requested and then delivered by the engine can be delivered either via a slow torque path request and/or fast torque path request. The slow torque path request is related to air charge management via the throttle control and/or intake valves control. The fast torque path request is related to spark advance control and/or FSO control.

The torque requestors decide via which method their torque shall be honored and make the request based on that. Both the fast and slow requests are each arbitrated separately. Thus, the slow path arbitration provides a slow path torque winner and, likewise, the fast path arbitration provides a fast path torque winner [71].

Slow torque request can be used to increase or decrease the amount of delivered torque. It is referred to as slow path because there is an inherent delay associated with this path related to intake manifold filling and emptying dynamics (breathing process of the engine).

In the fast path FSO control is hard FSO which means that the fuel is turned off completely in one instance for a given engine's cylinder and the same process is applied on the rest of the cylinders sequentially in a given pattern related to firing order at a given rate. The fast path torque request is referred to as fast because torque can

be delivered via spark adjustment and/or fuel injector activation almost instantaneously (some delay in the order of fraction of engine cycle can be expected related to programming of the drivers, combustion delay and engine's inertia effects). The fast path torque request is typically used to reduce torque during torque intervention from the various requestors. However, after utilizing it for torque reduction, fast path can be used to recover torque – that is bring it only up to the target level that is potentially achievable via the slow path. This torque level is often referred to as potential or feasible torque that is directly related to the amount of air charge trapped already in the combustion chamber and is ready to undergo the combustion process. Hence this potential or feasible torque can be approximated as a delayed or filtered version of the slow torque request slow.

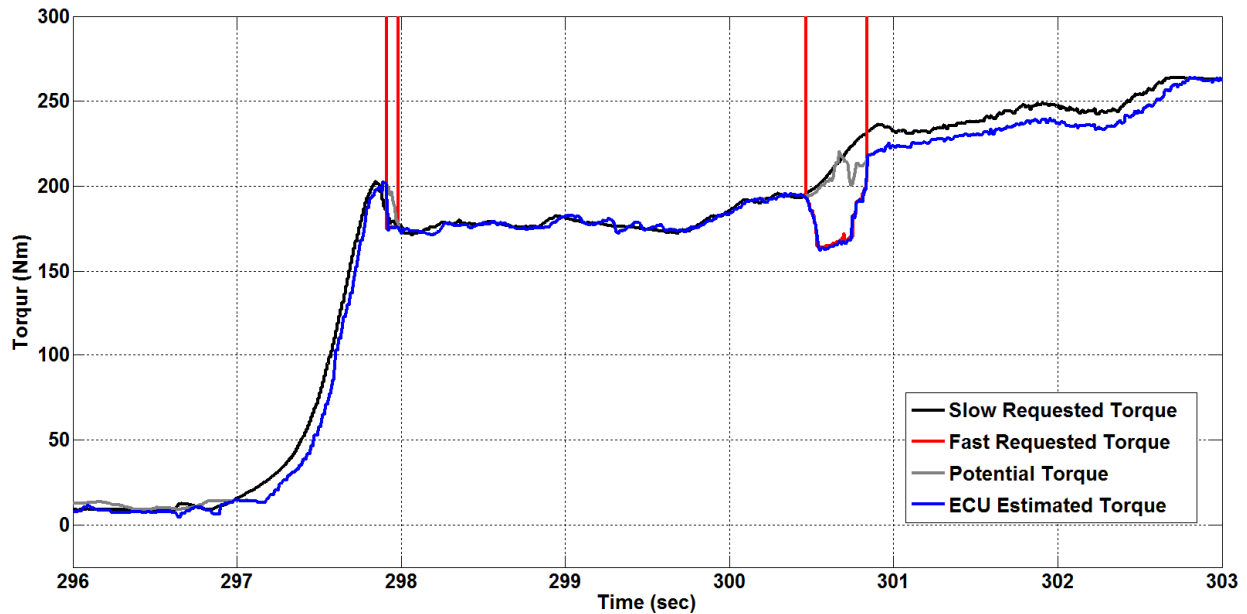


Figure 5.2 Typical torque signals for open loop torque control

As can be seen in Figure 5.2, the potential torque and hence the ECU estimated torques are close to the slow requested torque when there is not fast torque intervention (blue and grey signals are identical). Once fast torque intervention is requested (two

times in this plot for assisting transmission in up shifting), the ECU estimated torque will deviate away from the potential torque to achieve the requested fast torque.

Once the final slow torque request is determined from the arbitration, a desired engine air charge is then calculated based on lookup table that maps the relationship between the needed air charge that is required to generate the desired slow torque request based on quasi-steady state generated data. This desired air charge is then converted into a desired mass air flow to be achieved by controlling the electronic throttle position to achieve that original desired air charge based on models of the throttle that are typically built around compressible flow through restriction or orifice one way or the other. Next chapter elaborates more on this area. A feedback closed loop controller is often employed that utilizes the estimated air charge acquired from models that uses either MAF sensor or MAP sensor to close the loop on the error between estimated air charge and desired air charge. The desired throttle position itself is also controlled via closed loop feedback on the actual throttle position. Same closed loop concept is applied to the VVT positioning control. Figure 5.6 illustrates the available feedback loops related to the slow torque path realization.

Once the final fast torque request is determined from the arbitration, it gets converted into torque efficiency through a process that involves dividing that fast torque request by the potential torque to generate a torque percentage or torque efficiency. This efficiency is then looked up two times via two tables in a parallel process. The first table describes the relationship between torque efficiency to needed delta spark from MBT. The second table describes the relationship between torque efficiency to needed number of shut off cylinders. Between the two outputs of the two tables, a final

combination between spark adjustment from potential spark and FSO applied to certain cylinders is utilized to deliver the fast torque request. The aforementioned calibration table describing relationship between torque efficiency and the delta spark from MBT spark is highly nonlinear as can be seen from the graph depicted in Figure 5.2 below.

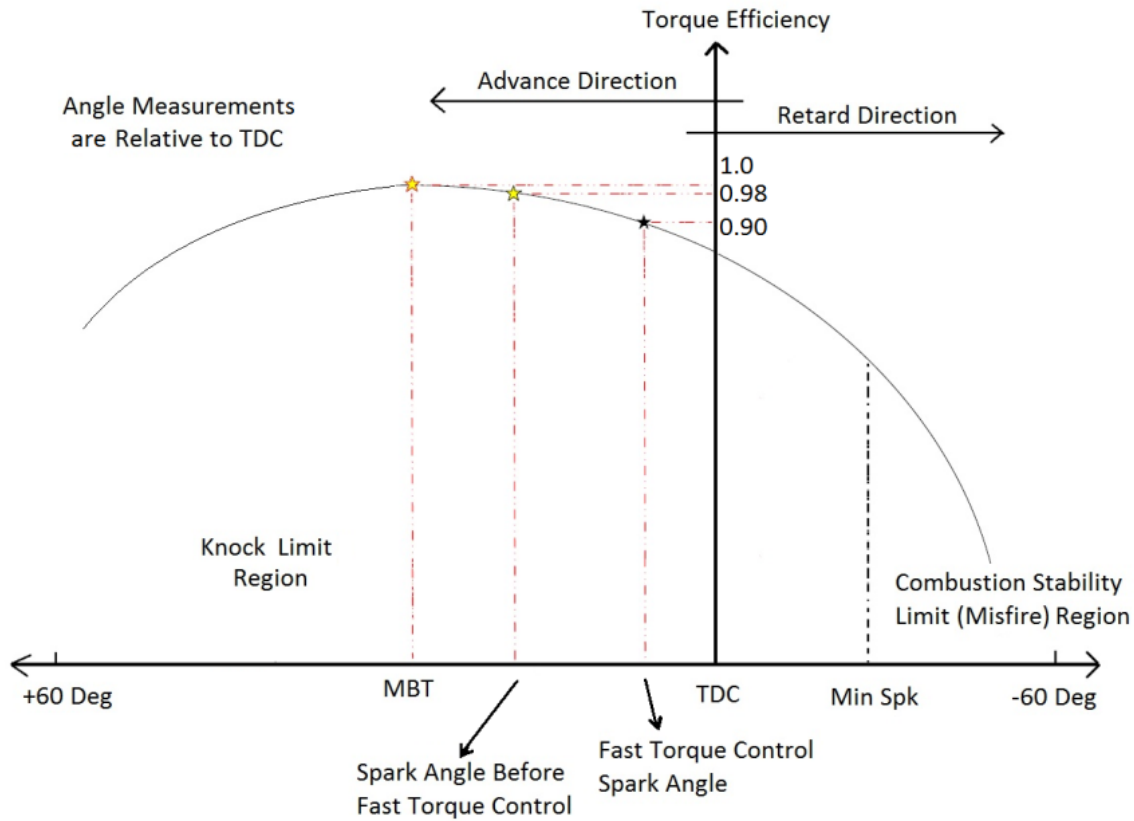


Figure 5.3 Averaged torque efficiency as a function of spark advance

Because of that nonlinearity and to a certain degree since the looked up delta spark for torque control away from potential spark (spark before fast torque control/intervention) is applied and treated the same for all operating points, not taking into account the effects of variable burn rates on spark efficiency at different operating points as it is complicated to model, these factors collectively contribute to the inaccuracies in final delivered torque and its reporting or estimation. This discussion is elaborated upon further in a subsequent section.

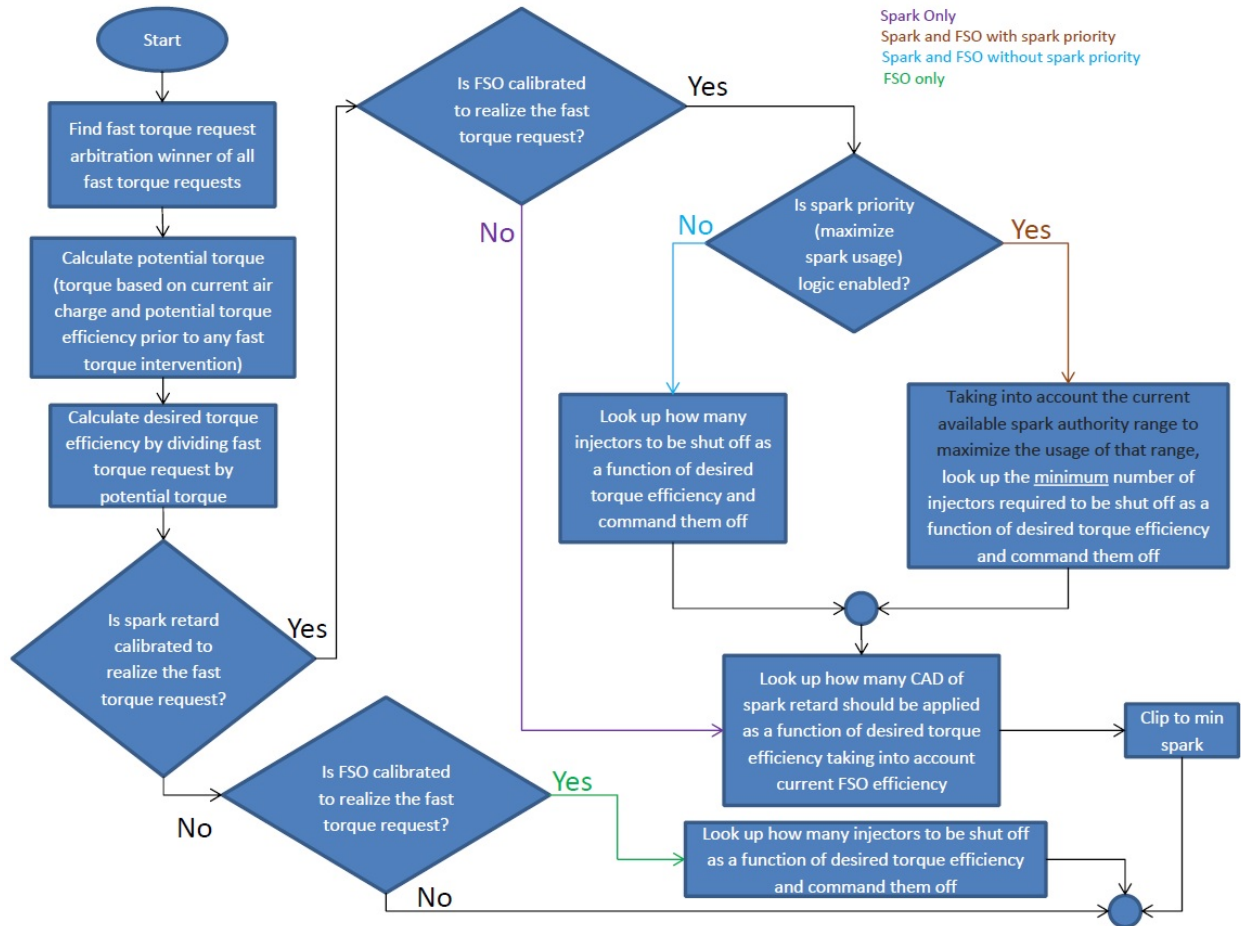


Figure 5.4 Summary of fast path torque realization between spark advance and FSO

Fast path torque realization is typically performed in an open loop process for the determination of both the required spark advance and FSO as currently there is no method to reduce these inaccuracies.

5.5 Estimations of Engine Losses

The interface between the engine and the various other components (transmission, transfer case etc.) is through the engine brake torque which is the final output of the engine. Hence, all torque requests are specified in the brake torque domain. From the indicated torque to the brake torque there are several losses that need to be considered. In addition, since torque realization acts on indicated torque, these losses

have to be estimated. The cylinder produces positive torque only during the power /expansion stroke. During the other three strokes, pumping losses occur. Engine friction is another loss which is complicated and not easy to estimate or measure [72]. Current methods use engine speed and engine temperature (effect of oil viscosity) to infer the frictional losses. Engine friction includes bearings and valve-train frictions. Engine friction is modeled as a mean value model since instantaneous model is very hard to measure or even model. There are also of course losses associated with driving all the accessories and auxiliaries such as the power assisted steering pump, alternator, heating, ventilation and air conditioning system (HVAC) etc. Those are event based losses and hence are treated separately from other accessories that are active all the time such as coolant pump, oil pump etc. that are lumped with the friction estimation since they are also function of engine speed and adding “friction” on the engine all the time. During idle speed control, since there is explicit closed loop control on engine speed, the I-term of the actuating torque used to control to the target idle speed is used as an adaption term to learn these engine losses. Hence, this adaption routine is currently only performed during engine idle speed control.

5.6 Estimations of Engine Torque

The torque subsystem has also to estimate engine torque. It performs this by executing to a certain extent the reverse calculations that it executed for scheduling torque with few exceptions. This starts by reading an estimation of trapped air flow in the cylinder which is derived from actual measured throttle positions taking into account manifold dynamics (filling and emptying) which involves the estimation of volumetric efficiency. This mass air flow is then converted to air charge which is then looked up

and converted to a base torque that gets adjusted based on spark efficiency (same curve as was shown before) λ efficiency, EGR efficiency, E85 percentage efficiency. These efficiencies are similar in characteristics to the spark one in terms of the nonlinearity that they exhibit. For example a typical λ efficiency curve is shown below:

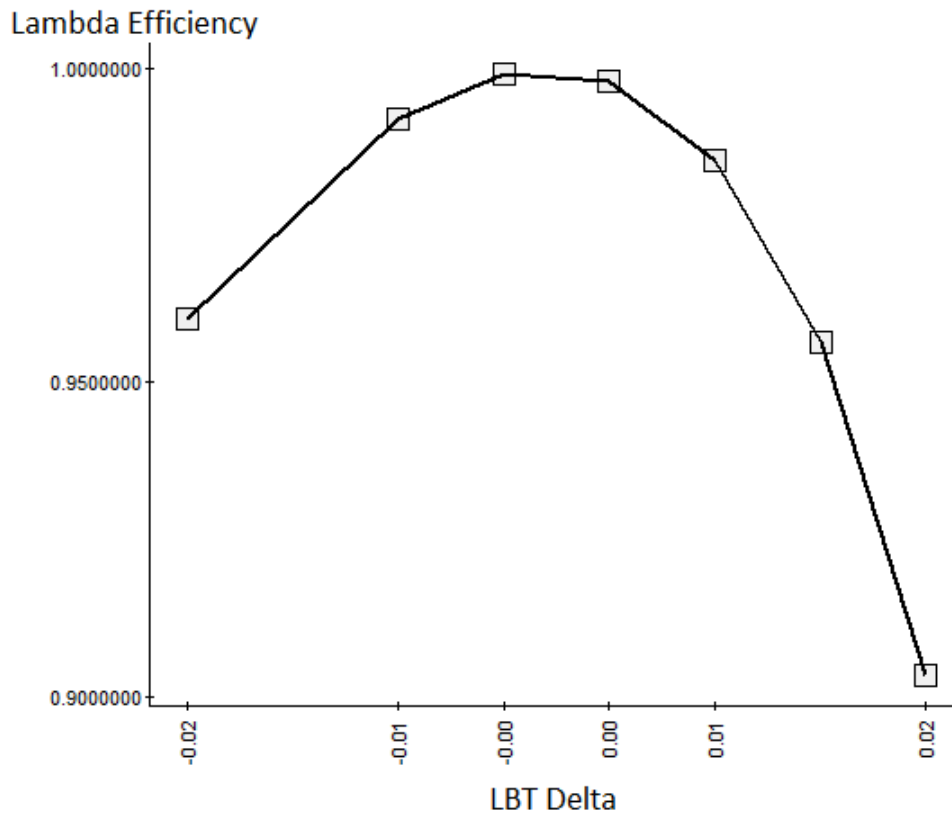


Figure 5.5 Torque efficiency curve as a function of LBT Delta

These efficiencies are typically calibrated by using the super position principle. This means that all are fixed at their best maximum value and only one is varied. However when these efficiencies are applied by multiplying them all together, the resultant combustion efficiency often times does not represent the true combustion efficiency. Hence when these efficiencies are used for adjusting the requested gross indicated torque and for adjusting the estimate of actual engine torques, errors of estimation unsurprisingly occur. A vital function of the engine torque management subsystem

is the torque realization. This implies that various engine's actuators have to be coordinated to deliver the final requested torque. The final requested torque can be delivered either via a slow torque path or fast torque path (or both). The torque requestors are arbitrated separately within these two distinct torque domains.

The slow torque path request is linked to air charge management via the throttle control and/or intake valves control. The fast torque path request is linked to spark advance control and/or fuel shutoff (FSO) control. The various torque requestors decide on which torque path(s) their request be realized with. Slow torque request can be used to increase or decrease the amount of torque delivered by the engine. It is referred to as slow path because there is an inherent significant delay (relative delay when compared to fast path) due to intake manifold filling and emptying dynamics (breathing process of the engine).

The fast path torque request is referred to as fast because torque can be delivered via spark adjustment and/or fuel injector activation/deactivation almost instantaneously (only a delay in the order of fraction of engine cycle can be expected). The fast path torque request is typically used to reduce torque during torque intervention from the various requestors such as transmission shift. During speed change phase, the transmission requests a specific fast engine torque in order to improve shift response. After engine response to the request, the torque can be increased to its original level prior to the transmission torque request that the slow path would have delivered. This torque level is often referred to as potential or feasible torque. This potential or feasible torque can be approximated as a delayed or filtered version of the slow torque request slow. FSO control is another form of fast path; it turns off the fuel completely in an

instance for a given engine's cylinder. The same process is applied to the rest of the cylinders sequentially (if needed based on the requested torque level) in the same order at which firing took place at a given rate. FSO control can also be used to modify the fraction of injected fuel amount in each cylinder to achieve certain torque levels based on torque efficiency. This approach is not common due to emissions side effects.

All of the slow torque requests from various requestors undergo comparison according to their magnitudes and priorities to determine the final slow torque request. Based on the final slow torque request, a desired engine air charge is then calculated based on the desired slow torque request through quasi-steady state generated engine mapping data. This desired air charge is then converted into a desired mass air flow to be achieved by controlling the electronic throttle position. The throttle model is based on compressible flow equation through a restriction or an orifice [55]. Essentially, these processes are the inverse models when compared to the models discussed previously in the engine plant model section. A feedback controller is often employed [4] that utilizes the estimated air charge, acquired from models that use sensors such as MAF or MAP to close the loop on the error between the estimated air charge and desired air charge. The desired throttle position itself is also controlled via feedback on the actual throttle position. The same closed-loop concept is applied to the VVT actuator positioning control [73]. Figure 5.6 illustrates the existing feedback loops (in black signal color) related to the slow torque path realization.

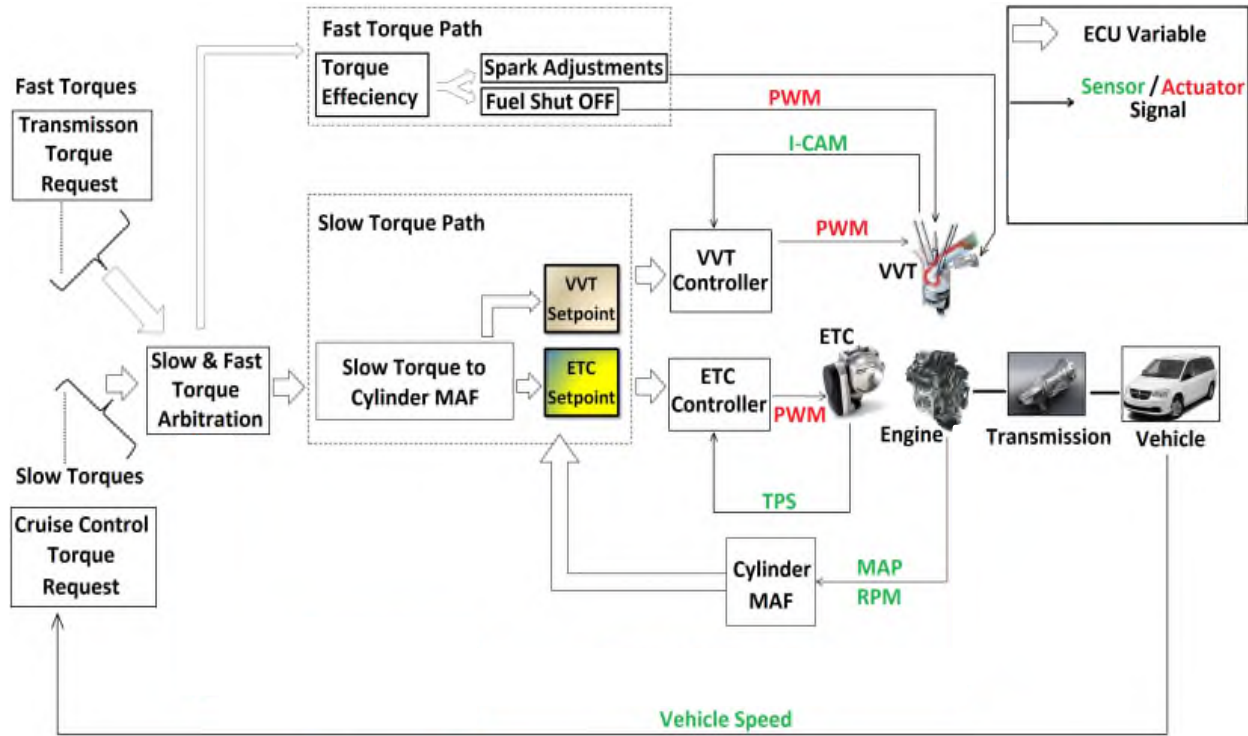


Figure 5.6 Illustration of existing control loops related to torque management

As shown in Figure 5.6, there is no feedback loop control applied on torque explicitly. The existing direct feedback loops involve only air and fuel feedback controls. For the air, throttle and/or variable valve timing is/are used to close the loop on desired engine mass air flow. On the other hand, fuel metering depends on the amount of air charge inducted by the engine. Closed-loop fuel control is employed using feedback from HEGO/UEGO sensors to maintain the air fuel ratio target, typically near the stoichiometric air fuel ratio for non-lean burn gasoline engines.

Once the final fast torque request is determined from fast torque arbitration, it is converted into desired torque efficiency. Using the desired torque efficiency, the spark and FSO are adjusted based on calibration tables without feedback to deliver the fast desired torque. There are several other schemes that can generate the requested spark

advance and FSO separately. These schemes are, however, beyond the scope of this paper. The aforementioned calibration table describing the relationship between the torque efficiency and delta spark away from the MBT spark is highly nonlinear and difficult to acquire as can be seen from the graph depicted in Figure 5.3.

CHAPTER 6: ALGORITHMS & CASCADE CONTROL STRUCTURE

6.1 Brake Torque Sensor Signal Processing

The SAW torque sensor measures the instantaneous engine brake torque pulsations [18]. As a result of that, and since all engine torque requestors specify their torque demands as mean torque signal, the sensor output has to be conditioned to create an average signal.

In addition, the sensor output signal is processed to compensate for the zero-torque-level offset that is shown in Figure 2.4 and Figure 2.5. The offset compensation is needed since the sensor output is not zero at zero-torque-level. The value is found to be around 12 N.m.

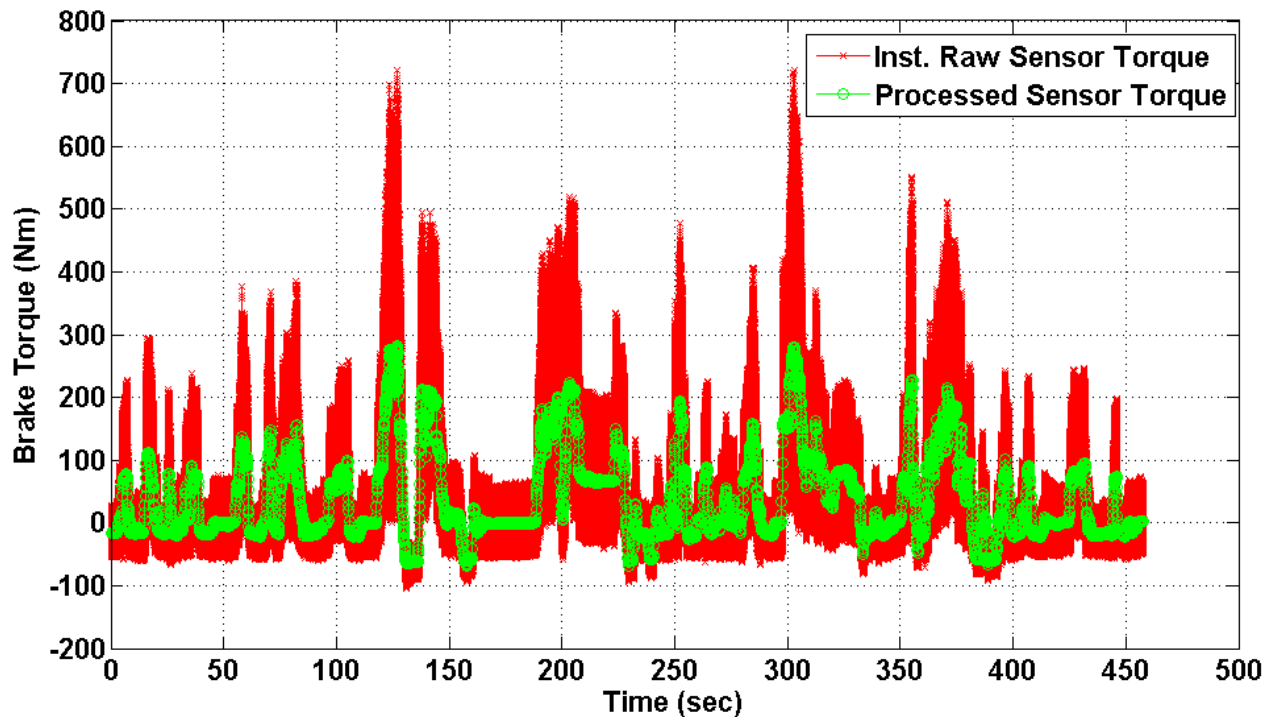


Figure 6.1 Raw SAW torque sensor reading and processed one

Figure 6.1 shows a typical raw SAW torque sensor output waveform and its average resolved over one engine cycle with zero-torque-level offset compensation. Data are collected in a city driving condition. Figure 6.2 shows a 3-engine cycle during neutral engine idling. As shown, the processed torque sensor signal is close to 0 Nm as expected. Every engine cycle, there are 6 torque peaks associated with six firing events. The processing algorithm establishes a window based on engine position (0-720 CAD) and sums up all torque sensor readings and then divides by the total number of acquired readings to come up with engine cycle resolved torque reading at the end of the cycle as the arrows show.

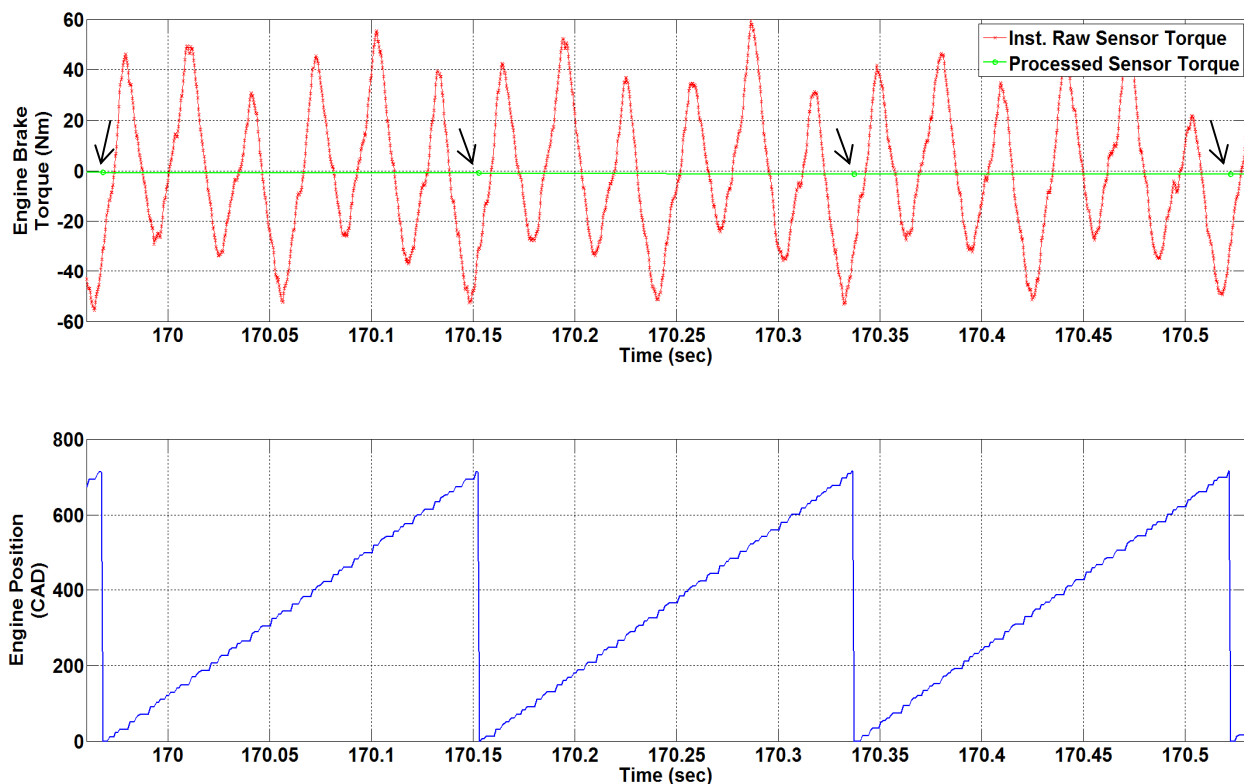


Figure 6.2 Three engine cycles zoomed-in view of SAW torque sensor reading and processed one during neutral engine idling

Figure 6.3 shows the processed sensor torque as well as the ECU estimated torque superimposed with the final requested torque. It shows the difference between the sensor reading and the estimated engine torque especially in the negative regime and near zero-torque-levels when engine enters fuel shut-off mode during deceleration.

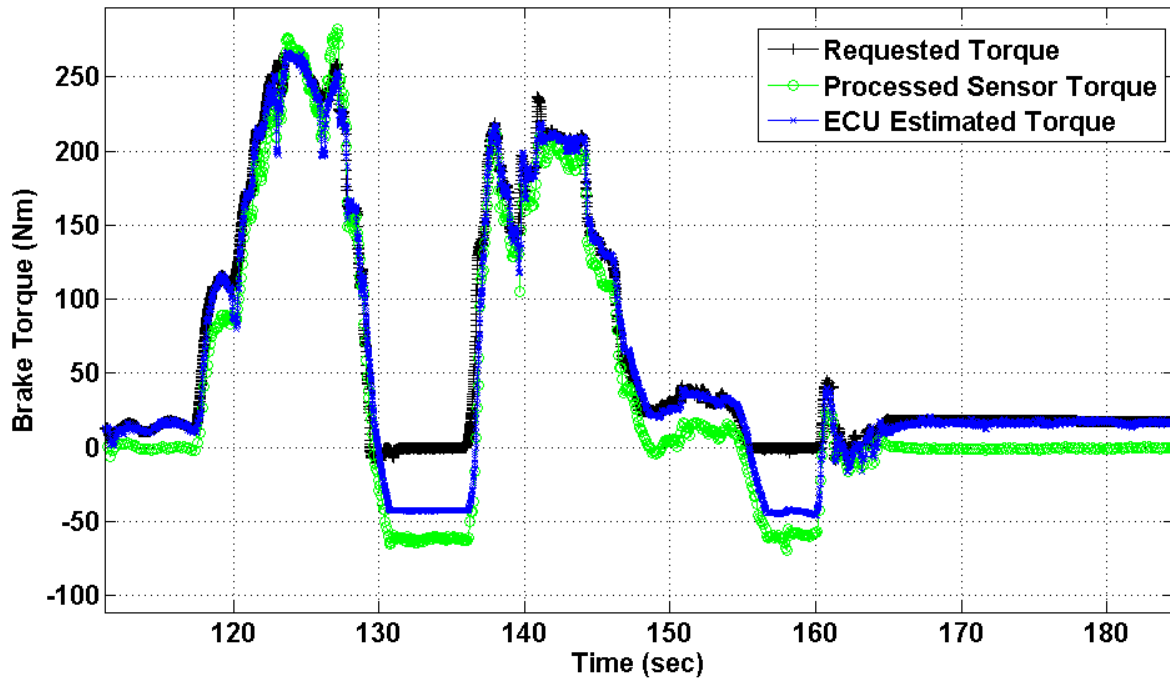


Figure 6.3 Requested engine brake torque, ECU's estimated one as well as the signal as measured by SAW torque sensor

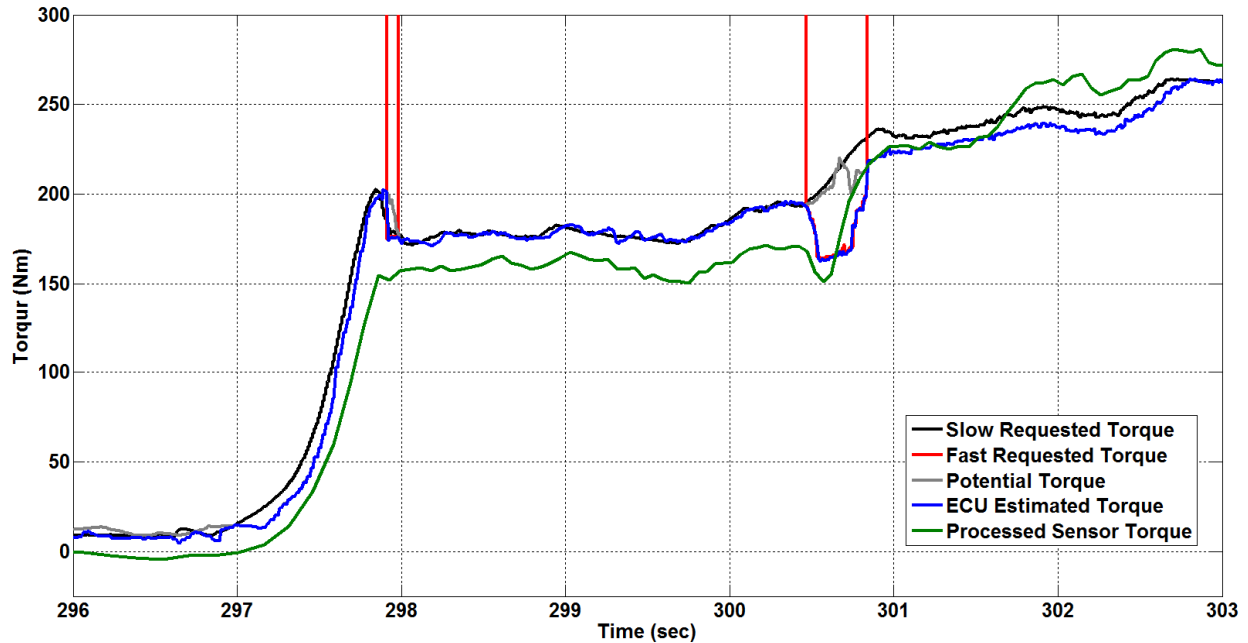


Figure 6.4 Processed brake torque sensor reading (green) compared to ECU estimated brake torque and commanded fast and slow torques

As can be seen in Figure 6.4, the actual brake torque as measured by the torque sensor indicates that the requested torques are not tracked accurately. During the second transmission torque intervention, the actual engine torque raises before the intervention is over. This is because spark advanced is not controlled using closed loop controller. The actual engine torque does undershoot the requested slow torque before $t = 300.5$ sec and does overshoot the requested slow torque by 25Nm after $t = 301.5$ sec. This is because slow torque request is not controlled using closed loop controller.

6.2 In-Cylinder Pressure Sensors Signal Processing

Processing of in-cylinder pressure sensors and its various aspects and details is well understood and covered significantly and thoroughly in public research such as those that can be found in [74] [75]. To overcome cycle-to-cycle variations in the in-cylinder pressure measurements and prevent instability issues of the closed loop

scheme, a low-pass filtering method is an appropriate technique to reduce the IMEP fluctuation around its mean value. The filter is implemented in the measurement hardware as described in the next section. In [76] the authors show a method to calculate IMEP for each cylinder and the engine overall IMEP. This method is adapted and used in this work. Figure 6.5 and Figure 6.6 show raw in-cylinder pressure data and their processed IMEPs using the method that is based on equations (2.1) and (2.2).

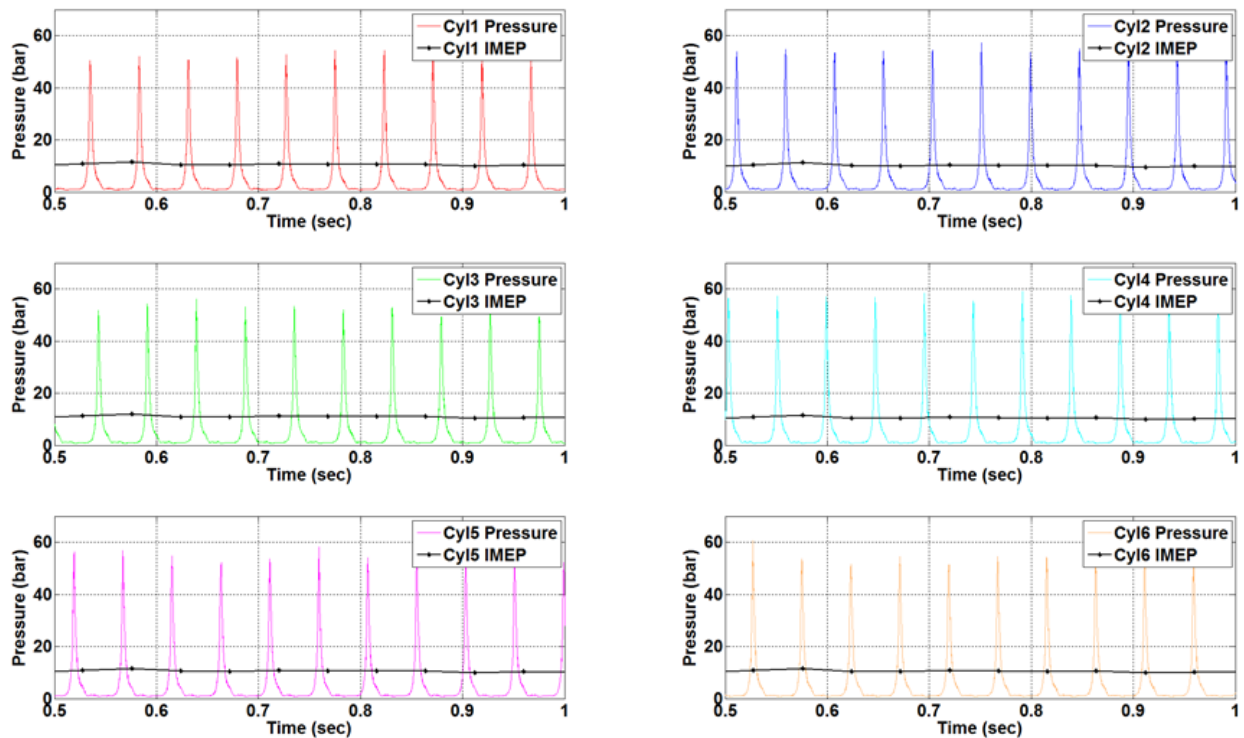


Figure 6.5 Instantaneous pressure and derived net IMEP for each cylinder at 2500RPM and max torque

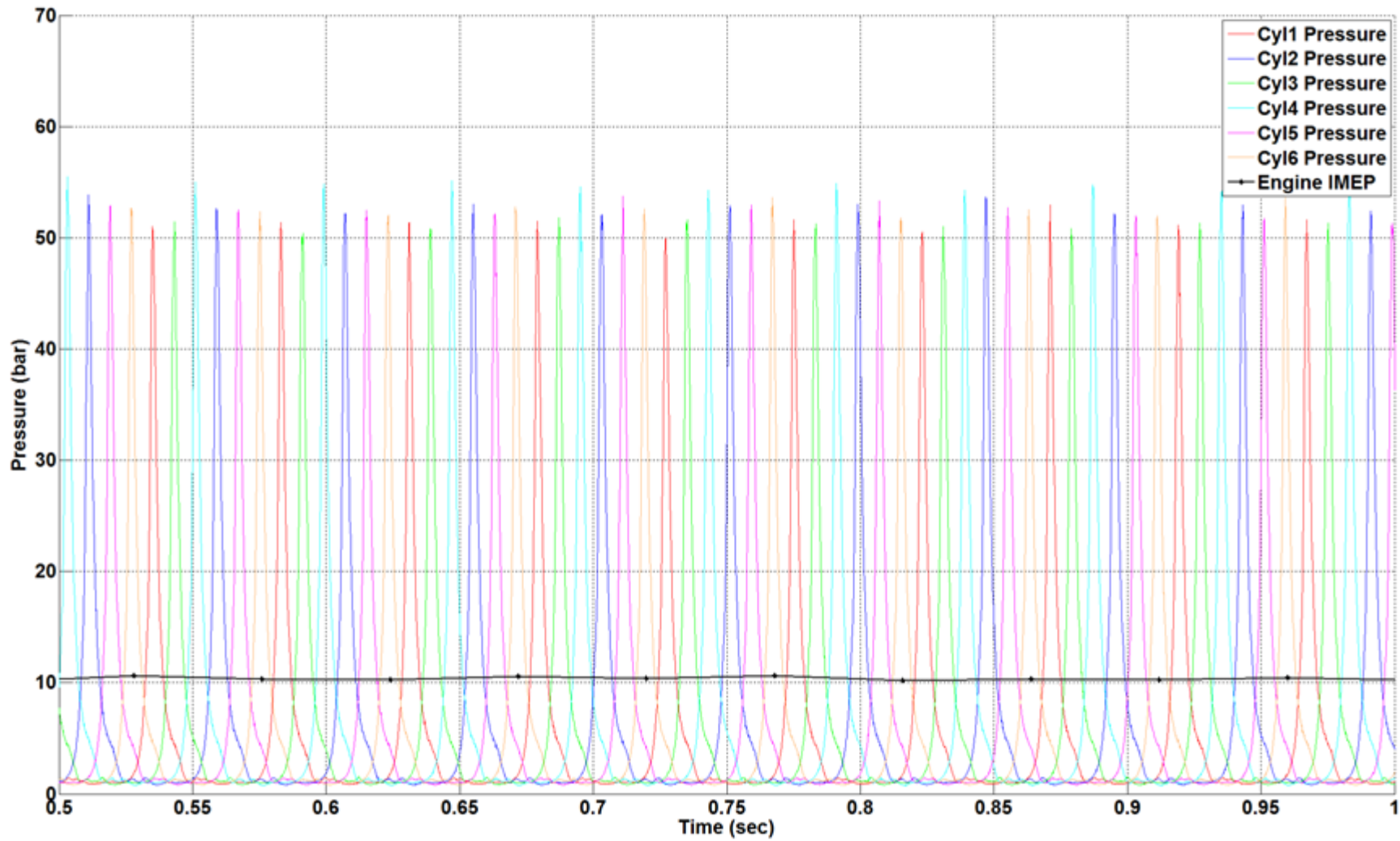


Figure 6.6 Superimposed instantaneous pressures for each cylinder and derived engine net IMEP at 2500RPM & max torque

6.3 Design of Feedback Control Systems

6.3.1 Control System Design Overview

Two controllers are introduced in this chapter for each of the three investigated control strategy. One controller for the slow torque control path (air path) and the other controller is for the fast torque control path (spark advance and fuel shut off) via adjustment of desired torque efficiency. The controllers used for this work are discrete Proportional-Integral-Derivative (PID) controllers [77] with variable gains as a function of the torque error between sensed and requested engine torques (indicated and brake). The investigated control strategies are (1) brake torque feedback (2) gross indicated torque feedback (3) brake and gross indicated torques feedbacks combined together.

Controller synthesis and integration into existing open loop scheme is done such that for slow torque request, the existing feed-forward term is adjusted by adding correction term from the new proposed torque feedback. For torque requestors that utilize the fast torque path such as transmission torque requests, the desired torque efficiency is adjusted (which will result in changes to spark advance and/or fuel shut off). Similarly, this is accomplished by adding a correction term to the existing feed-forward based on torque feedback. From this point of view, the system is SISO system for both slow and fast controllers. Meaning, slow torque request results in desired air charge request and fast torque request results in desired torque efficiency request as depicted in Figure 6.7.

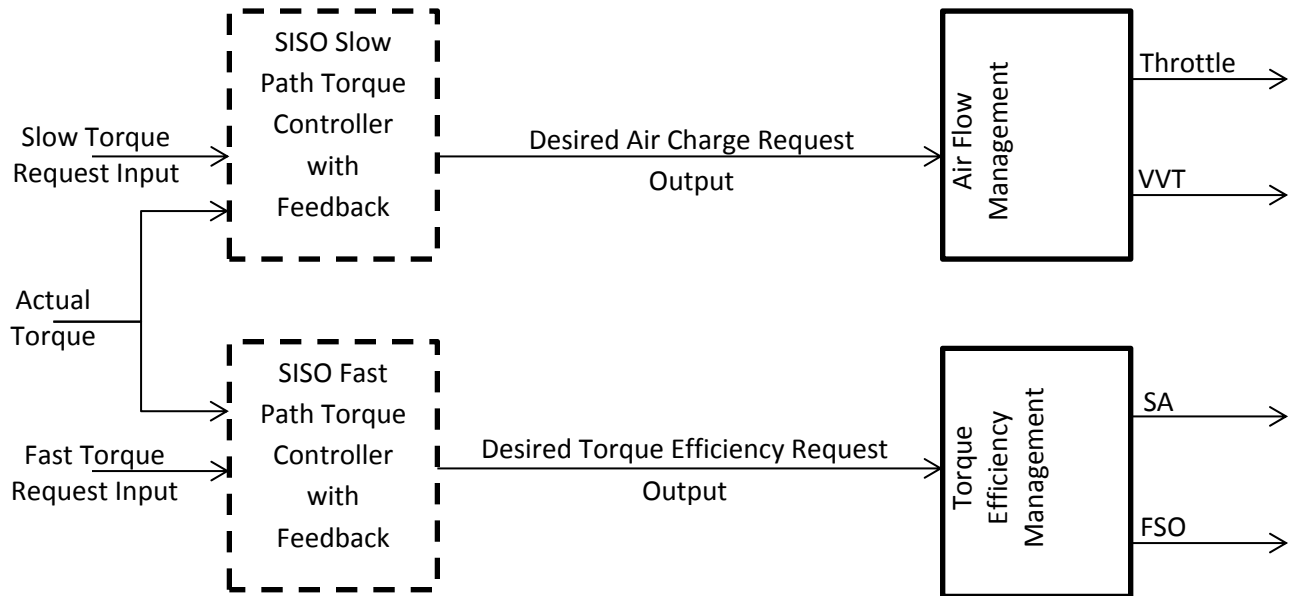


Figure 6.7 Illustration of SISO slow and fast paths feedback controllers

During fast torque path closed-loop control activation upon receiving a fast torque request, the slow torque path control loop is prevented from updating its feedback term in order to allow the fast torque path to handle the feedback torque control without having the two paths interfering. This means that the two paths operate one at a time based on the type of the torque request (slow or fast) or when control authority is reached by one path during which the other path can be utilized to complement the performance of the saturated one. For example, if there is a slow torque reduction request and the throttle reaches its minimum limit, then the fast path can be enabled to control to the desired torque. This way tracking control accuracy is maximized. This approach of coordinating the two paths is summarized in Figure 6.8

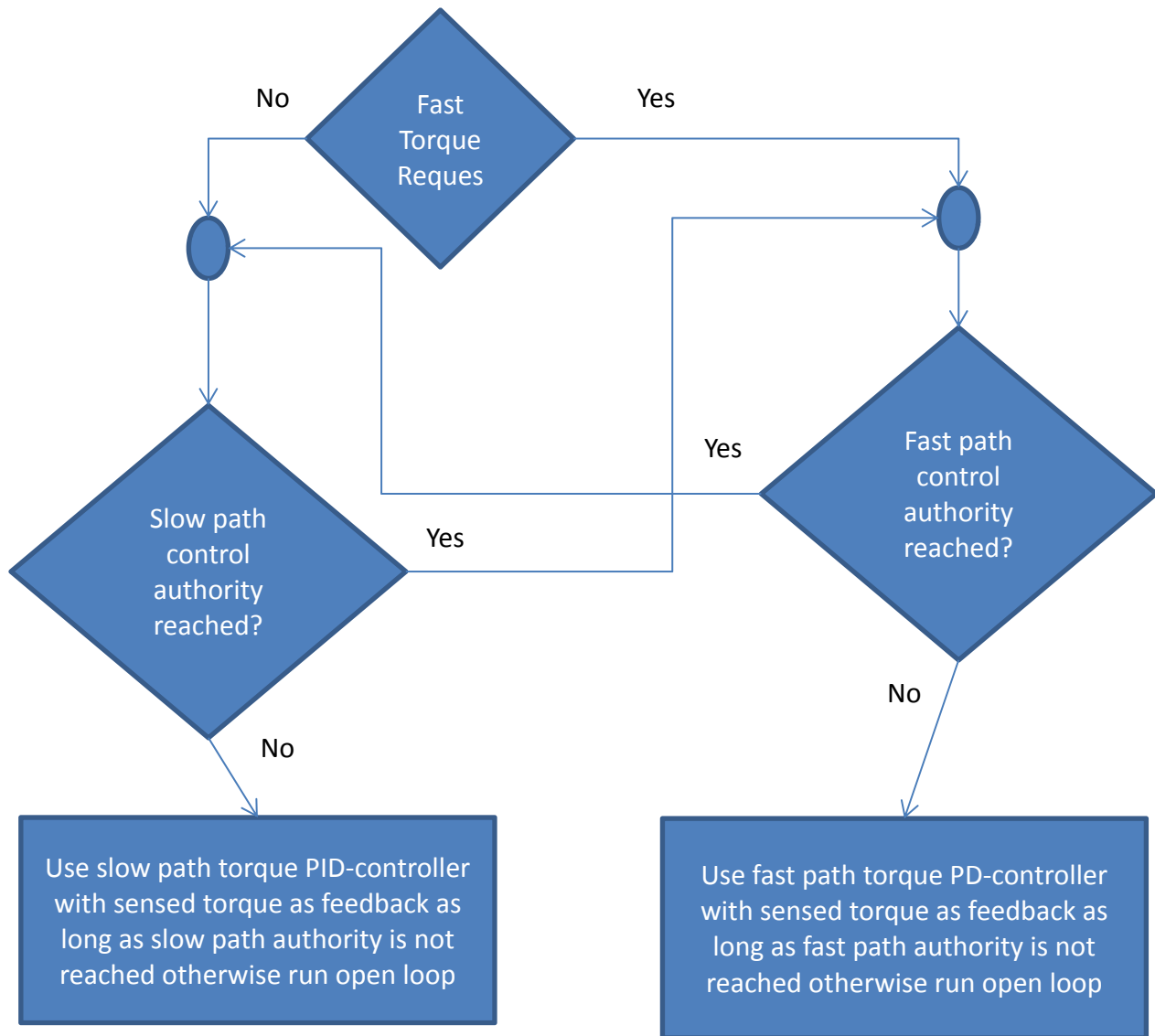


Figure 6.8 Fast and slow paths coordination algorithm overview

Alternatively, during fast torque requests, the slow path torque feedback does not have to freeze and can still be left activated by closing the loop on the potential torque instead of the actual torque. This way the actual torque can be used as a feedback on the fast path and the potential torque can be used as feedback on the slow path. Potential torque (estimated) should equal actual torque when there is no fast torque request intervention. This means actual torque can adapt potential torque such that potential torque tracks the actual torque when there is no fast torque request. When a

fast torque request is made, potential torque stops being adapted and gets used in lieu of the actual torque within the slow torque path and the actual torque gets used as a feedback within the fast torque control path. Any time a control actuator reaches its limits, proper integral anti-windup strategy is invoked. It is found that resetting the integral gain each time a new torque requestor changes, allows for faster torque tracking.

Adaptions are used as indicated by the arrows in Figure 6.10. At any given stable operating point and based on a sustained and stabilized integral term (I-term), a portion of the I-term is off loaded or subtracted from the I-term into an adaptive Keep Alive Memory (KAM) to be used every time this operating point is revisited again as part of the feedforward path. The logic used is similar to that described in [78]. This adaptive term is binned in either accessory load torque or friction torque depending on whether or not an accessory load is activated in order to enhance torque losses estimation model which means achieving better torque tracking accuracy. This is a clear advantage of closing the loop on torque as without this scheme, this can only be done during idle control because engine speed is being explicitly controlled using feedback from engine speed sensor.

As stated before, the current engine torque control subsystem performs torque control in an open loop / feed-forward method. As a result, errors in the reported torque relative to the requested torque can occur due to calibrations, airflow model inaccuracies, combustion phasing error, errors associated with loads, friction and pumping losses estimations, and others. Adding an explicit torque feedback closed-loop control to the current methodology would result in improved torque accuracy which

can provide drivability improvements and potential fuel economy and emissions improvements as well. The following control methods are introduced:

6.3.2 Closed loop indicated torque control

Using cylinder pressure sensors, the actual indicated mean effective pressure (IMEP) for each cylinder is calculated and from which the actual engine's indicated torque is computed. The gross indicated torque of the engine is then compared to the desired engine's indicated torque and used as an input to a closed-loop controller that minimizes the indicated engine torque error. This method assumes the engine losses are calibrated and estimated correctly and are appropriate at all times which is not the case all the time as explained previously. As a result, while the target IMEP is attained, there may still be some error in the output engine brake torque. This closed-loop has fast response associated with it due to fast responses of pressure sensors. The fast response that is referred to here is in the order of TDC to TDC scale. However, in practice the variations of pressures from cylinder to cylinder and cycle to cycle due to stochastic noise of the sensors and combustion variation might be problematic for such fast feedback control. One possible solution is to average the IMEP readings over few engine cycles. It is possible that the averaging will take away the advantage of fast torque response. Therefore, another alternative is to allow only slow path feedback as opposed to allow both fast and slow paths feedback. In this approach, the measured gross indicated torque will be controlled in order to track the requested slow gross indicated torque. This requires that the pressure sensors shall be processed in order to extract from them only the pressure values over the compression and power strokes only (gross information). This is the first advantage of this approach which is namely

tracking of gross indicated torque. However, the final brake torque is not controlled explicitly with this approach. At the same time, since the entire pressure wave forms can be processed over the entire four strokes including the intake and the exhaust strokes, the net indicated and pumping torques can be measured. Therefore, this information can be utilized to apply adaptations on the ECU estimated pumping losses. This is because if the requested gross indicated torque is known and if the gross indicated torque is controlled, then any error in the gross indicated torque is contributed to errors in estimating the pumping losses. This is the second advantage of this control scheme.

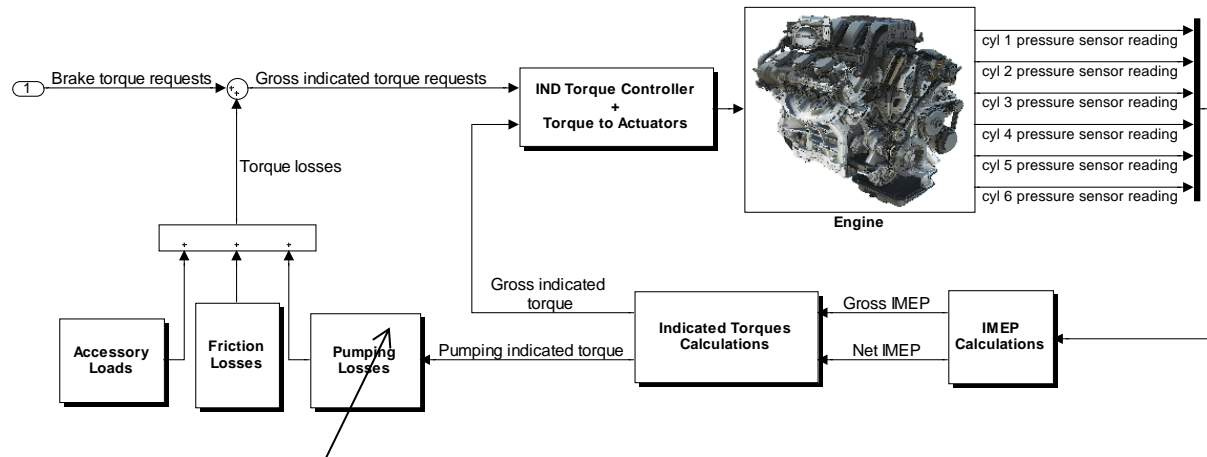


Figure 6.9 Illustration of indicated torque feedback structure with adaptation area

6.3.3 Closed loop brake torque control

Using a brake torque sensing technology, the actual brake torque for the engine is measured. This torque is then compared to the desired brake torque to calculate a torque error term which is used as an input to a closed-loop controller which minimizes that brake torque error. The output of the controller is added to the original existing feedforward brake torque path. This method assumes the engine losses are calibrated correctly and are appropriate which is not the case all the times. As a result, while the target brake torque may be attained, there may still be some error in indicated torque.

This closed loop can be set up to act directly on the requested brake torque as depicted in the next diagram. This control would utilize the throttle or VVT as actuators to fine-tune the delivered torque for better torque accuracy when slow torque request is made. The main advantage of this approach is that the brake torque is controlled which is the final output of the engine that the rest of the systems (transmission, traction, etc.) consider and take into account. Another byproduct of this approach is the ability to perform adaptations on the modeled accessory loads and modeled frictional losses. This can possibly be done because any steady-state repeating error between the requested and actual brake torque could be assumed to be contributed to inaccuracies in these losses models rather than torque-to-air conversion model or the air flow model which have closed loop controls that can adjust and adapt the air flow errors.

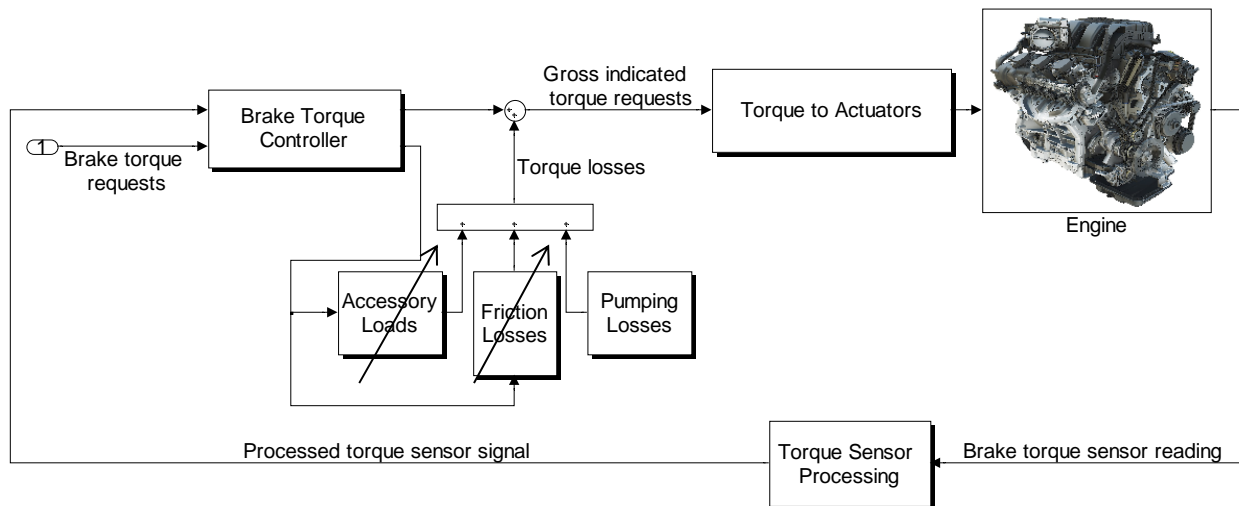


Figure 6.10 Illustration of brake torque feedback structure with adaptation area

6.3.4 Combined closed-loop indicated and brake torque control

Combining the two methods above allows the entire torque generation capability of the engine to be controlled and adapted. In this case the individual cylinder indicated torque controller will ensure the target gross indicated torque is always attained as well

as the ability to adapt the pumping losses. The desired brake torque will be compared to the actual brake torque as sensed by the brake torque sensor and will be used to adapt the engine's losses and accessory load torques as appropriate. The proposed control topology for this approach is depicted in Figure 6.11. Here, an explicit outer control feedback loop is added to close the loop on the brake torque.

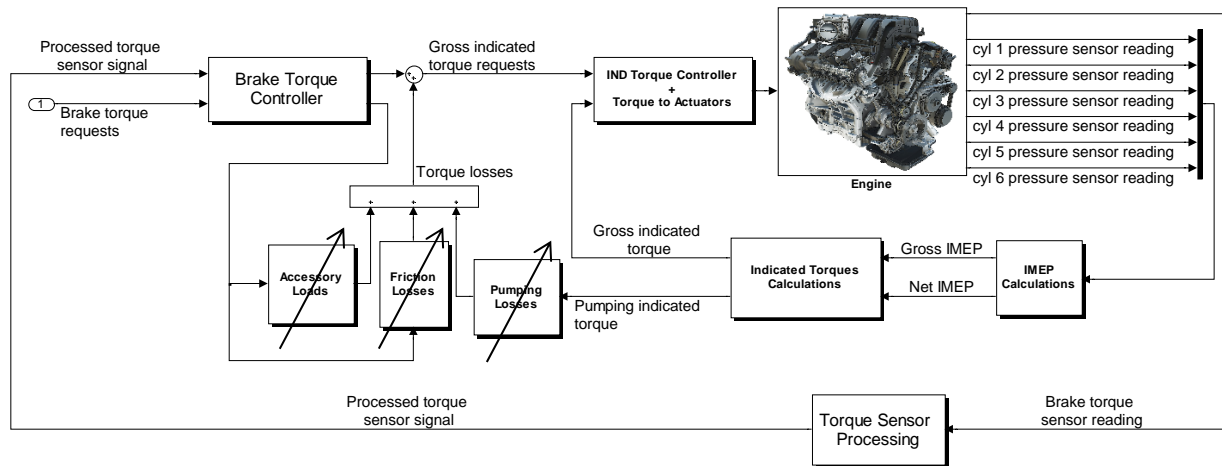


Figure 6.11 Illustration of brake and indicated torque feedback structure with adaptations area

For all these three structures, it is possible that the existing MAF feedback control loop (see Figure 6.12) can be turned off to reduce calibration efforts and simplify design. However, keeping this feedback loop has advantages that will be discussed in the next chapter.

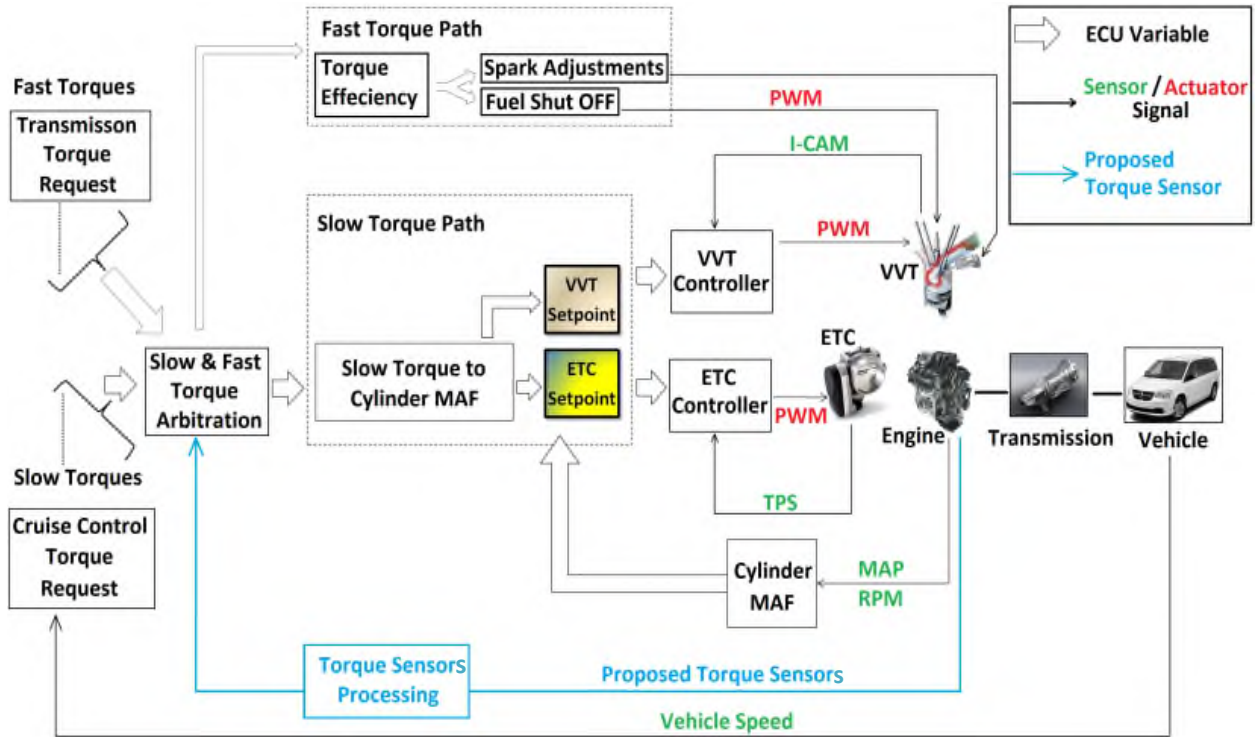


Figure 6.12 Pictorial diagram of torque sensors feedback with existing feedback loops

CHAPTER 7: SIMULATIONS AND RESULTS

7.1 Steady State Data Fitting Results

Figure 7.1 through Figure 7.5 show the results of fitting the steady state data obtained by GT-SUITE simulations.

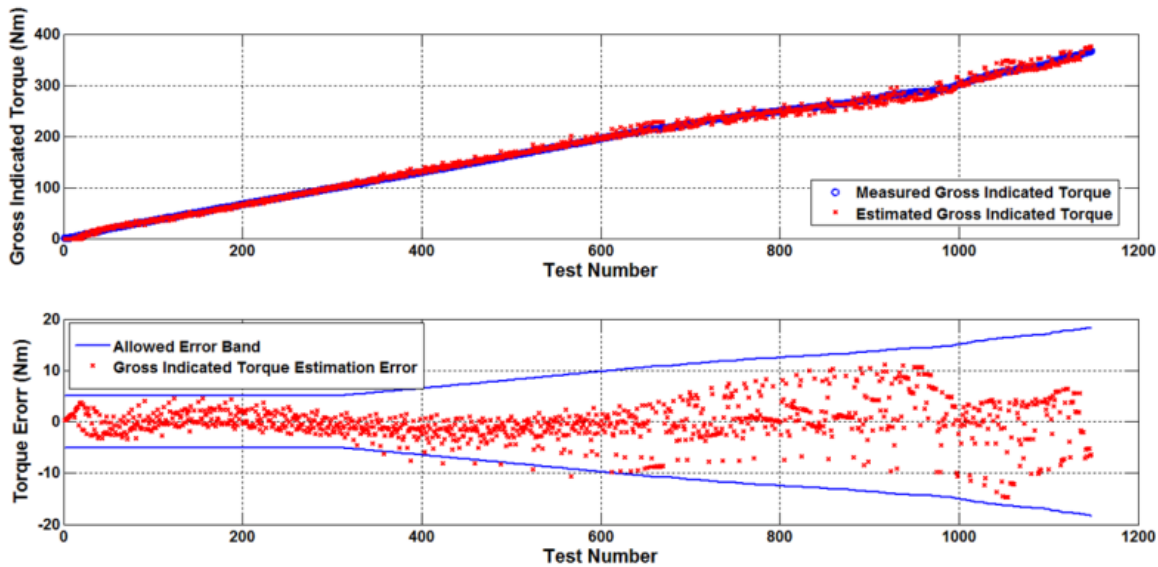


Figure 7.1 Steady state fitting of indicated torque and the error of fitting

The goodness of fit for the gross indicated torque estimation is 0.99 for the adjusted R-squared. Some points could not be kept in the targeted error band. The goodness of fit for the MAF, torque losses, throttle CdA, VVT are all close to 0.98 for the adjusted R-squared. However, spark and LBT torque efficiencies are only 0.85 and 0.65 respectively. This is due to the variation of the combustion efficiency as predicted by GT-Power which makes the case for using torque feedback stronger as ECU estimated spark and LBT efficiencies cannot predict these variations because of mandates to use simplified models due to ECU computational power limitations.

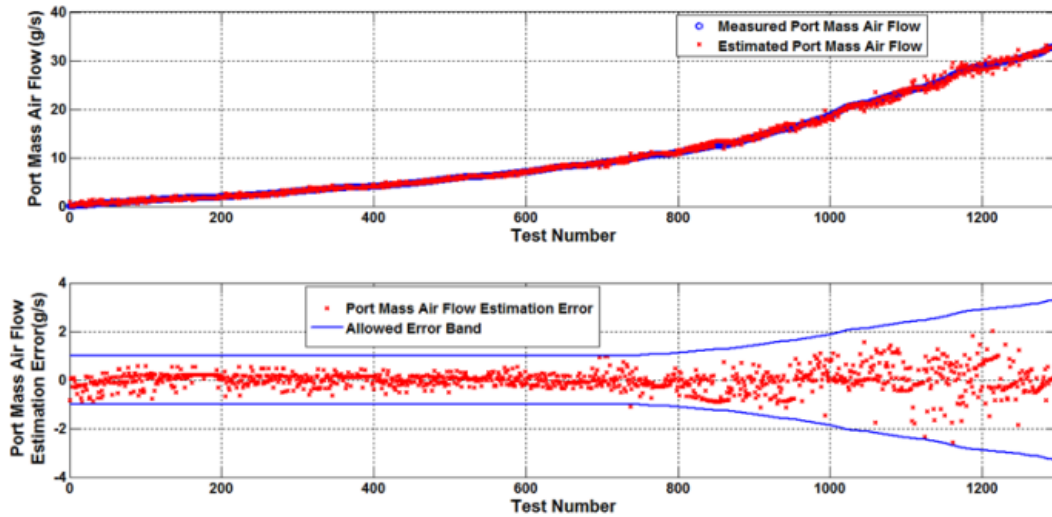


Figure 7.2 Steady state fitting of cylinder MAF and the error of fitting

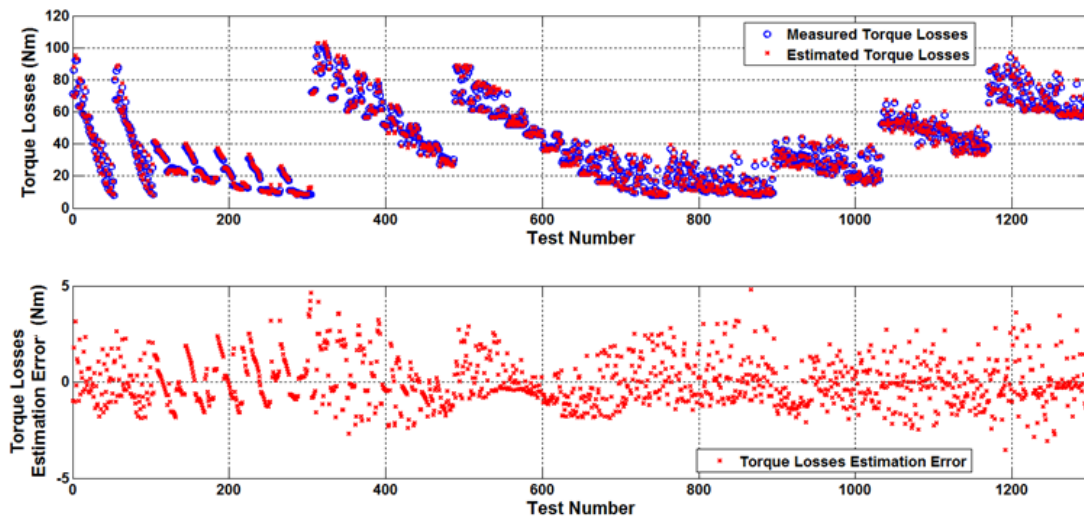


Figure 7.3 Steady state fitting of cylinder Torque Losses and fitting error

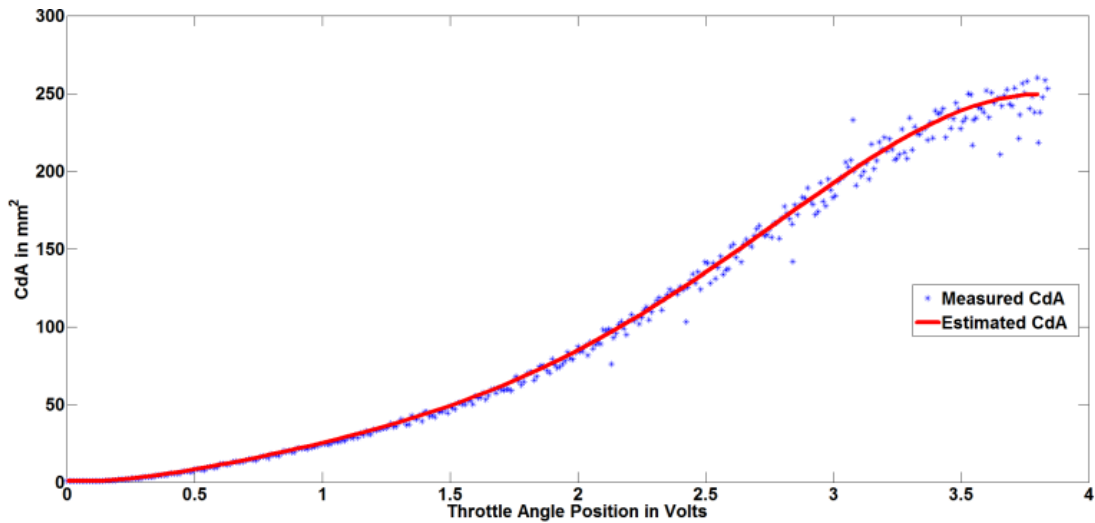


Figure 7.4 CdA data fitting

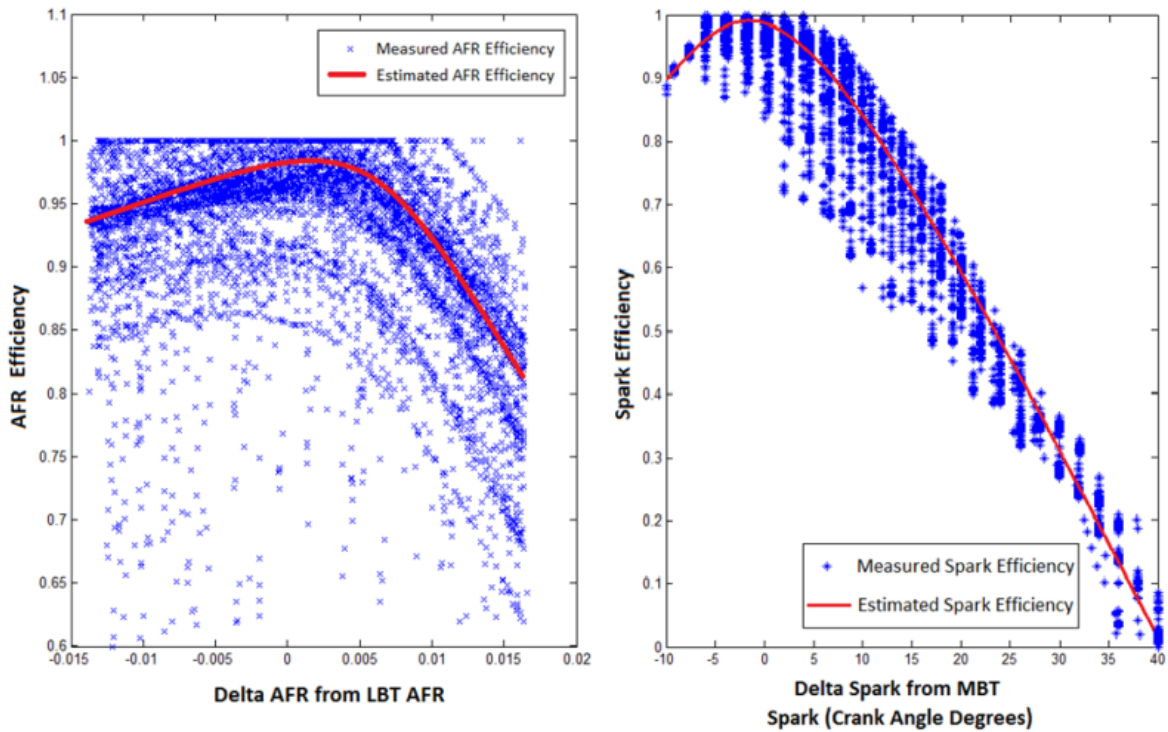


Figure 7.5 Fitting of AFR and spark efficiency data

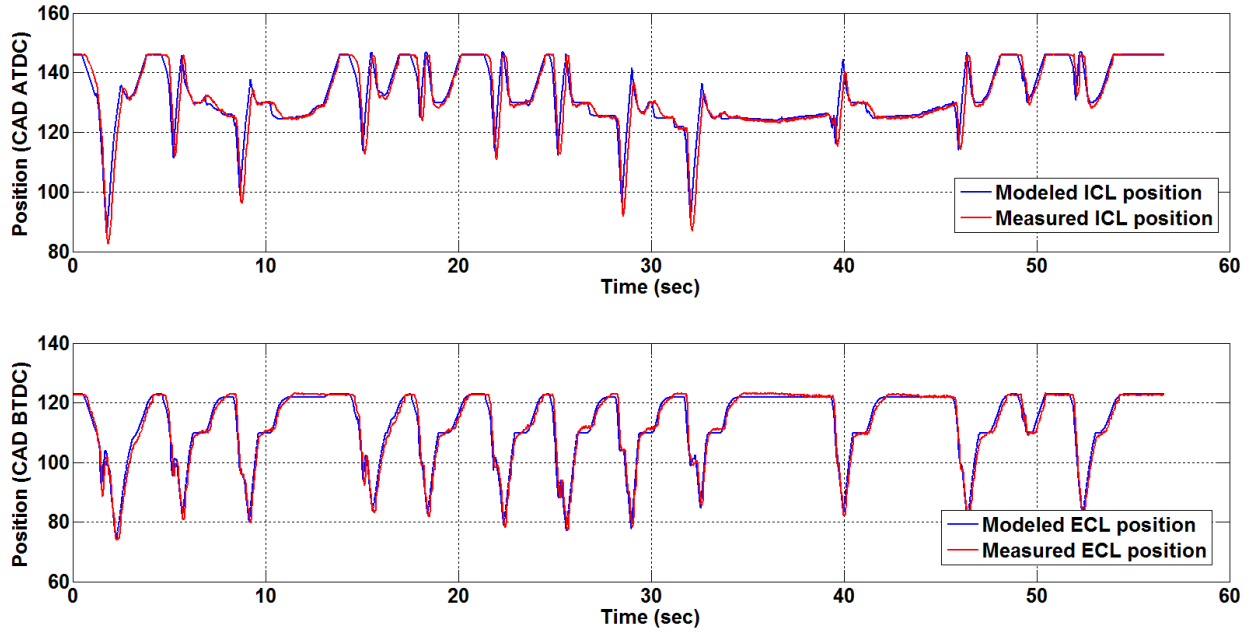


Figure 7.6 Validation of modeled VVT positions against ECU measured ones

The results in Figure 7.5 agrees with those shown in [79] as expected which justifies the structure used in equation (3.17). However, the variations in spark efficiency significantly affect torque modeling accuracy as stated previously.

The steady state measured engine dyno data for both cycle-resolved averaged engine brake torque and inlet mass air flow are used to validate the obtained steady state models given by equation and equation as shown in Figure 7.7 and Figure 7.8.

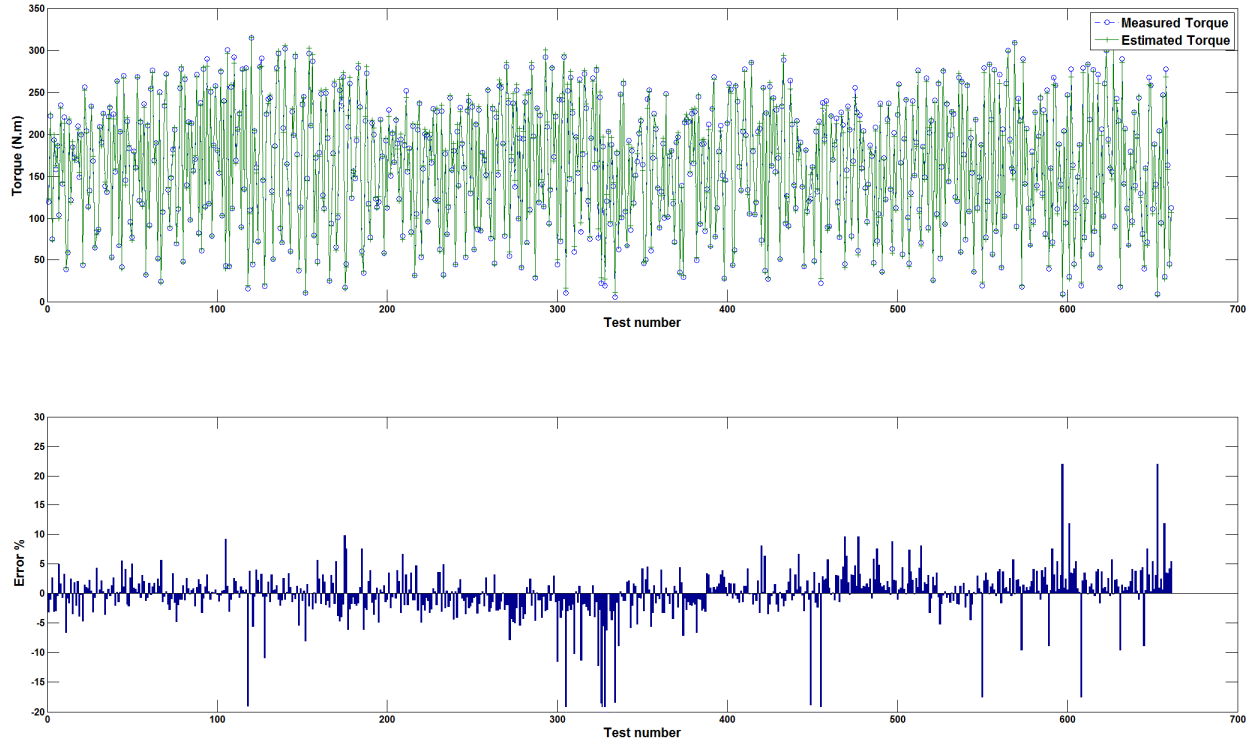


Figure 7.7 Validation of modeled against dyno measured torque data

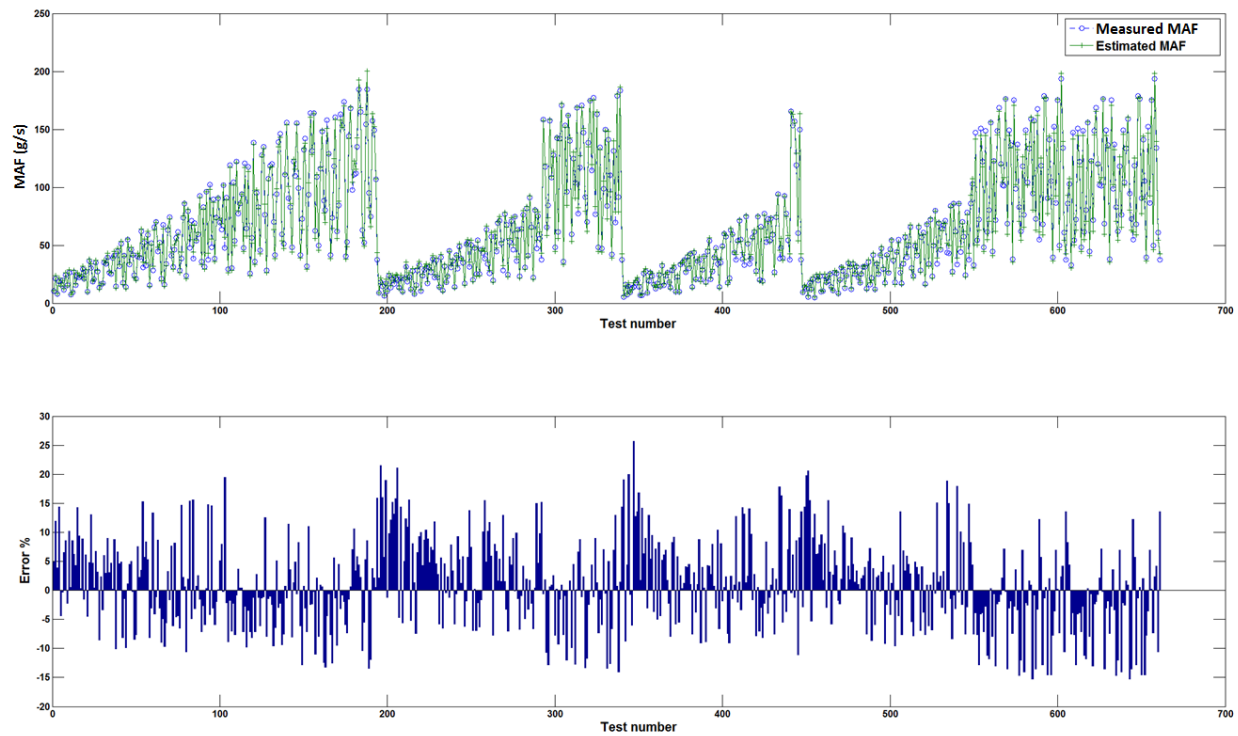


Figure 7.8 Validation of modeled against sensor measured MAF data

It is important to notice that validating CAC model using throttle mass air flow is a valid approach because at steady state operations, there is not transport delay associated with the manifold filling and emptying dynamics. Therefore, during steady state operations, the inlet mass air flow through the throttle, measured by MAF sensor, is the same as the mass air flow passing out of the intake manifold into the combustion chamber of the cylinder through the intake port. The modeled cylinder air charge is converted to cylinder mass air flow taking into account the steady state operating engine speed to perform the validation as shown in Figure 7.8.

7.2 Transient Data Fitting Results

To capture the transient effects of the engine, the constants of the ODEs (3.2), (3.3), (3.14), (3.31) and (3.41) are adjusted in order to fit the transient data collected previously from a real vehicle and the high fidelity GT-SUITE engine plant model as shown in Figure 7.9. The constants are initially set to their nominal values based on the physics and the hardware specifications but then manually adjusted slightly for achieving model accuracy by fitting the transient data. The following plots in Figure 7.10 and Figure 7.11 show the final validation of the main model state and output variables for a transient driving cycle.

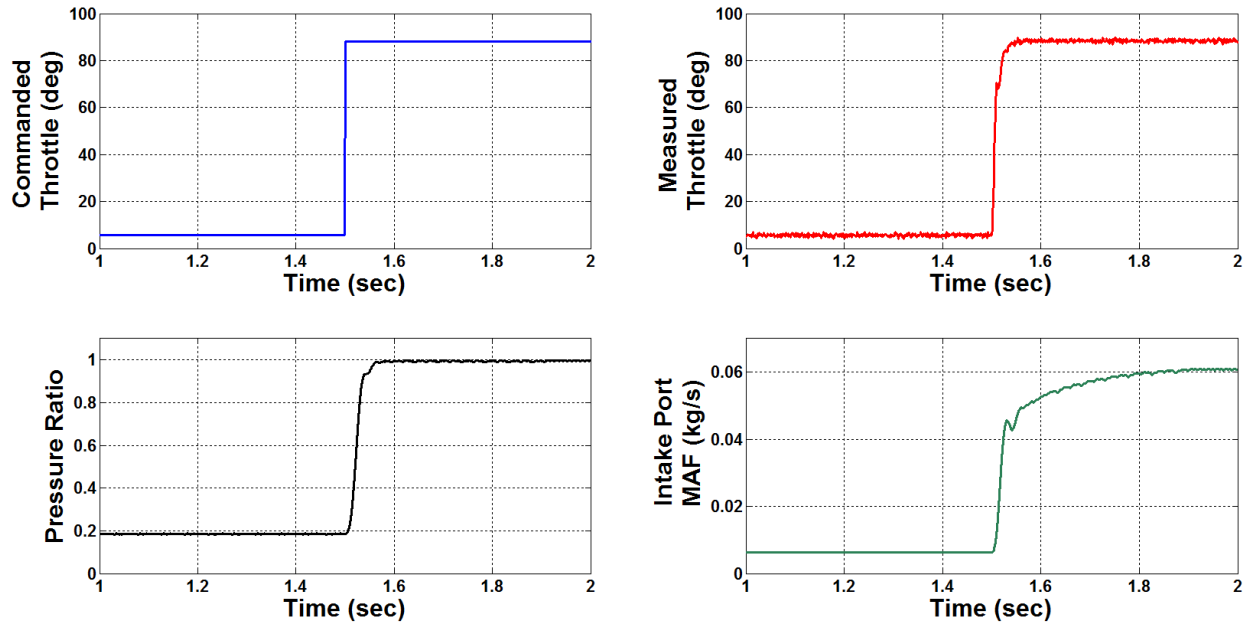


Figure 7.9 GT-Power transient throttle opening data at engine speed = 2500RPM

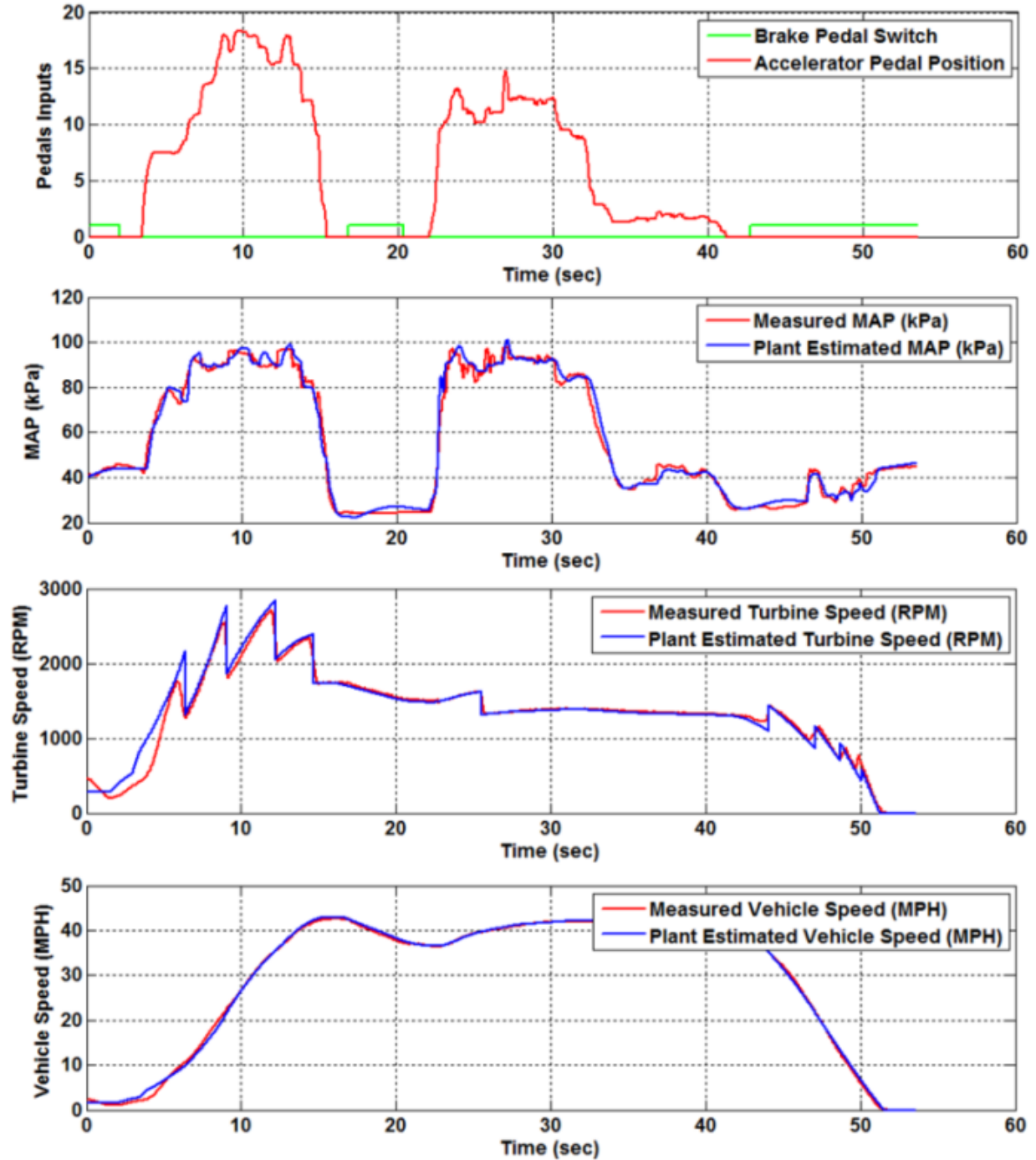


Figure 7.10 Pedal and brake inputs and modeled vs measured values of MAP, transmission turbine speed and vehicle speed

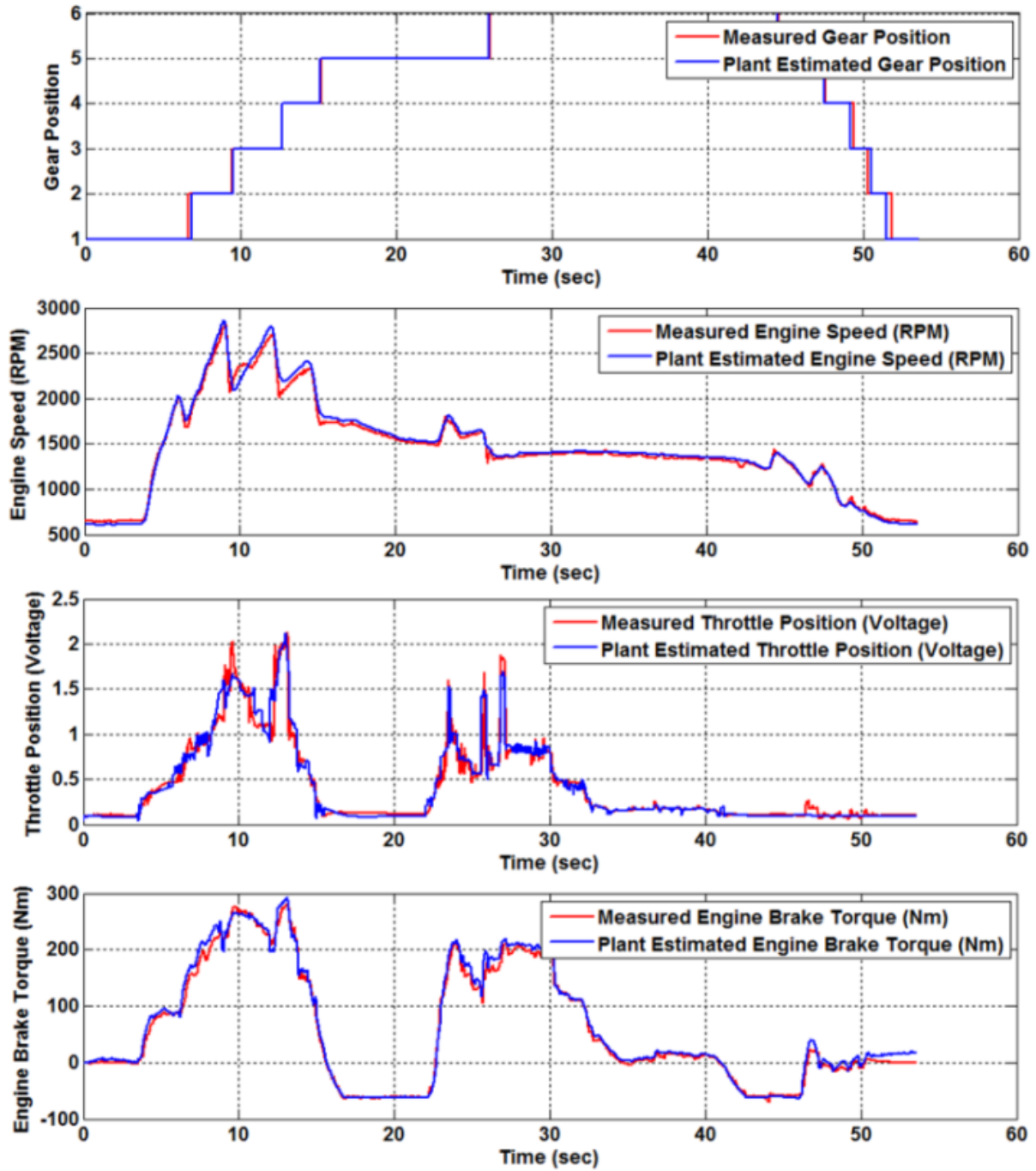


Figure 7.11 Modeled vs measured values of transmission gear, engine speed, throttle and engine brake torque

7.3 Controllers Simulation Results

Simulations of combined plant and controllers models are implemented using MATLAB® and Simulink®. The model is simulated two times to generate two sets of data that are superimposed and plotted in the graphs shown below. The first set (designated by the red colored plots) serves as a baseline for comparison purposes to compare the existing control scheme as a known reference with the new one. The second data set (designated by the blue colored plots) is generated from the new proposed strategy. The baseline strategy performs open loop control for the desired brake torque whereas the new proposed strategy performs an explicit feedback control on the brake torque on top of the existing open loop feed forward control. In order to appreciate the potential advantages, it was decided to test it in cruise control mode. The simulations are focused on three main areas: (1) the performance of vehicle's speed tracking when cruise control is engaged (2) disturbance rejection capabilities when disturbance is injected (3) transients' performance when driver steps on the accelerator pedal. The test scenario is designed such that driver gas pedal is depressed as a step input from engine idle creeping vehicle speed at time $t=10$ sec. Once the vehicle speed reached around 62mph the driver gas pedal is let go at time $t \sim 17$ sec and ~ 18 sec causing the vehicle to coast down up until vehicle speed reached 50mph upon which cruise control is engaged. When vehicle speed is maintained by the cruise controller, a disturbance is injected by simulating a steep hill mimicking a 4% grade. With the new proposed inner torque-based loop, aggressive calibrations of the cruise control speed-based outer loop are utilized. Simulations showed that the vehicle speed tracking performance is improved while at the same time better torque tracking

is realized. Disturbance rejection is also significantly enhanced. The sample and execution times of these loops had to be chosen such that an outer loop runs at a slower rate than an inner loop to ensure stability and control robustness.

It is important to notice that the plot in Figure 7.12 shows that for a given driver pedal input, the vehicle speed in the system that utilizes closed loop torque feedback control is higher than the system that runs only open loop torque control for the same pedal. This means that the driver has to step more on the pedal in the case of the open loop torque to get the same result with closed loop torque system. Such closed loop torque control system can aid in enhancing pedal feeling experience by customers and reduce pedal busyness.

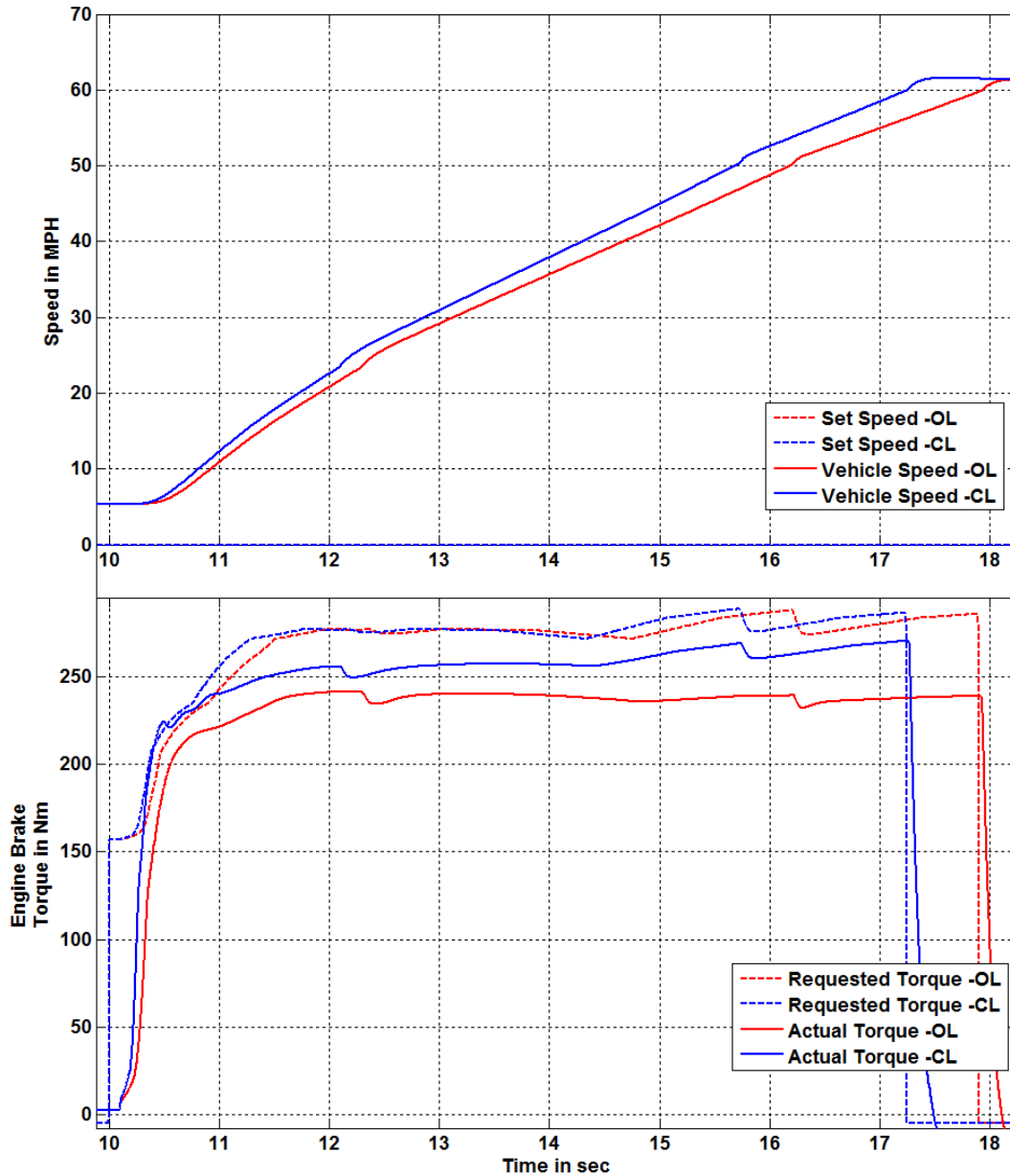


Figure 7.12 Plots of initial vehicle launch simulation

Figure 7.13 shows simulation results upon activating and engaging cruise control at 50 mph set-point just right after a period of vehicle deceleration due to accelerator pedal not being depressed. The simulations are run for the existing strategy and the newly proposed one with torque feedback. The cruise control controller gains are kept the same for the two strategies. Torque feedback not only enhanced the torque tracking

error by more than 20N.m during torque steady state but also improved vehicle speed tracking error as well.

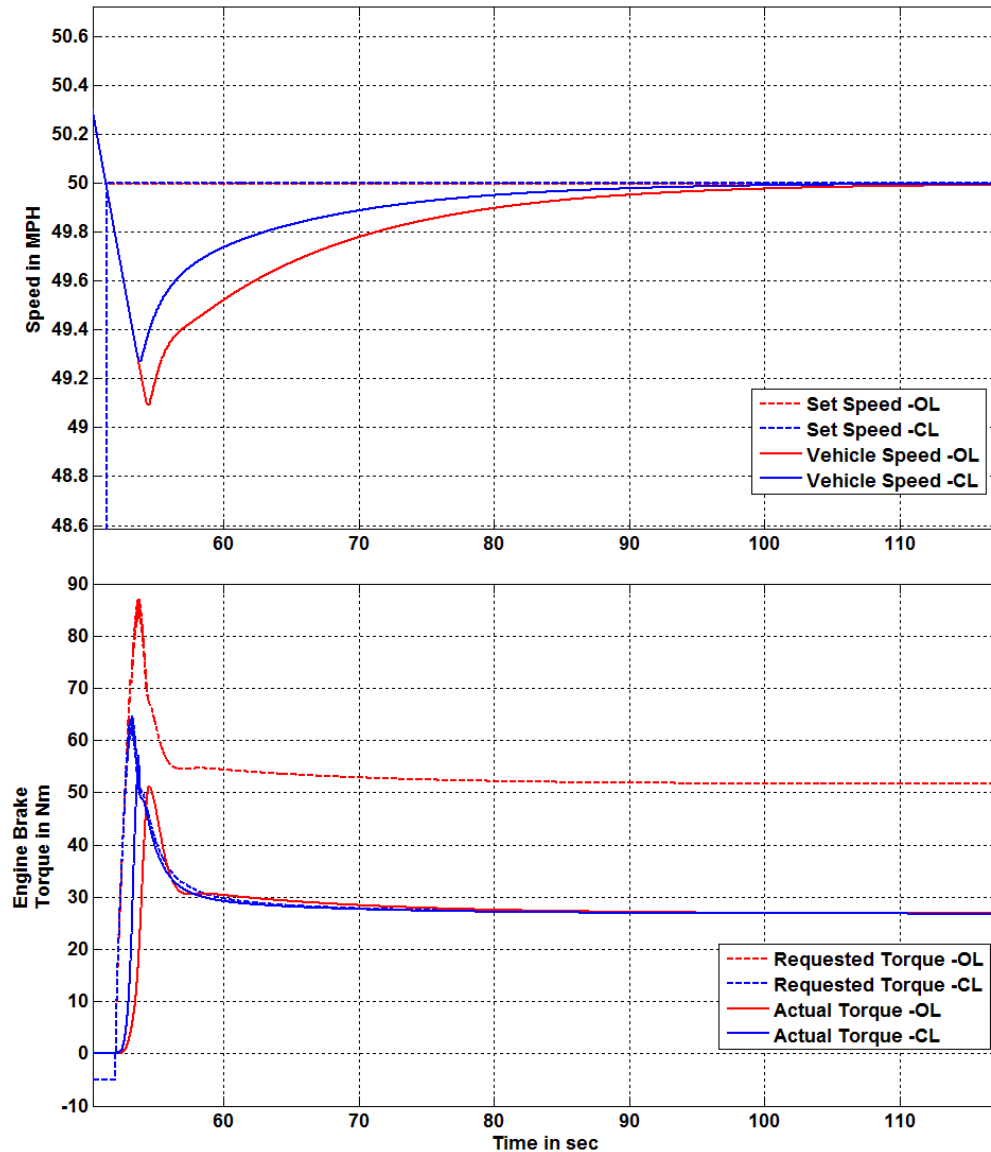


Figure 7.13 Plots of activation of cruise control simulation using the same cruise control gains for the two strategies

Figure 7.14 shows simulation results for testing the capability of rejecting disturbances when a 6%-sloped hill is injected at the moment when the vehicle speed error is zero. Cruise control gains are kept the same between the two strategies. There

is not significant improvement in disturbance rejection when cruise control controller gains are kept the same.

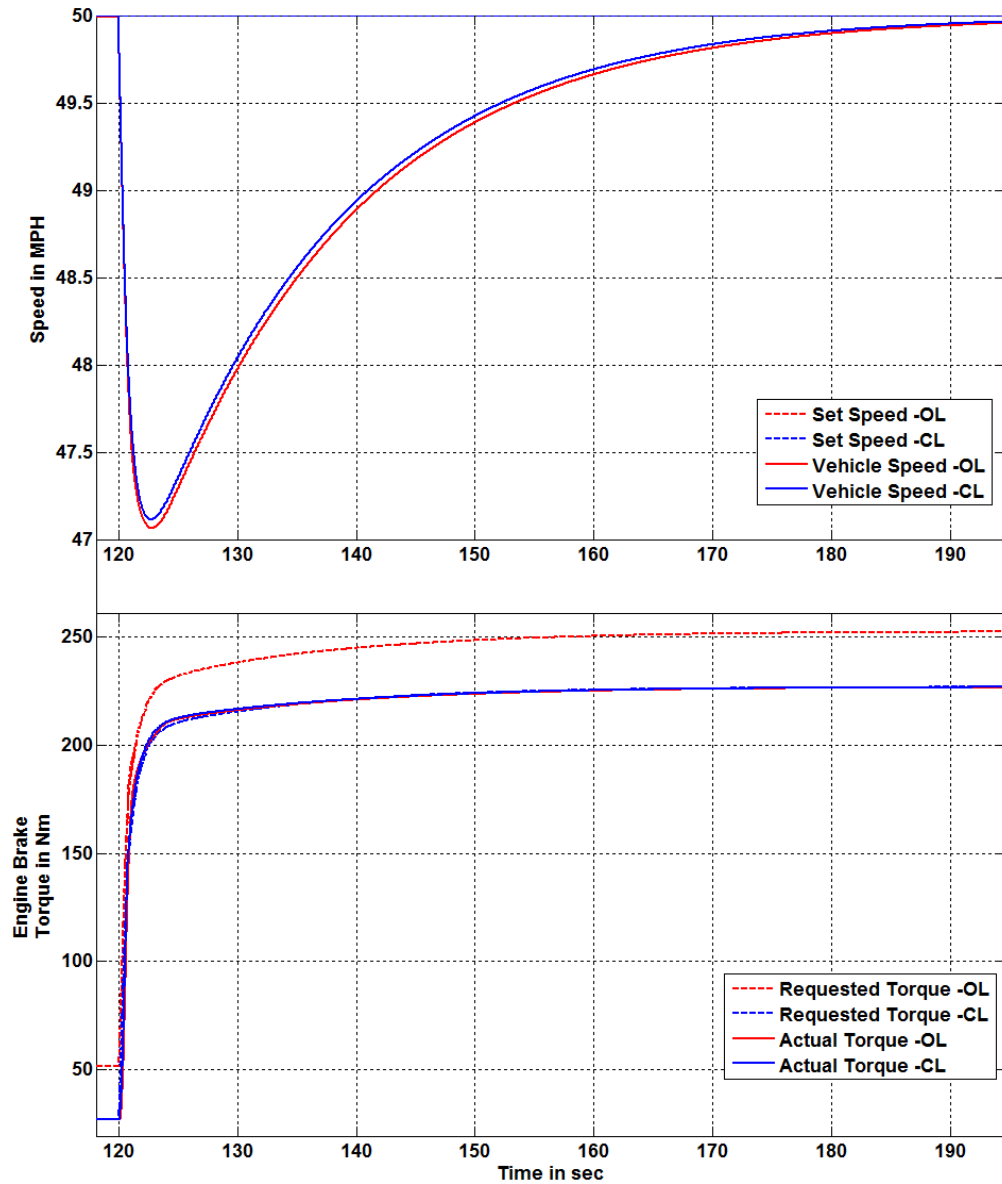


Figure 7.14 Vehicle speed and engine brake torque with hill disturbance injection during cruise control whilst cruise control gains are kept the same between the two strategies

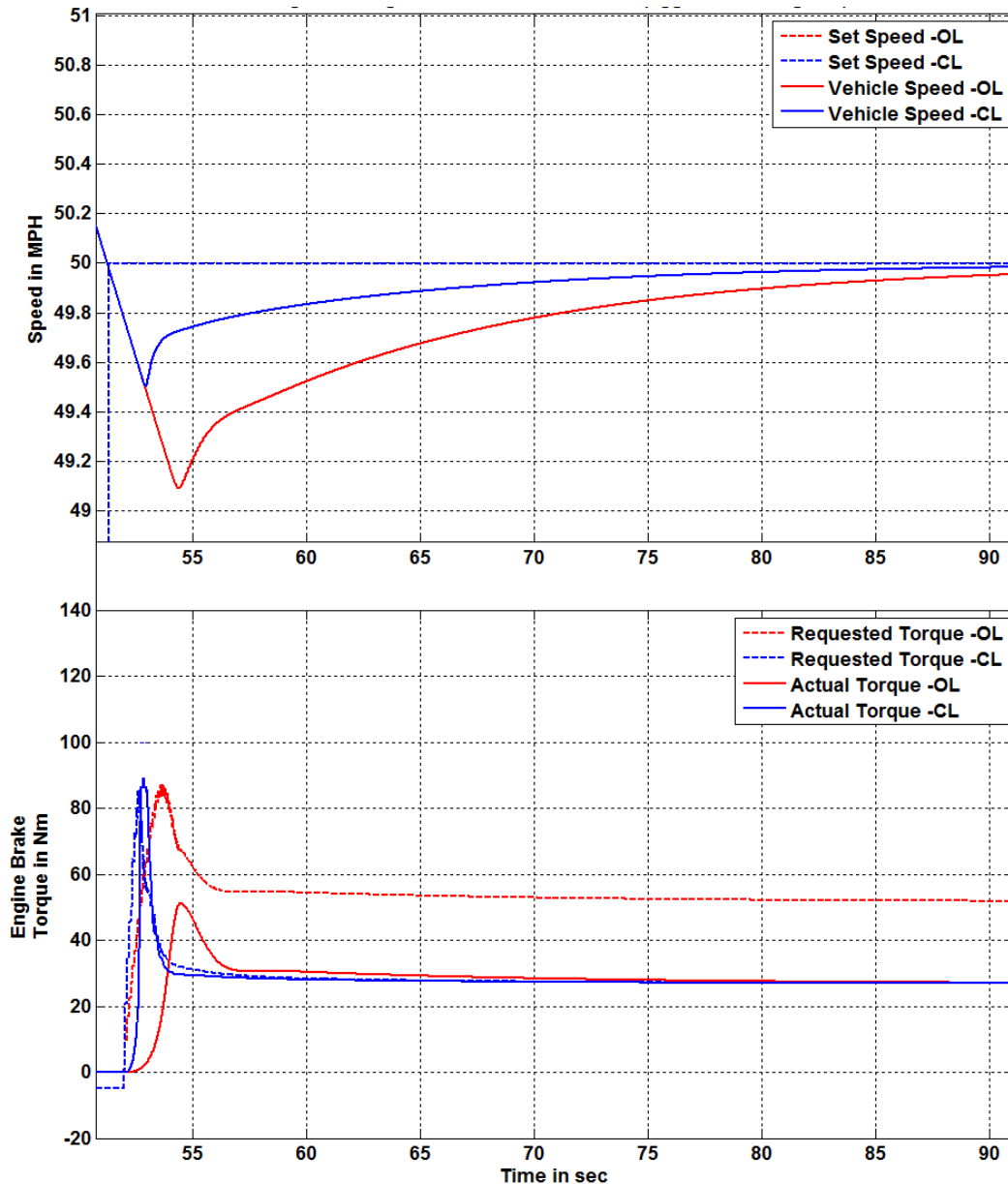


Figure 7.15 Activation of cruise control simulation results with aggressive cruise control gains for the closed loop strategy

Conversely, Figure 7.15 and Figure 7.16 show simulation results for the same test scenarios as the ones shown in Figure 7.13 and Figure 7.14 respectively but with utilization of aggressive cruise control controller gains only for the newly proposed strategy with torque feedback control. These aggressive gains are possible because of the utilization of the inner torque control loop. Without the proposed inner torque control

feedback loop, the utilization of aggressive cruise control controller gains will cause unacceptable drivability and controller performance issues such as excessive vehicle speed overshoots and undershoots. These aggressive gains utilized in the newly suggested control strategy clearly improved vehicle speed tracking and enabled better disturbance rejection.

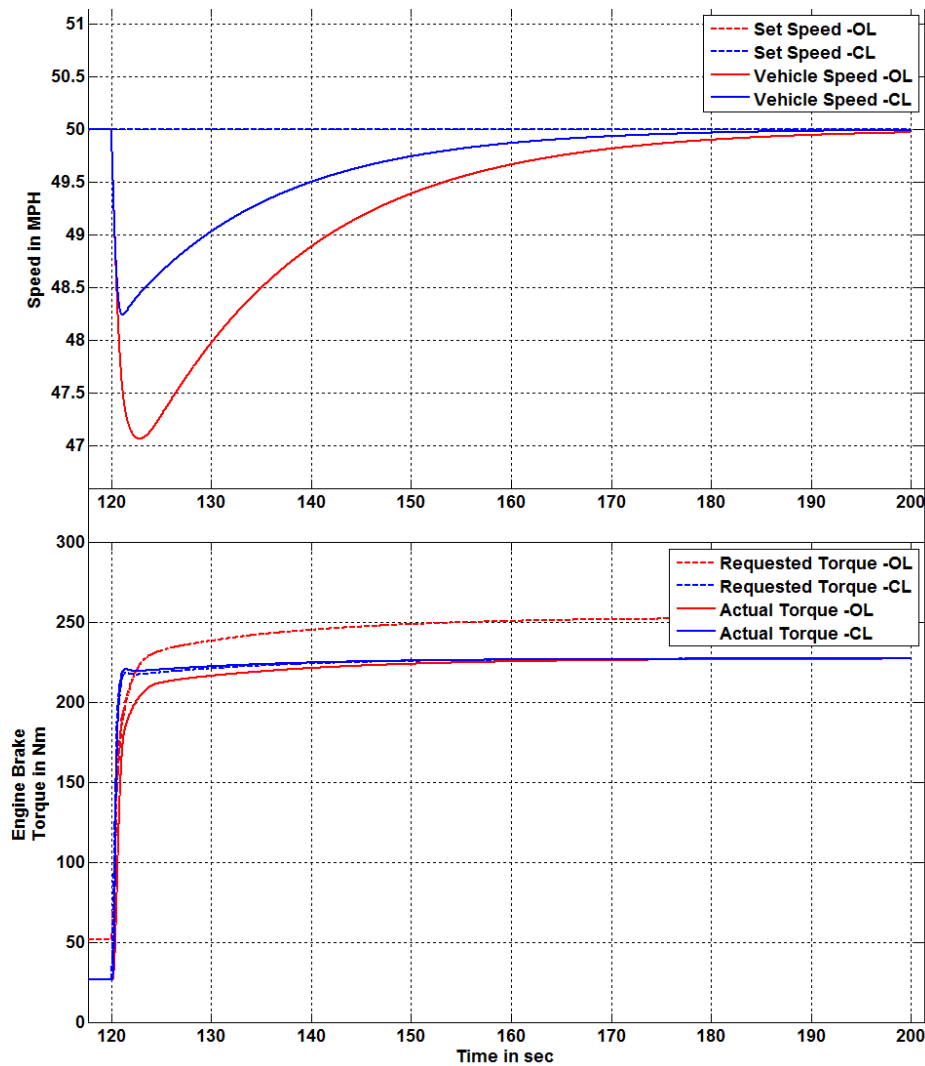


Figure 7.16 Vehicle speed and engine brake torque with up-hill disturbance injection during cruise control with aggressive cruise control gains for the closed loop strategy

The simulation results for the fast path torque request are illustrated in Figure 7.17 and Figure 7.18. The conducted test in Figure 7.17 is meant to simulate a transmission fast torque intervention. The open loop control strategy response does not track the requested torque but the closed loop controller is able to achieve adequate and better tracking. The test is conducted in dyno mode by fixing engine speed at 2500 RPM.

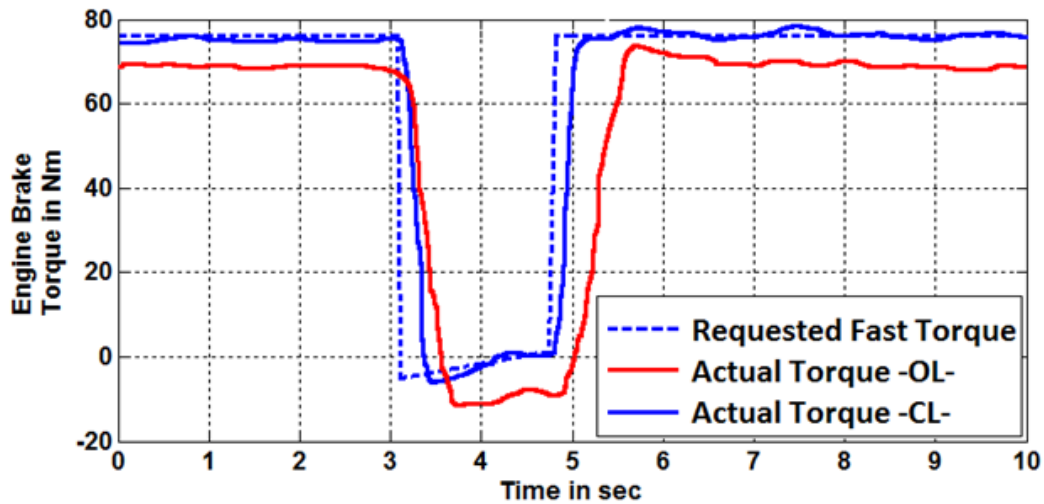


Figure 7.17 Open vs closed loop control response to fast torque request at engine speed 4500 RPM in dyno mode

In Figure 7.18, the test simulates a vehicle cruising at a target set speed of 50 MPH and at $t = 120$ sec of the simulation the vehicle undergoes a down-hill of around 1% grade. The closed loop torque control strategy is able to achieve improved response by using the torque feedback until the slow (air path) reaches its minimum limit (control authority) and thus invoking fast torque path to continue the control.

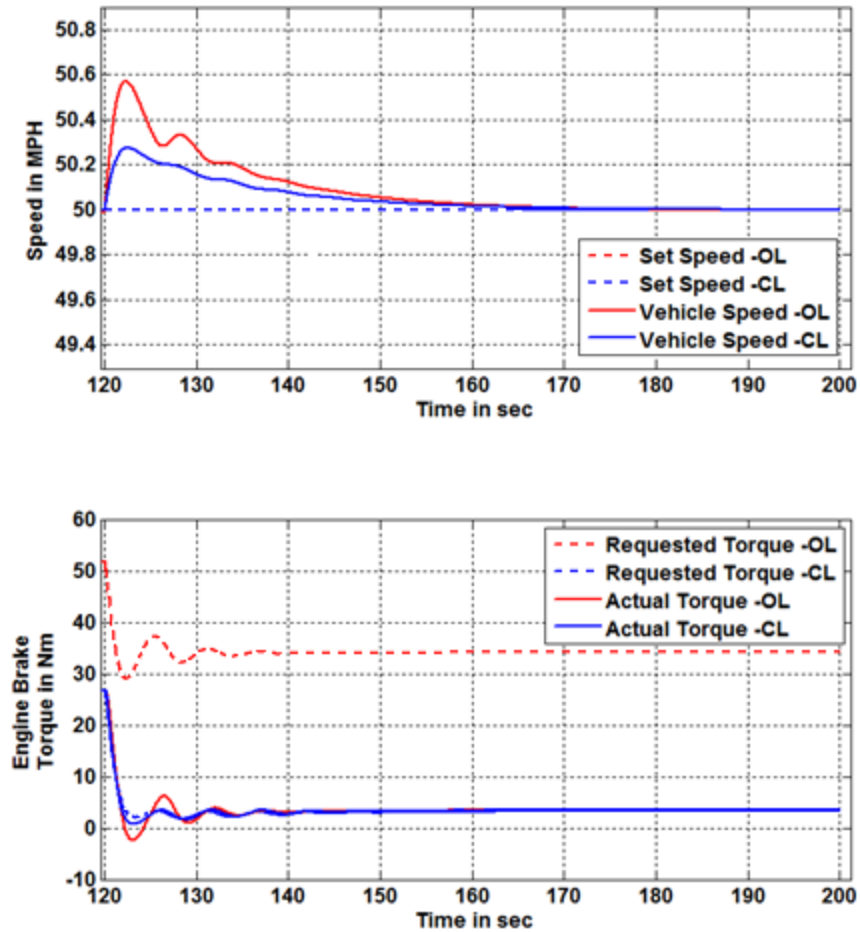


Figure 7.18 Vehicle speed and engine brake torque with down-hill disturbance injection during cruise control with aggressive cruise control gains for the closed loop strategy

CHAPTER 8: SYSTEM ANALYSIS AND CONCLUSION

8.1 Control System Analysis

This section shows that the addition of an inner feedback control loop for torque feedback (green signal line in Figure 8.1) enhances the gain and phase margins of the existing vehicle speed control when closing the outer feedback loop on vehicle speed. This analysis will be focused on the slow torque path since the cruise control is handled typically by the slow torque path request. The idea here is to compute two total open loop transfer functions (without closing the loop on vehicle speed) with and without the torque feedback to compare the gain and phase margins for these two options. To do this, the system needs to be linearized around the equilibrium operating point at which simulations are run. This equilibrium point is namely $VS = 50$ MPH, $N = 1520$ RPM, $MAP = 40$ kPA. $THR = 0.22$ V

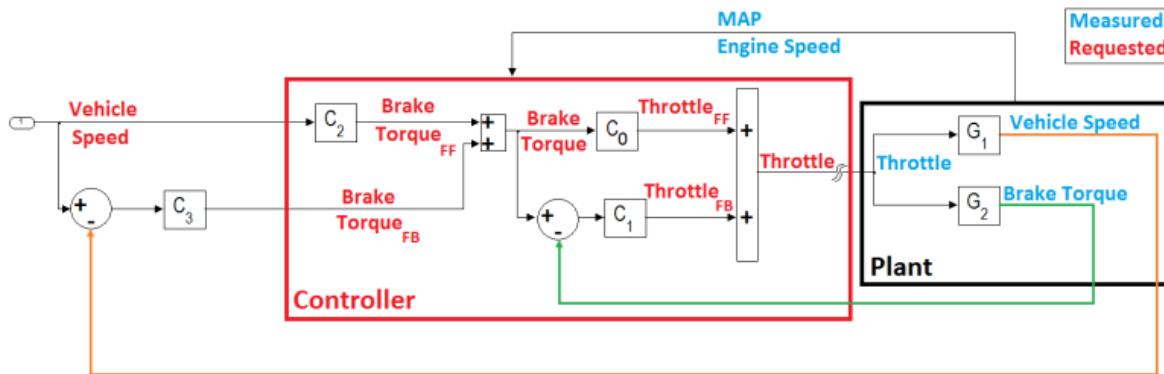


Figure 8.1 Illustration of plant and slow controller using linearized transfer functions

By observing Figure 8.1, the transfer functions G_1 and G_2 need to be calculated. G_1 maps the input/commanded throttle to vehicle speed. G_2 maps the input/commanded throttle to engine brake torque. The transfer function of the controller C_0 is $\frac{1}{\hat{G}_2}$.

For the purpose of performing torque control in general and for this analysis, \hat{G}_2 is set equal to the nominal value of G_2 . G_2 is the plant itself and can change overtime (due to component aging, drifting etc.) whereas \hat{G}_2 is chosen to be fixed and set to be equal to the nominal value of the plant G_2 . C_1 is the new proposed controller (PID) under study and C_2 is an existing cruise control feed forward controller that is typically a function of commanded vehicle speed and current engine speed (or by observing Figure 8.1 $C_2 = \frac{1}{\hat{C}_0 \hat{G}_1}$).

By defining the following succinct vector notation,

$$\mathbf{x} = \begin{bmatrix} x_1 \\ x_2 \\ x_3 \end{bmatrix} \text{ where, } x_1 := \text{MAP} \quad x_2 := \text{N} \quad x_3 := \text{VS}$$

$u := \text{THR}$ (for the slow torque control system only).

$$\mathbf{y} = \begin{bmatrix} y_1 \\ y_2 \end{bmatrix} \text{ where, } y_1 := \text{VS} \quad y_2 := T_{\text{Brake}}$$

then combining the developed plant model equations provided previously, one can write the following lumped two system nonlinear differential equations [80]:

$$\dot{\mathbf{x}} = \mathbf{f}(\mathbf{x}, u)$$

$$\mathbf{y} = \mathbf{g}(\mathbf{x}, u)$$

where \mathbf{f} is a function mapping $\mathbb{R}^3 \times \mathbb{R}^1 \rightarrow \mathbb{R}^3$ and \mathbf{g} a function mapping $\mathbb{R}^3 \times \mathbb{R}^1 \rightarrow \mathbb{R}^2$: $\mathbf{x} \in \mathbb{R}^3$, $u \in \mathbb{R}^1$ & $\mathbf{y} \in \mathbb{R}^2$

The rest of the system inputs such as spark, air/fuel ratio, gear etc. are treated as known disturbances and their values at the equilibrium point are used in the equations.

The transport delay that is present in equation (3.23) is approximated by a rational s-domain transfer function using fifth order Padé approximation [62].

By using the Jacobian linearization method, the LTI system matrices for the two outputs are calculated as in the following:

$$A := \left. \frac{\partial f}{\partial x} \right|_{\substack{x=\bar{x} \\ u=\bar{u}}} \quad B := \left. \frac{\partial f}{\partial u} \right|_{\substack{x=\bar{x} \\ u=\bar{u}}} \quad C := \left. \frac{\partial g}{\partial x} \right|_{\substack{x=\bar{x} \\ u=\bar{u}}} \quad D := \left. \frac{\partial g}{\partial u} \right|_{\substack{x=\bar{x} \\ u=\bar{u}}}$$

For G_1 , clearly the first row of the matrices C and D are [0 0 1] and [0] respectively because the output y_1 for G_1 is the state vehicle speed itself.

For G_2 , the output y_2 which is T_{Brake} is a linear combination of the system state variables and input. Hence, the second row of C and D matrices are determined by:

$$C := \left. \frac{\partial T_{Brake}}{\partial x} \right|_{\substack{x=\bar{x} \\ u=\bar{u}}} \quad D := \left. \frac{\partial T_{Brake}}{\partial u} \right|_{\substack{x=\bar{x} \\ u=\bar{u}}}$$

Finally, the transfer functions G_1 and G_2 are found using $C(sI - A)^{-1}B + D$. From Figure 8.2 the overall open loop (without the vehicle speed orange color feedback) transfer function of the newly proposed system (with torque feedback) is given by:

$$H_{CL} = C_1 C_2 G_1 - \frac{C_1 G_1 (C_2 C_1 G_2 + \frac{C_2 G_2}{\hat{G}_2})}{1 + C_1 G_2} + \frac{C_2 G_1}{\hat{G}_2}$$

Similarly, the overall open loop (i.e. without the vehicle speed orange color feedback) transfer function of the original system (without torque feedback, $C_1 = 0$) is given by:

$$H_{OL} = \frac{C_2 G_1}{\hat{G}_2}$$

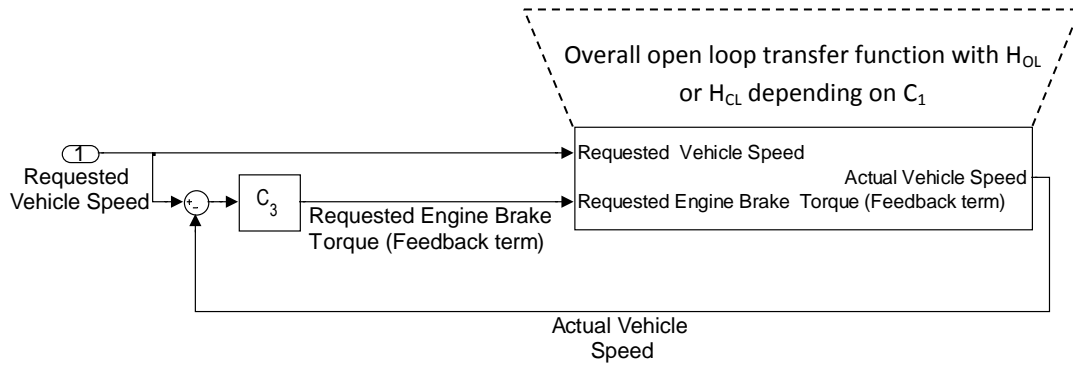


Figure 8.2 Overall open loop equivalent system with closed loop feedback closing the loop on vehicle speed.

Plotting the Bode plot of these two transfer functions shows that the gain margin is increased from 283dB to 323dB (an increase by 40dB) and phase margin is increased from 85.3deg to 137deg (an increase by 51.7deg). Hence, more aggressive cruise control gains can be used when torque feedback loop is utilized which confirms the previous observations from simulations of the original non-linear model. That is an advantage on top of the better torque tracking control.

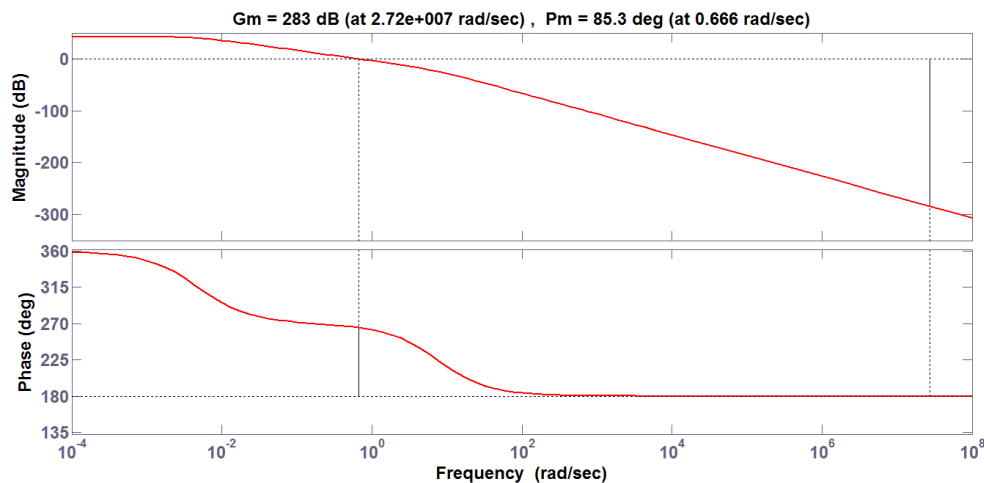


Figure 8.3 Bode Plot of the OL torque control system

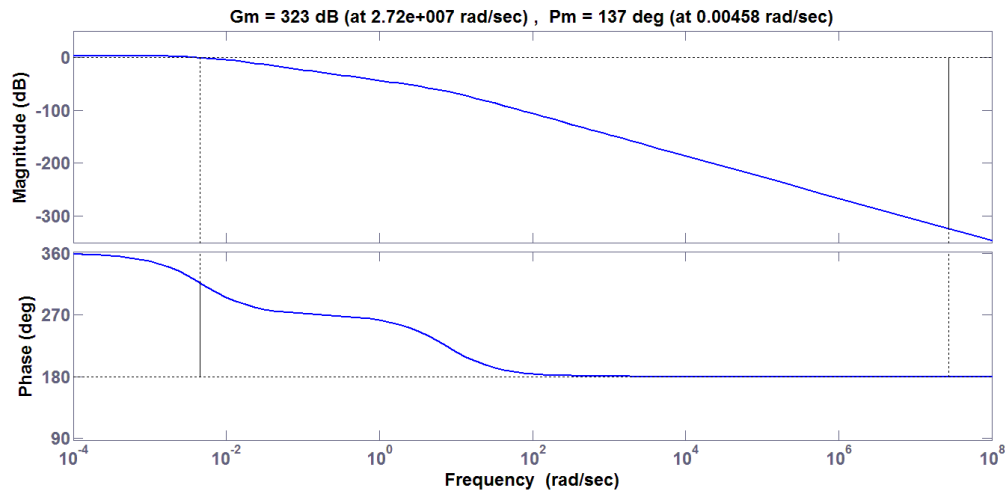


Figure 8.4 Bode plot of the system including inner torque control feedback loop

Using the same argument and similar analysis, keeping the MAF feedback loop will allow the torque control system to have an increased phase and gain margins. Hence, it is recommended to keep this most inner feedback control loop. Another reason for wanting to keep this control loop is that this loop allows for air flow error to be adapted whilst the torque control loops (brake and indicated) allow the torque losses errors to be adapted.

8.2 Conclusion and Suggested Future Work

All of the aforementioned challenges related to estimation of delivered torque and tracking of requested torque can be potentially addressed with a system that employs an enhanced controller that utilizes explicit torque feedback from the newly suggested sensors namely pressure and brake SAW torque sensors. The simulation work presented herein shows several advantages of using such control strategy. These advantages include: the ability of performing torque adaption off idle, reduce pedal busyness, achieving improved and consistent torque tracking control , ability to utilize more aggressive cruise control gains due to achieving better gain and phase margins.

These advantages are enablers to better optimizing vehicle launches and transient response, and engine starts especially for engines equipped with engine stop start features, potential improvements in driveline oscillations control as well as accomplishing better transmission shift quality. PID and PD controllers are designed to track both the slow and fast torques, respectively, in a coordinated manner using inner-outer loop control structure. The suggested future work is to investigate using only one in-cylinder pressure sensor to calculate engine's IMEP and to implement this design in an actual vehicle to assess the promising results of the simulation work. This simulation work may possibly be enhanced if the model is changed from mean value model to cylinder by cylinder model with crank angle resolved measurements. In other words, I am suggesting as a next step to increase the fidelity of the plant model. This can also be done by including, cylinder combustion model, burn rate and burn fraction estimation (Wiebe function), closed loop fuel controller with exhaust gas oxygen sensor feedback model. Furthermore, including a high fidelity driveline model will assist in performing simulations related to controlling transient driveline oscillations using torque feedback.

APPENDIX: LIST OF USED SYMBOLS

Description	Variable	Units	Description	Variable	Units
Cylinder Swept Volume	V_{dc}	m^3	Engine Speed	N	rev/s
In-Cylinder Pressure	P_{icyl}	Pascal	Specific Gas Constant of Air	R_s	J/(Kg.K)
Work Done by Cylinder	W_{cyl}	Joule	Inlet Air Temperature	IAT	K
Instantaneous Displacement Volume of Cylinder	V_{icyl}	m^3	Intake Manifold Volume	V_m	m^3
Indicated mean effective pressure of cylinder	$IMEP_{cyl}$	Pascal	The Gross Indicated Torque at Full Efficiency	$T_{G_Ind} _{full_eff}$	N.m
Number of Revolutions per Cycle	n_r	rev/cycle	Spark Efficiency Function	η_{spk}	%
Engine Displacement	V_d	Liter	Lambda Efficiency Function	η_{af}	%
Supply Voltage	V_s	V	Torque Efficiency Associated with the Cylinder Fuel Shut-Off	η_{FSO}	%
Throttle Angle	φ_{thr}	rad	Raw FSO Efficiency Prior to Filtering	η_{RAW_FSO}	%
Total Throttle Gear Ratio	GR_{thr}	unitless	Filter Time Constant	τ_c	s
Angular Speed of the Motor	ω_m	rad/s	Final Gross Engine Indicated Torque	T_{G_Ind}	N.m
Angular Speed of the Throttle Plate Shaft	ω_{thr}	rad/s	Variable Torque Production Delay	t_d	s

Description	Variable	Units	Description	Variable	Units
Back emf Voltage	V_{emf}	V	Engine Pumping Losses Torque	T_{P_Losses}	N.m
Motor's Back emf Constant	K_{me}	V.s/rad	The Net Indicated Torque	T_{N_Ind}	N.m
Throttle Plate Angular Velocity	ω_{thr}	rad/s	Crankshaft Position	θ	rad
Controller Duty Cycle of PWM signal	DC_{PWM}	%	Angular Speed of the Engine's Crankshaft	ω_e	rad/s
DC Motor's Armature Equivalent Resistance	R_a	Ω	Angular Acceleration of Engine's Crankshaft	α_e	rad/s ²
Current Through the DC Motor's Armature	i_a	A	Equivalent Moment of Inertia of the Engine and Transmission Impeller	J_{ei}	N.m.s ² /rad
DC Motor's Armature Equivalent Inductance	L_a	H	Engine's and Transmission Impeller's Damping Coefficient or Rotational Friction	C_{ei}	N.m.s/rad
Equivalent Total Inertia of the ETB	J_{ETB}	N.m.s ² /rad	Stiffness of Engine and Transmission Impeller's or Coefficient of Torsion	K_{ei}	N.m/rad
DC Motor Applied Torque	T_m	N.m	External Load Torque on the Engine	T_{Load}	N.m
Friction Torque	T_f	N.m	Impeller Torque	T_{Imp}	N.m
Motor Torque Constant	K_{mt}	N.m/A	Turbine Speed	N_T	rad/s

Description	Variable	Units	Description	Variable	Units
DC Motor's Viscous Friction Damping Constant	K_b	N.m.s/rad	Turbine Torque	T_T	N.m
Spring Constant	K_s	N.m/rad	Transmission Input Speed	N_{in}	rad/s
Spring Torque Function	$f n_1(\varphi_{thr}, K_s)$	N.m	Transmission Gear Ratio Based on the Current Gear.	R_{gear}	unitless
Spring Pre-Loaded Torque Function	$f n_2(\varphi_{thr})$	N.m	Transmission Output Speed	N_{out}	rad/s
Constant Spring Pre-Loaded Torque	T_{PL}	N.m	Vehicle Wheel Speed (RPM) Derived From the Vehicle Model	spd_w	Rev/s
Air Mass Variation in the Intake Manifold	$\frac{dm_{air_m}}{dt}$	g/s	Wheel Torque	T_w	N.m
Mass Flow Rate of Air Passing Through the Throttle	\dot{m}_{air_thr}	g/s	Load Torque	T_l	N.m
Mass Flow Rate of Air in a Given Individual Cylinder i	$\dot{m}_{air_cyl,i}$	g/s	Vehicle Speed	VS	MPH
Engine's Total Number of Cylinders	total_cyls	cylinders	Road Grade Angle	θ_r	°
Pressure Upstream of the Throttle	p_o	kPa	Braking Torque Applied by the Driver's Brake Pedal	T_{BP}	N.m

Description	Variable	Units	Description	Variable	Units
Intake Manifold Pressure Downstream the Throttle	p_m	kPa	Vehicle's Inertia	J_v	N.m.s ² /rad
Pressures Ratio	p_r	unitless	Vehicle Angular Acceleration	α_v	rad/s ²
Ratio of Specific Heat Capacities (c_v/c_p) of Inlet Air	γ	unitless	Estimated Cylinder Air Charge for the i^{th} Operating Point Measurement	\overline{CAC}_i	g/s
Specific Heat Capacity at Constant Pressure	c_p	J/(mol.K)	Mean of all Cylinder Air Charge Measurements	\overline{CAC}	g/s
Specific Heat Capacity at Constant Volume	c_v	J/(mol.K)	i^{th} Operating Point Cylinder Air Charge Measurement	CAC_i	g/s
Throttle Discharge Coefficient	C_D	unitless	Adjusted Coefficient of Determination	\bar{R}^2	%
Engine Volumetric Efficiency	η_v	%	Manifold Intake Air Density	ρ_{air_m}	g/L

REFERENCES

- [1] D. W. Guenther and J. Gerhardt, "MOTRONIC – torque guided engine management systems to meet future challenges in emissions and fuel consumption reduction," in *SAE technical paper 2000-01-1420*, 2000.
- [2] T. Bertram, R. Bitzer, R. Mayer and A. and Volkart, "CARTRONICS – an open architecture for networking the control systems of an automobile," in *SAE technical paper no. 980200*, 1998.
- [3] J. Gerhardt, N. Benninger and W. Hess, "Torque based system structure of electronic engine management system (ME7) as a new base for drivetrain systems," in *Proceedings of the FISITA Congress*, Paris, France, July 1998.
- [4] J. W. Grizzle, J. A. Cook and W. P. Milam, "Improved cylinder air charge estimation for transient air fuel ratio control," in *Proceedings of the American Control Conference*, Baltimore, MD, June 1994.
- [5] M. Vojtišek and M. Kotek, "Estimation of Engine Intake Air Mass Flow using a generic Speed-Density method," *Journal of Middle European Construction and Design of Cars*, vol. 12, no. 1, pp. 7-15, December 2014.
- [6] I. Brahma, M. C. Sharp and T. R. Frazier, "Estimation of Engine Torque from a First Law Based Regression Model," in *SAE Technical Paper 2008-01-1014*, 2008.
- [7] B. Mencher, H. Jessen, L. Kaiser and J. Gerhardt, "Preparing for CARTRONIC - Interface and New Strategies for Torque Coordination and Conversion in a Spark Ignition Engine-Management System," in *SAE Technical Paper 2001-01-0268*, 2001.

- [8] N. Heintz, M. Mews, G. Stier, A. J. Beaumont and A. D. Noble, "An approach to torque-based engine management systems," in *SAE technical paper 2001-01-0269*, 2001.
- [9] A. Haj-Fraj and F. Pfeiffer, "Optimal Control of Gear Shift Operations in Automatic Transmissions," *Journal of the Franklin Institute*, vol. 338, no. 2-3, pp. 371-390, 2001.
- [10] Z. Zhong, G. Kong, Z. Yu, X. Xin and X. Chen, "Shifting control of an automated mechanical transmission without using the clutch," *International Journal of Automotive Technology*, vol. 13, no. 3, pp. 487-496, 2012.
- [11] M. Gäfvert, K. Årzén, B. Bernhardsson and L. M. Pedersen, "Simple feedback control and mode switching strategies for GDI engines," in *SAE technical paper 2000-01-0263*, 2000.
- [12] P. Willibald, S. Thomas, S. Joachim and T. Oliver, "The BMW active cruise control ACC," in *SAE technical paper No. 2000-01-0344*, 2000.
- [13] P. Worrawut, T. Somphong and P. Manukid, "Adaptive cruise control for an intelligent vehicle," in *2008 IEEE International Conference on Robotics and Biomimetics*, Bangkok, Thailand, 22-25 Feb. 2009.
- [14] W. J. Fleming, "Automotive torque measurement: A summary of seven different methods," *IEEE Transactions on Vehicular Technology*, vol. 31, no. 3, pp. 117-124, August 1982.
- [15] N. Cavina, F. Ponti and R. G., "Fast Algorithm for On-Board Torque Estimation," in *SAE Technical Paper 1999-01-0541*, 1999.
- [16] P. Azzoni, D. Moro, F. Ponti and G. Rizzoni, "Engine and load torque estimation with application to electronic throttle control," in *SAE Technical Paper 980795*, 1998.
- [17] J. Franco, M. Franchek and K. Grigoriadis, "Real-time brake torque estimation for internal

- combustion engines," *Journal of Mechanical Systems and Signal Processing*, vol. 22, no. 2, pp. 338-361, 2008.
- [18] V. Kalinin, R. Lohr, A. Leigh and G. Bown, "Application of Passive SAW Resonant Sensors to Contactless Measurement of the Output Engine Torque in Passenger Cars," in *Frequency Control Symposium, Joint with the 21st European Frequency and Time Forum. IEEE International*, Geneva, Switzerland, May 29 - June 1 2007.
- [19] S. Larsson and I. Andersson, "An Experimental Evaluation of Torque Sensor Based Feedback Control of Combustion Phasing in an SI-engine," in *SAE Technaical Paper 2005-01-0060*, 2005.
- [20] S. Larsson and I. Andersson, "Self-optimising control of an SI-engine using a torque sensor," *Control Engineering Practice*, vol. 16, no. 5, pp. 505-514, 2008.
- [21] S. Schagerberg and T. McKelvey, "Instantaneous crankshaft torque measurements – modeling and validation," in *Society of Automotive Engineering, Paper no. 2003-01-0713.*, 2003.
- [22] S. Larsson and S. Schagerberg, "SI-engine cylinder pressure estimation using torque sensors," in *Society of Automotive Engineering Paper no. 2004-01-1369*, 2004.
- [23] G. A. Ingram, M. A. Franchek, V. Balakrishnan and G. Surnilla, "Spark ignition engine torque management," in *Proceedings of the 2003 American Control Conference*, Denver, CO, 2003.
- [24] M. Hong, M. Ouyang and T. Shen, "Torque-based optimal vehicle speed control," *International Journal of Automotive Technology*, vol. 12, no. 1, pp. 45-49, 2011.
- [25] M. Hong, M. Ouyang, T. Shen and J. Li, "Model-based PI Feedback Control of Engine

- Torque," in *8th IEEE International Conference on Control and Automation*, Xiamen, China, 2010.
- [26] T. Nagata and M. Tomizuka, "Engine torque control based on discrete event model and disturbance observer," in *ASME International Mechanical Engineering Congress and Exposition*, Seattle, Washington, November 11–15, 2007.
- [27] G. W. Pestana, "Engine control methods using combustion pressure feedback," in *SAE Technical Paper 890758*, 1989.
- [28] Y. Chamaillard, P. Higelin and A. Charlet, " A simple method for robust control design, application on a non-linear and delayed system: engine torque control," *Control Engineering Practice*, vol. 12, no. 4, pp. 417-429, 2004.
- [29] C. A. Amann, "Cylinder-Pressure Measurement and Its Use In Engine Research," in *Society of Automotive Engineering Paper no. 852067*, 1985.
- [30] H. S. Rai, M. F. J. Brunt and C. P. Loader, "Quantification and reduction of IMEP errors resulting from pressure transducer thermal shock in an S.I. engine," in *Society of Automotive Engineering Paper no. 1999-01-1329.*, 1999.
- [31] D. R. Lancaster, R. B. Krieger and J. H. Lienesch, "Measurement and Analysis of Engine Pressure Data," in *Society of Automotive Engineering Paper no. 750026*, 1975.
- [32] M. Brunt and G. G. Lucas, "The effect of crank angle resolution on cylinder pressure analysis," in *Society of Automotive Engineering Paper no. 910041*, 1991.
- [33] M. Hong, T. Shen and M. Ouyang, "Nonlinear Observer-based Torque Control for SI Engine," in *2009 ICCAS-SICE*, Fukuoka, Japan, 2009.

- [34] R. Müller and B. Schneider, "Approximation and control of the engine torque using neural networks," in *SAE Technical Paper 2000-01-0929*, 2000.
- [35] D. Liu, H. Javaherian, O. Kovalenko and T. Huang, "Adaptive Critic Learning Techniques for Engine Torque and Air–Fuel Ratio Control," *IEEE Transactions on Systems, Man, and Cybernetics, Part B: Cybernetics*, vol. 38, no. 4, pp. 988-993, August 2008.
- [36] N. S. Nise, *Control systems engineering*, Hoboken, NJ: Wiley, 2004, p. 547.
- [37] H. e. a. Bauer, *Automotive Sensors*, Stuttgart, Germany: Robert Bosch GmbH, 2002, pp. 85-93.
- [38] J. Fraden, *Handbook of modern sensors physics, designs, and applications*, New York: AIP Press/Springer, 2004, p. 344.
- [39] F. Scoppe, "Magnetostrictive Torque Transducer," *Instrumentation Technology*, vol. 16, pp. 95-99, October 1969.
- [40] I. J. Garshelis and C. R. Conto, "A torque transducer utilizing a ring divided into two oppositely polarized regions," *Applied physics*, vol. 79, no. 8, pp. 4756-4758, 1996.
- [41] A. Mamishev, K. Sundara-Rajan, F. Yang, Y. Du and M. Zahn, "Interdigital sensors and transducers," *Proceedings of the IEEE*, vol. 92, no. 5, pp. 808-845, 2004.
- [42] B. Lee, G. Rizzoni, Y. Guezennec, A. Soliman, M. Cavalletti and J. Waters, "Engine Control Using Torque Estimation," in *SAE Technical Paper 2001-01-0995*, 2001.
- [43] S. Hadden, L. Hulls and E. Sutphin, "Remote Diagnosis of Internal Combustion Engines," *Instrumentation Technology*, vol. 23, pp. 43-48, July 1976.

- [44] D. Moyer, "Electronic Engine Control By On-Board Computer," in *IEEE-SAE International Conference On Automotive Electronics And Electric Vehicles*, Dearborn, Michigan, September 20, 1976.
- [45] J. Qualman and E. Egbert, "Fluid Couplings," *Chapter 19, Design Practices - Passenger Car Automatic Transmissions, SAE Advances in Engineering*, vol. 5, pp. 183-197, 1973.
- [46] U. Kiencke and L. Nielsen, *Automotive Control Systems*, Berlin, Germany: Springer-Verlag, 2000.
- [47] B. Richard and F. Schäfer, *Internal combustion engine handbook : basics, components, systems, and perspectives*, Warrendale, Pa: SAE International, 204, p. 507.
- [48] J. Fraden, *Handbook of modern sensors physics, designs, and applications*, New York: AIP Press/Springer, 2004, p. 496.
- [49] R. N. K. Loh, T. Pornthanomwong, J. S. Pyko, A. Lee and M. N. Karsiti, "Modeling, parameters identification, and control of an electronic throttle control (ETC) system," in *Proceedings of the International Conference on Intelligent and Advanced Systems*, Kuala Lumpur, Malaysia, November 2007.
- [50] J. Deur, J. Petric, J. Asgari and D. Hrovat, "Recent advances in control-oriented modeling of automotive power train dynamics," *IEEE/ASME Transactions on Mechatronics*, vol. 11, no. 5, pp. 513-523, 2006.
- [51] A. G. Stefanopoulou, J. S. Freudenberg and J. W. Grizzle, "Variable camshaft timing engine control," *IEEE Transactions on Control Systems Technology*, vol. 8, no. 1, pp. 23-34, 2000.
- [52] Z. Ren and G. Zhu, "Modeling and control of an electric variable valve timing system for SI

- and HCCI combustion mode transition," in *Proceedings of 2011 American Control*, San Francisco, CA, June-July 2011.
- [53] T. K. Lee and Z. S. Filipi, "Nonlinear model predictive control of a dual-independent variable valve timing engine with electronic throttle control," *Proceedings of the Institution of Mechanical Engineers, Part D: Journal of Automobile Engineering*, vol. 225, no. 9, pp. 1221-1234, 2011.
- [54] A. Beydoun, L. Wang, J. Sun and S. Sivashankar, "Hybrid control of automotive powertrain systems: A case study," *Hybrid Systems: Computation and Control*, vol. 1386, pp. 33-48, 1998.
- [55] J. B. Heywood, *Internal Combustion Engine Fundamentals*, New York, NY: McGraw-Hill, 1988.
- [56] A. G. Stefanopoulou, J. A. Cook, J. W. Grizzle and J. S. Freudenberg, "Joint air-fuel ratio and torque regulation using secondary cylinder air flow actuators," *ASME Journal of Dynamic Systems, Measurement, and Control*, vol. 121, no. 4, pp. 638-647, 1999.
- [57] R. Pursifull, A. J. Kotwicki and S. Hong, "Throttle Flow Characterization," in *SAE Technical Paper 2000-01-0571*, 2000.
- [58] R. K. Jurgen, *Automotive electronics handbook*, New York: McGraw-Hill, 1999, p. xxx.
- [59] J. A. Cook, J. Sun, J. H. Buckland, I. V. Kolmanovsky, H. Peng and J. W. Grizzle, "Automotive powertrain control — a survey," *Asian Journal of Control*, vol. 8, no. 3, pp. 237-260, 2006.
- [60] P. Yoon, S. Park and M. Sunwoo, "A Nonlinear Dynamic Model of SI Engines for Designing Controller," in *FISITA World Automotive Congress*, Seoul, S. Korea, June 2000.

- [61] A. Ali and J. P. Blath, "Application of Modern Techniques to SI-Engine Torque Control," in *International Conference on Control Applications*, Munich, Germany, October 4-6, 2006.
- [62] G. Baker and P. Graves-Morris, "Padé approximants," *2nd edition, Encyclopedia of mathematics and its applications*, vol. 59, 1996.
- [63] G. Labreuche, A. Da Costa, Y. Chamai lard, A. Charlet, P. Higelin and C. Perrier, "Total friction effective pressure and torque," in *MECA*, Italy, 2001.
- [64] M. Ibamoto, H. Kuroiwa, T. Minowa, K. Sato and T. Tsuchiya, "Development of smooth shift control system with output torque estimation," in *SAE technical paper number 950900*, 1995.
- [65] K. Hebbale, C. Lee, F. Samie, C. Kao, X. Chen, J. Horgan and S. Hearld, "Model Based Torque Converter Clutch Slip Control," in *SAE technical paper 2011-01-0396*, 2011.
- [66] U. Kiencke and L. Nielsen, *Automotive Control Systems*, New York: Springer-Verlag, 2000, pp. 130-131.
- [67] W. B. Ribbens, *Understanding automotive electronics*, Boston, MA: Newnes, 2003, p. 160.
- [68] G. Dahlquist and Å. Björck, *Numerical Methods*, Englewood Cliffs, N.J.: Prentice-Hall, 1974, pp. 196-198.
- [69] H. e. a. Bauer, *Gasoline-engine management*, Stuttgart, Germany: Robert Bosch GmbH, 1999, pp. 307, 330 and 361.
- [70] H. Bauer, *Automotive handbook*, Cambridge, MA: Robert Bosch GmbH via Bentley Publishers, 2004, p. 641.

- [71] H. Bauer, Gasoline-engine management, Cambridge, MA: Robert Bosch GmbH via Bentley Publishers, 2004, pp. 294-300.
- [72] M. Kamil, M. M. Rahman and R. A. Bakar, "An Integrated Model for Predicting Engine Friction Losses in Internal Combustion Engines," *International journal of automotive and mechanical engineering*, vol. 9, pp. 1695-1708, 2014.
- [73] D. Hrovat and W. F. Powers, "Modeling and Control of Automotive Power Trains," *Control and Dynamic Systems*, vol. 37, pp. 33-64, 1990.
- [74] A. L. Randolph, "Methods of Processing Cylinder-Pressure Transducer Signals to Maximize Data Accuracy," in *Society of Automotive Engineering Technical Paper no. 900170*, 1990.
- [75] M. F. J. Brunt and A. L. Emtage, "Evaluation of IMEP Routines and Analysis Errors," in *Society of Automotive Engineering Technical Paper no. 960609*, 1996.
- [76] S. Oh, D. Kim, J. Kim, B. Oh, K. Lee and M. Sunwoo, "Real-time IMEP estimation for torque-based engine control using an in-cylinder pressure," in *Society of Automotive Engineering Technical Paper 2009-04-20*, 2009.
- [77] R. C. Dorf and R. H. Bishop, Modern control systems, Upper Saddle River, NJ: Pearson Prentice Hall, 2005, p. 813.
- [78] W. Gang, "A Table Update Method for Adaptive Knock Control," in *SAE Technical Paper 2006-01-0607*, 2006.
- [79] L. Guzzella and C. Onder, Introduction to modeling and control of internal combustion engine systems, Second ed., Berlin: Springer, 2010, pp. 73-74.
- [80] B. Friedland, Control system design : an introduction to state-space methods, New York:

McGraw-Hill, 1986, pp. 22-24.

- [81] K. J. Åström and B. Wittenmark, *Computer-Controlled Systems - Theory and Design*, Upper Saddle River, N.J: Prentice Hall, 1997.
- [82] V. Ganesan, *Computer Simulation of Spark-ignition Engine Processes*, Hyderabad, India: University Press (India) Limited, 1996.
- [83] R. Stone, *Introduction to Internal Combustion Engines*, Basingstoke, Hampshire: Macmillan Press Limited, 1999.
- [84] A. G. Stefanopoulou, J. Grizzle and J. Freudenberg, "Engine air-fuel ratio and torque control using secondary throttles," in *Proceedings of the 33rd IEEE Conference on Decision and Control*, Lake Buena Vista, FL, Dec 1994.
- [85] A. G. Stefanopoulou, J. Cook, J. Freudenberg, J. Grizzle, M. Haghgoie and P. Szpak, "Modeling and control of a spark ignition engine with variable cam timing," in *Proceedings of 1995 American Control Conference - ACC'95*, Seattle, WA, Jun 1995.

ABSTRACT**TORQUE ACCURACY IMPROVEMENT VIA EXPLICIT TORQUE
FEEDBACK CONTROL FOR INTERNAL COMBUSTION SPARK
IGNITION ENGINES**

by

ANWAR ALKEILANI**May 2016****Advisors:** Dr. Hao Ying and Dr. Le Yi Wang**Major:** Electrical Engineering**Degree:** Doctor of Philosophy

At the present time, both control and estimation accuracies of engine torque are causes for under-achieving optimal drivability and performance in today's production vehicles. The major focus in this area has been to enhance torque estimation and control accuracies using existing open-loop torque control and estimation structures. Such an approach does not guarantee optimum torque tracking accuracy and optimum estimation accuracy due to air flow and efficiencies estimations errors. Furthermore, current approach overlooks the fast torque path tracking which does not have any related feedback. Recently, explicit torque feedback control has been proposed in the literature using either estimated or measured torques as feedback to control the torque using the slow torque path only. I propose the usage of a surface acoustic wave torque sensor and in-cylinder pressure sensor to measure the engine brake and indicated torques respectively and feedback the signals to control the torques using both the fast and slow torque paths utilizing an inner-outer loop control structure. The fast torque

path feedback is coordinated with the slow torque path by a novel method using the potential torque and is adapted to the sensors readings. The torque signals enable a fast and explicit torque feedback control that can correct torque estimation errors and improve drivability, emission control, and fuel economy. Control-oriented engine models for the 3.6L engine are developed. Computer simulations are performed to investigate the advantages and limitations of the proposed control strategy, versus the existing open loop control strategies. The findings include an improvement of 14% in gain margin and 60% in phase margin when the torque feedback is applied to the cruise control torque request at the simulated operating point. This study demonstrates that the direct torque feedback is a powerful technology with promising results for improved powertrain performance and fuel economy.

AUTOBIOGRAPHICAL STATEMENT

Anwar Alkeilani

Education:

Masters of Science in Electrical Engineering

Bachelors of Science in Electrical Engineering

Patents:

- US Patent Publication Number: US 20140156156

“Real time modeling of engine load addition due to alternator with an over-run clutch”

- Pending US Patent Publication Number: US 20140158097

“Supercharged engine and method of control”

Publications:

1. Main author of ASME paper titled: “DIRECT TORQUE FEEDBACK FOR ACCURATE ENGINE TORQUE DELIVERY AND IMPROVED POWERTRAIN PERFORMANCE” in proceedings of the ASME 2015 Internal Combustion Engine Division Fall Technical Conference ICEF2015, November 8-11, 2015, Houston, Texas, USA Paper # ICEF2015-1069